

A generalizable foundation model for intraoperative understanding across surgical procedures

Kanggil Park^{1,2,3}, Yongjun Jeon^{2,3}, Soyoung Lim¹, Seonmin Park^{1,2},
 Jongmin Shin^{1,2}, Jung Yong Kim¹, Sehyeon An³, Jinsoo Rhu¹, Jongman Kim¹,
 Gyu-Seong Choi¹, Namkee Oh^{1,2*}, Kyu-Hwan Jung^{2,3*}

¹Department of Surgery, Samsung Medical Center, Seoul, South Korea.

²Clinical Robotics and Embodied AI Research Center, Smart Healthcare Research Institute, Research Institute for Future Medicine, Samsung Medical Center, Seoul, South Korea.

³Department of Medical Device Management and Research, Samsung Advanced Institute for Health Sciences & Technology (SAIHST), Sungkyunkwan University, Seoul, South Korea.

*Corresponding author(s). E-mail(s): namkee.oh@samsung.com;
kyuhwanjung@gmail.com;

Abstract

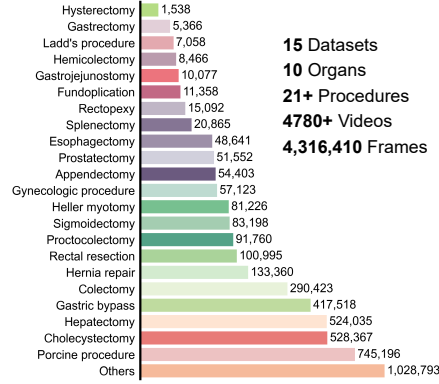
In minimally invasive surgery, clinical decisions depend on real-time visual interpretation, yet intraoperative perception varies substantially across surgeons and procedures. This variability limits consistent assessment, training, and the development of reliable artificial intelligence systems, as most surgical AI models are designed for narrowly defined tasks and do not generalize across procedures or institutions. Here we introduce ZEN, a generalizable foundation model for intraoperative surgical video understanding trained on more than 4 million frames from over 21 procedures using a self-supervised multi-teacher distillation framework. We curated a large and diverse dataset and systematically evaluated multiple representation learning strategies within a unified benchmark. Across 20 downstream tasks and full fine-tuning, frozen-backbone, few-shot and zero-shot settings, ZEN consistently outperforms existing surgical foundation models and demonstrates robust cross-procedure generalization. These results suggest a step toward unified representations for surgical scene understanding and support future applications in intraoperative assistance and surgical training assessment.

Keywords: Foundation Model, Minimally Invasive Surgery, Self-Supervised Learning, Surgical Video Analysis

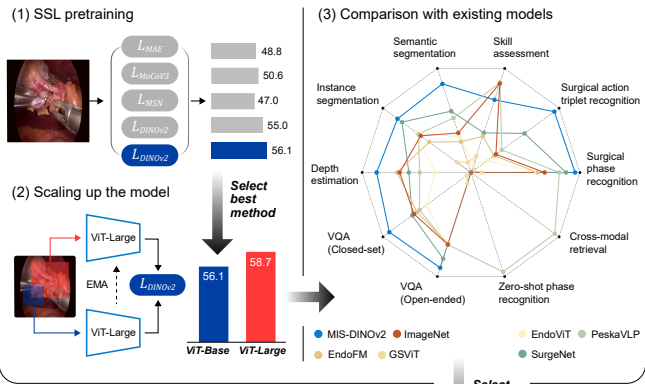
Introduction

Minimally invasive surgery (MIS) is now the standard of care for many procedures, providing reduced postoperative pain, shorter hospital stays, and faster recovery compared to open surgery [1–3]. Despite these advantages, MIS introduces greater procedural complexity, as surgeons must operate with limited visual and tactile feedback [4, 5]. Consequently, intraoperative decision-making in MIS remains highly dependent on individual surgeon experience and local practice patterns [6]. Variability in anatomical recognition, workflow interpretation, and situational awareness contributes to preventable complications, technical errors, and inconsistent training outcomes [7]. Since MIS relies on real-time endoscopic video, computational video analysis is essential to improve intraoperative decision-making and patient safety [8, 9]. Recent advances in artificial intelligence (AI) have shown strong potential for surgical video analysis in

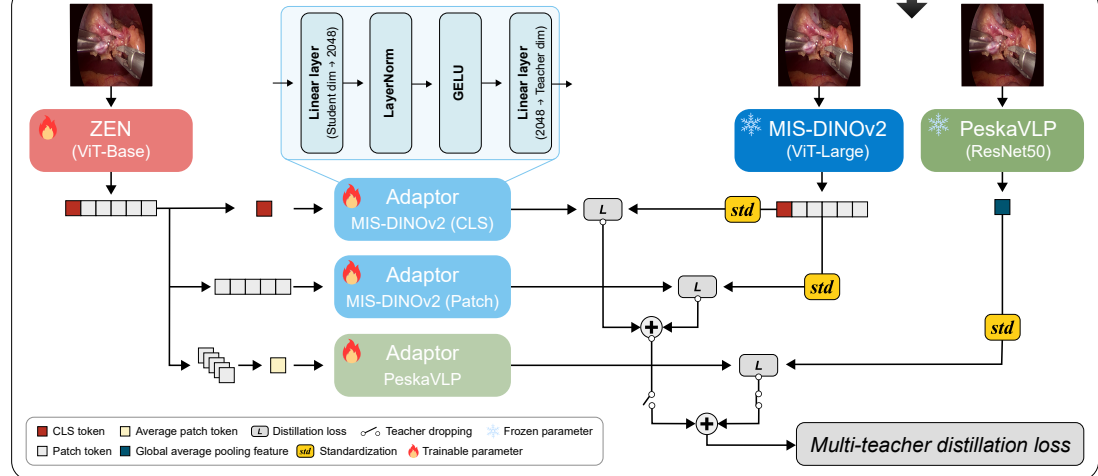
a. Large-scale minimally invasive surgery dataset



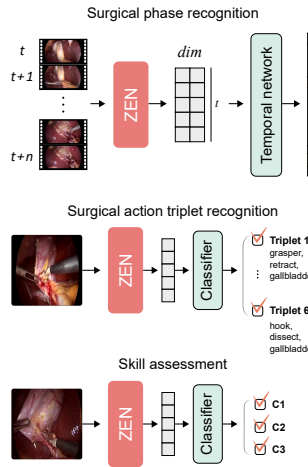
b. Comparison of pretraining strategies



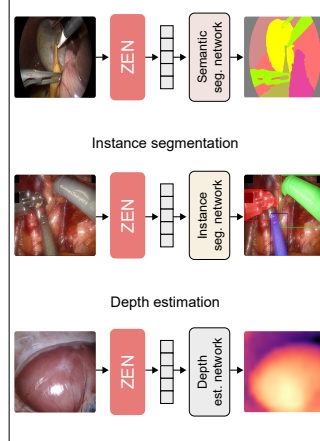
c. Architecture



d. Surgical workflow understanding



e. Dense spatial understanding



f. Vision-language understanding

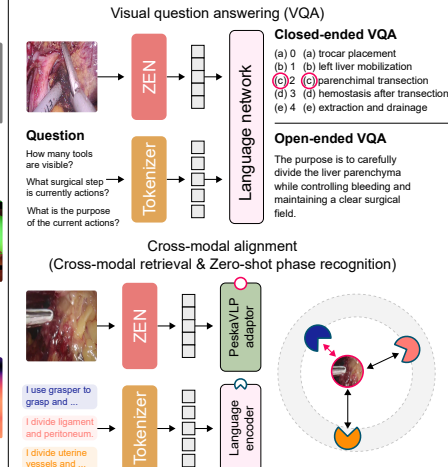


Fig. 1 Overview of this study. **a**, Large-scale pretraining dataset comprising over 4.3 million frames from over 4,780 minimally invasive surgery videos, spanning over 21 procedures across 10 organs. **b**, Comparison of pretraining strategies. Various self-supervised methods were evaluated across surgical downstream tasks, after which the best-performing strategy was scaled up and compared against existing pretrained models. **c**, Architecture of ZEN and the multi-teacher distillation framework. ZEN is trained via feature-level distillation from multiple frozen expert teachers, including MIS-DINOv2 (ViT-Large) and PeskaVLP. **d–f**, Downstream surgical evaluation tasks. **d**, Surgical workflow understanding: surgical phase recognition, surgical action triplet recognition, and skill assessment. **e**, Dense spatial understanding: semantic segmentation, instance segmentation, and monocular depth estimation. **f**, Vision-language understanding: closed-ended and open-ended visual question answering, cross-modal retrieval, and zero-shot phase recognition.

tasks such as surgical workflow analysis [10–14]. Despite this progress, clinically deployable systems remain limited. A major barrier is poor generalizability. Most existing models are developed for narrowly defined tasks within single procedures or institutions and fail to transfer across variations in anatomy, surgical technique, equipment, and operative context [15]. In addition, reliance on large, manually annotated datasets—particularly for video—poses substantial scalability challenges [16], limiting clinical translation.

Foundation models (FM) have emerged as a powerful paradigm to overcome these limitations. Pre-trained on large datasets, FMs show broad generalization across diverse tasks and perform well even when labeled data are limited [17]. Building on these advances, medical AI is shifting towards domain-specific FMs [18–22]. As open-access surgical video datasets continue to grow, this trend is expanding into the surgical field, and initial efforts to develop surgical FMs have begun to emerge [23–28]. However, several key questions remain unresolved. Previous work has relied on varying pretraining datasets and strategies, making it unclear which approaches are most effective for the surgical domain. Moreover, most existing models focus on workflow analysis, with only a few extending to tasks such as tool or anatomy segmentation (Fig.2a). Consequently, it remains uncertain whether current approaches can support the diverse and complex tasks required for real-world clinical use. Therefore, a comprehensive evaluation across a broader range of downstream tasks is essential for developing FMs that generalize reliably within the surgical domain.

To address this gap, we curated a large-scale pretraining dataset comprising 4,316,410 frames from over 4,780 videos spanning 10 organs and over 21 procedures (Fig.1a). Additionally, we established 20 clinical benchmarks covering surgical workflow understanding (phase recognition, action triplet recognition, and skill assessment) (Fig.1d), dense spatial understanding (semantic and instance segmentation, and depth estimation) (Fig.1e), and vision–language understanding, including VQA and cross-modal alignment tasks (cross-modal retrieval and zero-shot phase recognition) (Fig.1f). Using this unified resource, we conducted the first systematic comparison of various self-supervised learning (SSL) methods and evaluated them alongside existing surgical FMs (Fig.1b and Extended Fig.1). To ensure a rigorous comparison, all SSL methods were initially trained on the same pretraining dataset using a Vision Transformer (ViT) [29] Base architecture and were evaluated under identical downstream conditions. Our evaluation revealed that SimDINOv2 [30] exhibited the strongest overall performance. Motivated by this result, we scaled SimDINOv2 to a ViT-Large encoder to enhance model capacity, producing “MIS-DINOv2”. When benchmarked against existing surgical FMs, MIS-DINOv2 demonstrated superior performance across most downstream tasks. Notably, PeskaVLP [26] retained its advantage in cross-modal alignment tasks (cross-modal retrieval and zero-shot phase recognition), reflecting its training with vision–language contrastive learning [31], whereas other vision-only models lack this capability. These findings show that individual pretraining strategies offer distinct strengths across downstream tasks.

To unify these complementary strengths within a single framework, we introduce ZEN, a generalizable FM for MIS video analysis. Specifically, we introduce a self-supervised multi-teacher distillation strategy [32–35] to synergize MIS-DINOv2 and PeskaVLP, enabling ZEN to inherit both robust spatial representations and precise vision–language alignment (Fig.1c). Across our comprehensive benchmark evaluation, ZEN not only demonstrates advanced cross-modal alignment capabilities but also consistently outperforms existing surgical FMs (Fig.2b). Moreover, ZEN demonstrates this superior performance across diverse evaluation settings, including limited labeled data and frozen-backbone settings, underscoring its robust generalization as a FM for the surgical domain.

Results

Overall performance

We evaluated ZEN and other surgical FMs using a clinical benchmark comprising 20 tasks across nine surgical procedures. These tasks cover three core domains: surgical workflow understanding (three phase recognition, two action triplet recognition, and one skill assessment task); dense spatial understanding (three semantic segmentation, one instance segmentation, and two depth estimation tasks); and vision–language understanding, comprising VQA (two closed- and one open-ended VQA) and vision–language alignment (text-to-image and image-to-text retrieval, and three zero-shot phase recognition tasks). The five vision–language alignment tasks were evaluated in a zero-shot setting, while the remaining 15 tasks used supervised evaluation. For supervised tasks, we evaluated the representation quality using a frozen-backbone setting and model adaptability using full fine-tuning. Overall performance was summarized using the average of each task’s representative metric, complemented by task-level rankings to account for heterogeneity in evaluation metrics across tasks.

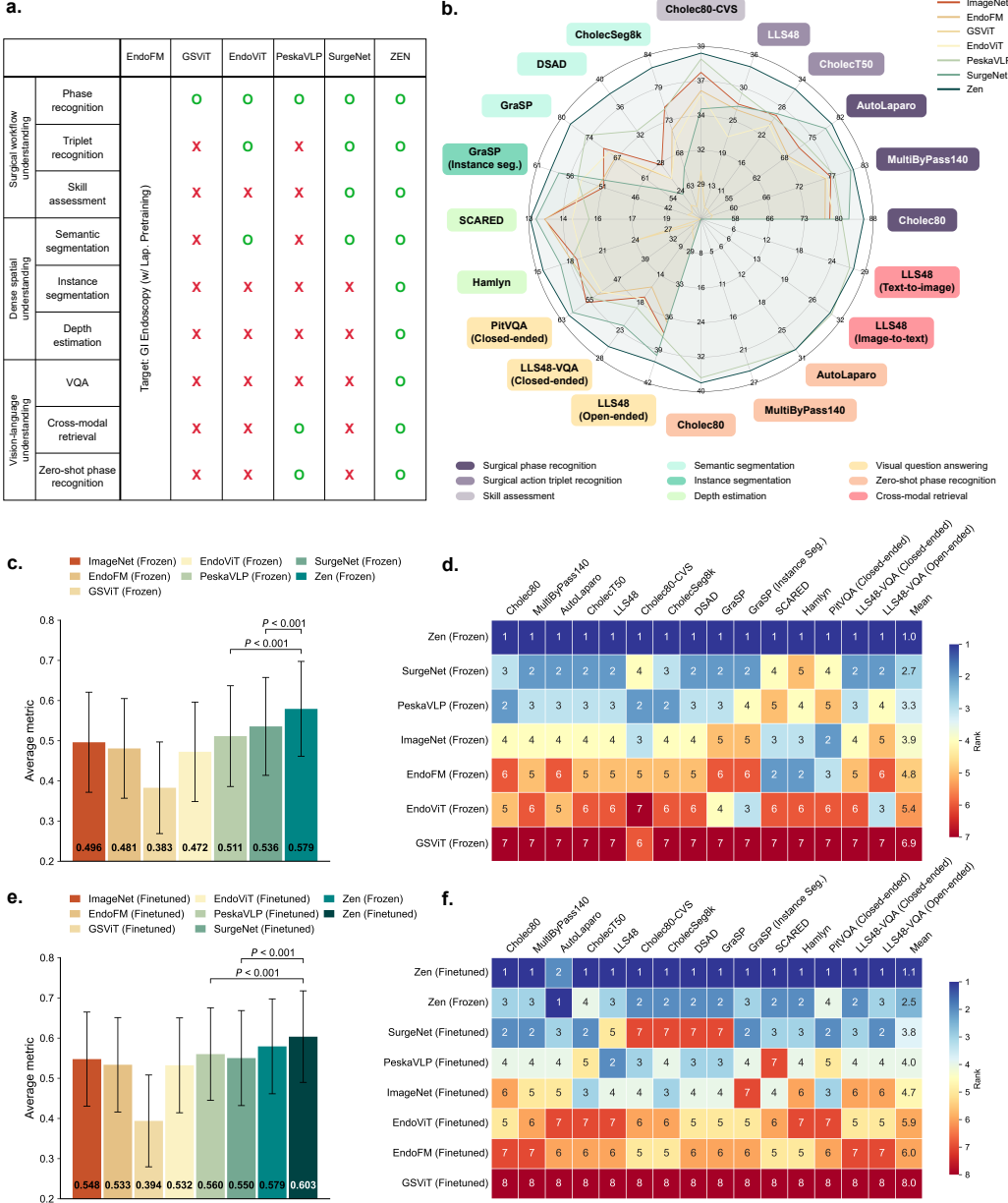
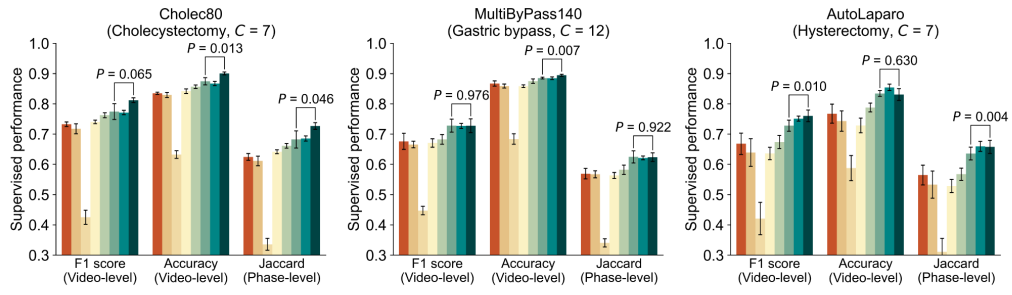


Fig. 2 Generalization performance of surgical foundation models on comprehensive clinical benchmarks. **a**, Comparison of downstream tasks targeted by existing surgical foundation models. Note that although EndoFM [24] utilizes MIS videos for pretraining, its target tasks primarily focused on gastrointestinal endoscopy. **b**, ZEN outperforms other pretrained models across 20 clinical tasks in surgical video. **c**, Average performance in the frozen-backbone setting across 15 supervised tasks, computed using task-specific representative metrics: video-level macro F1 score and accuracy for phase recognition; triplet (IVT) mean average precision (mAP) for action triplet recognition; mAP for skill assessment; Dice score for semantic segmentation; the average of detection and segmentation mAP for instance segmentation; 1 – absolute relative error for depth estimation; the average of macro F1 score and balanced accuracy for closed-ended VQA; and the average of BLEU, ROUGE-L, and METEOR for open-ended VQA. **d**, Ranking heatmap across the supervised tasks in the frozen-backbone setting, based on representative task-level metrics. **e**, Average performance in the fine-tuned backbone setting across the supervised tasks, computed using representative metrics. **f**, Ranking heatmap across the supervised tasks in the fine-tuned backbone setting. Error bars in **c** and **e** indicate 95% confidence intervals. P values were calculated using a two-sided Wilcoxon signed-rank test.

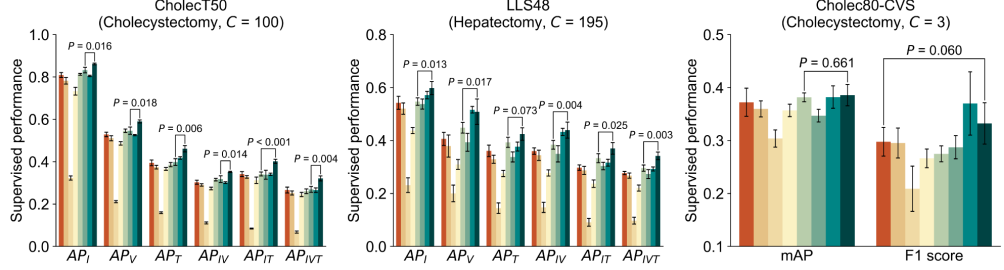
In the frozen-backbone setting, ZEN achieved the highest average score (0.579) and the best mean rank of 1.0, outperforming the next-best model, SurgeNet (score 0.536; rank 2.7) (Fig. 2c,d). In the full fine-tuning setting, ZEN again achieved the top performance with an average score of 0.603 and a mean rank of 1.1. Notably, the frozen ZEN model (score 0.579; rank 2.5) exceeded the performance of all other fully fine-tuned FMs, including SurgeNet (score 0.550; rank 3.8) (Fig. 2e,f). When compared with the second- and third-best performing models, ZEN achieved significantly higher average performance ($P < 0.001$) in



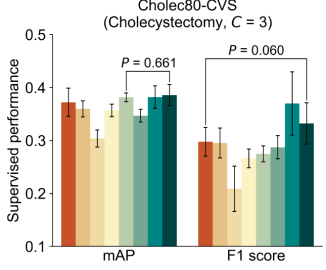
a. Surgical phase recognition



b. Surgical action triplet recognition



c. Skill assessment



d. Few-shot surgical phase recognition

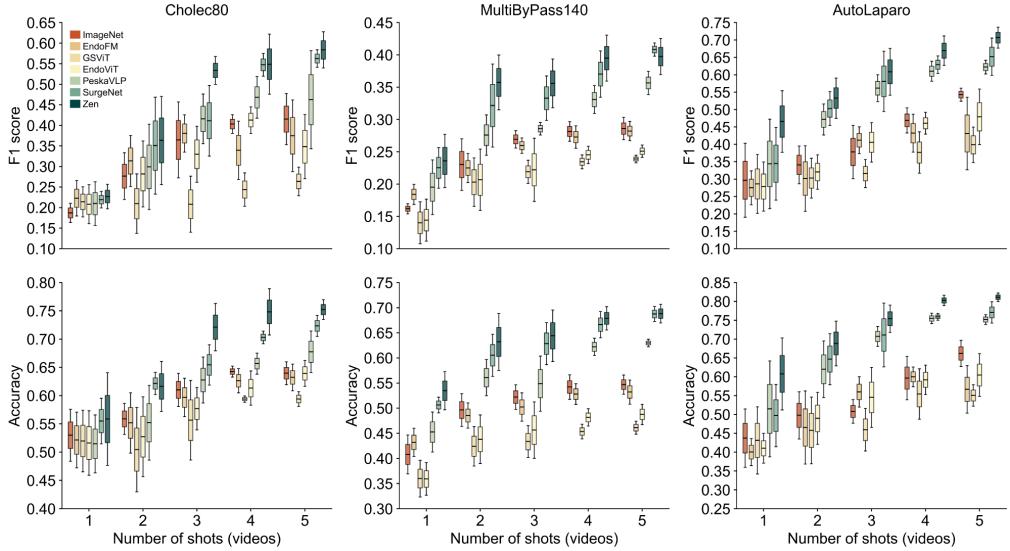


Fig. 3 Performance comparison for surgical workflow understanding. **a.**, Performance of ZEN and other pretrained models on surgical phase recognition across three datasets in the fine-tuned backbone setting. Metrics include video-level macro F1 score, accuracy, and phase-level Jaccard index. C denotes the number of phases. **b.**, Surgical action triplet recognition performance across two datasets in the fine-tuned backbone setting. Performance is evaluated using mean average precision (mAP) for instrument (I), verb (V), and target (T) components, as well as their combinations. C denotes the number of triplet (IVT) classes. **c.**, Skill assessment performance in the fine-tuned backbone setting, evaluated using mAP and macro F1 score. C denotes the number of safety criteria. **d.**, Few-shot surgical phase recognition performance using 1–5 training videos across three datasets. Results represent five independent runs ($n = 5$) for each model and shot condition. The center of each box indicates the mean, box bounds denote the standard error, and whiskers indicate the lower and upper bounds of the 95% confidence interval (CI). For **a–c**, error bars represent 95% CIs over five independent runs ($n = 5$). P values were calculated using two-sided paired t -test.

both the frozen and fine-tuning settings. Together, these results demonstrate ZEN’s strong generalization capabilities across diverse tasks in surgical domain.

Surgical workflow understanding

Surgical workflows follow a hierarchical structure in which combinations of instruments, verbs, and targets define individual actions, and sequences of these actions form surgical phases. Skill assessment complements this hierarchy by evaluating whether key safety criteria are satisfied throughout the procedure. To assess ZEN’s understanding of surgical workflows at multiple levels of granularity, we benchmarked the model on three representative tasks: surgical phase recognition [10–14], which captures the temporal progression of procedure phases; surgical action triplet recognition [36–39], which models fine-grained instrument–verb–target (I–V–T) combinations; and skill assessment [40], which evaluates whether predefined surgical safety criteria are satisfied during the procedure.

Surgical phase recognition

Surgical phase recognition was evaluated on three public laparoscopic datasets: Cholec80 [10] (cholecystectomy), MultiBypass140 [41] (Roux-en-Y gastric bypass surgery) and AutoLaparo [42] (hysterectomy). ZEN consistently outperformed other FMs on all three surgical phase recognition datasets under full fine-tuning, across multiple evaluation metrics including video-level F1 score, accuracy, and phase-level Jaccard index (Fig.3a and Supplementary Tables 1–3). In the frozen-backbone setting, ZEN also achieved the strongest overall performance across the three datasets (Extended Fig.2a and Supplementary Tables 4–6). Notably, the frozen ZEN model remained competitive with fully fine-tuned models, underscoring the strength of its pretrained representations (Fig.3a). We further evaluated ZEN under few-shot settings (limited task-specific data conditions), using 1–5 training videos. Across all datasets, ZEN demonstrated competitive performance relative to other models (Fig.3d and Supplementary Tables 7–21). Additional results for phase-level precision and recall are included in the aforementioned Supplementary Tables.

Surgical action triplet recognition

Surgical action triplet recognition was evaluated on two procedures using the open-access CholecT50 [43] dataset (cholecystectomy) and an in-house LLS48 [44] dataset (hepatectomy). Both datasets provide frame-level multi-label annotations of surgical actions, with each action represented as a combination of instrument (I), verb (V), and target (T). ZEN demonstrated superior performance across the two datasets in both full fine-tuning and frozen-backbone settings. Under the full fine-tuning setting, ZEN attained the highest full triplet (IVT) mean average precision (mAP), outperforming the second-best model, SurgeNet [27], by +5.2% on CholecT50 ($P = 0.004$) and +6.9% on LLS48 ($P = 0.003$) (Fig.3b and Supplementary Tables 22, 23). ZEN also achieved the highest performance on individual and paired sub-components (I, V, T, IV, and IT). In the frozen-backbone setting, ZEN achieved the top performance for all component (all $P \leq 0.002$) (Extended Fig.2b and Supplementary Tables 24, 25). Together, these results demonstrate ZEN’s robust capability for fine-grained surgical workflow understanding at the action level.

Skill assessment

We evaluated ZEN’s skill assessment performance using the critical view of safety (CVS), a widely adopted safety concept for laparoscopic cholecystectomy proposed by Strasberg [45]. CVS is defined by three criteria: (1) only two structures are clearly identified entering the gallbladder; (2) the lower third of the gallbladder is dissected off the liver bed; and (3) the hepatocystic triangle is completely cleared to expose all cystic structures. This task was evaluated on the Cholec80-CVS [46] dataset with expert annotations of CVS achievement. The three CVS criteria were formulated as a multi-label format, with each criterion predicted as satisfied or not. Overall, ZEN achieved strong performance in both the full fine-tuning and frozen-backbone settings. In the full fine-tuning setting, ZEN reached an mAP of 0.386 and a macro F1 score of 0.332, showing performance comparable to PeskaVLP (mAP 0.382; $P = 0.661$) and higher performance than the ImageNet-pretrained model [29] (macro F1 0.298; $P = 0.060$) (Fig.3c). In the frozen-backbone setting, ZEN achieved an mAP of 0.382 and a macro F1 of 0.370, comparable to PeskaVLP (mAP 0.369; $P = 0.517$) and SurgeNet (macro F1 0.327; $P = 0.342$) (Extended Data Fig. 2c). Notably, even without task-specific fine-tuning, the frozen ZEN model obtained higher mAP and macro F1 than any other fully fine-tuned model, highlighting the strength of its pretrained representations (Supplementary Table 26).

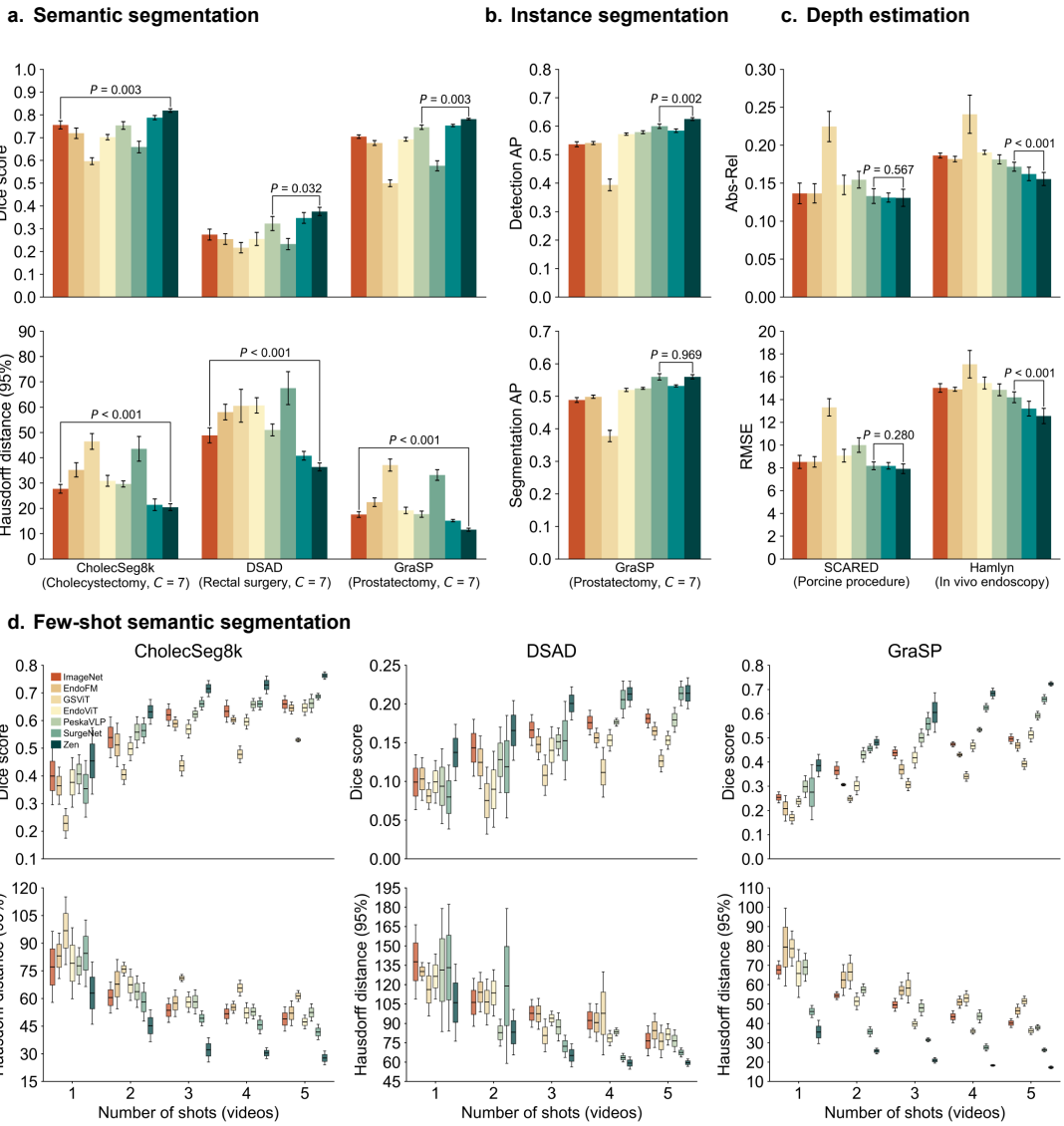


Fig. 4 Performance comparison for dense spatial understanding. **a.**, Semantic segmentation performance across three datasets in the fine-tuned backbone setting. Performance is measured using Dice score and 95% Hausdorff distance. C denotes the number of classes. **b.**, Instance segmentation performance in the fine-tuned backbone setting. Performance is evaluated using mean Average Precision (mAP), averaged over Intersection over Union thresholds from 0.5 to 0.95. Results are reported for bounding box detection (Detection AP) and segmentation masks (Segmentation AP). C denotes the number of classes. **c.**, Depth estimation performance across two datasets in the fine-tuned backbone setting. Metrics include Absolute Relative Error (Abs-Rel) and Root Mean Squared Error (RMSE). **d.**, Few-shot semantic segmentation performance (label efficiency) using 1–5 training videos across three datasets. Data represent five independent runs ($n = 5$) for each model and shot condition. The center of the box represents the mean, the bounds of the box indicate standard error, and the whiskers denote the lower and upper bounds of the 95% confidence interval (CI). For **a–c**, error bars represent 95% CIs over five independent runs ($n = 5$). P values were calculated using two-sided paired t -tests.

Dense spatial understanding

Unlike open surgery, MIS relies exclusively on video data for intraoperative guidance and postoperative analysis. Consequently, the accurate extraction of spatial and physical information from surgical videos—such as anatomical structure localization [47, 48], tool trajectories [49, 50] and depth estimation [51–53]—is critical for advanced clinical applications, including surgical navigation and automated skill assessment. To assess pixel-, instance-level, and geometric understanding, we evaluated ZEN on three dense prediction tasks: semantic segmentation of tools and anatomy, instance segmentation of surgical instruments, and monocular depth estimation.

Semantic segmentation

To evaluate pixel-level semantic understanding, we used three public datasets: CholecSeg8k [54] (cholecystectomy; instruments and anatomy), DSAD [55] (rectal surgery; abdominal organs), and GraSP [56] (prostatectomy; instruments). Under the full fine-tuning protocol, ZEN outperformed all other models across all datasets. ZEN achieved higher Dice scores than the second-best model by 6.3% on CholecSeg8k ($P = 0.003$), 5.3% on DSAD ($P = 0.032$), and 3.6% on GraSP ($P = 0.003$). In parallel, ZEN achieved lower 95% Hausdorff distances by 7.26, 12.50, and 6.02, respectively (all $P < 0.001$; Fig.4a and Supplementary Table 27). Under the frozen-backbone setting, ZEN also achieved higher performance than the second-best model across all datasets ($P < 0.05$) (Extended Fig. 3a and Supplementary Table 28). Notably, frozen ZEN surpassed all other fully fine-tuned other models, indicating that ZEN learns transferable spatial semantics during pretraining. Furthermore, in few-shot settings (1–5 videos), ZEN consistently achieved the best performance across all three datasets (Fig.4d and Supplementary Table 29–33). Qualitative segmentation examples are provided in Extended Fig. 4.

Instance segmentation

We evaluated instance-level instrument localization on the GraSP [56] dataset using mAP computed over intersection-over-union thresholds from 0.5 to 0.95 for both bounding box (bbox) detection and mask segmentation. In the full fine-tuning setting, ZEN achieved the best performance for both bbox detection and mask segmentation. Specifically, ZEN surpassed the second-best model, SurgeNet, by 2.5% in bbox detection ($P = 0.002$) and by 0.16% in segmentation ($P = 0.969$) (Fig.4b). This trend continued in the frozen-backbone setting, where ZEN outperformed SurgeNet by 4.4% in bbox detection ($P = 0.001$), with comparable segmentation performance (+0.2%; $P = 0.716$) (Extended Fig.3b). Results for both full fine-tuning and frozen-backbone settings are summarized in Supplementary Table 34. Qualitative examples are provided in Extended Fig.4.

Depth estimation

We also assessed the model’s capacity to capture 3D geometric structures via monocular depth estimation using the SCARED [57] (porcine procedure) and Hamlyn [58] (in vivo endoscopy video) datasets. In the full fine-tuning setting, ZEN achieved the best performance in terms of Absolute Relative error (Abs-Rel) and Root Mean Square Error (RMSE). On the SCARED dataset, ZEN demonstrated performance comparable to the second-best model, SurgeNet, recording an Abs-Rel of 0.131 and RMSE of 7.92 (SurgeNet: 0.133 and 8.18; $P > 0.05$). On the Hamlyn dataset, ZEN achieved significantly lower errors than SurgeNet, with an Abs-Rel of 0.155 and RMSE of 12.55 (SurgeNet: 0.172 and 14.20; both $P < 0.001$; Fig.4c and Supplementary Tables 35, 36). In the frozen-backbone setting, ZEN consistently achieved the lowest errors across both datasets. On the SCARED dataset, ZEN outperformed the second-best model, EndoFM [24], achieving an Abs-Rel of 0.131 and RMSE of 8.18 (EndoFM: 0.154 and 9.52; $P < 0.05$). On the Hamlyn dataset, ZEN surpassed EndoFM with an Abs-Rel of 0.155 and RMSE of 12.55 (EndoFM: 0.172 and 14.20; $P < 0.05$; Extended Data Fig.3c and Supplementary Tables 37, 38). Additional metrics, including square relative error, log-scale RMSE, and accuracy under threshold, are detailed in Supplementary Tables, with qualitative examples provided in Extended Data Fig.5.

Vision–Language understanding

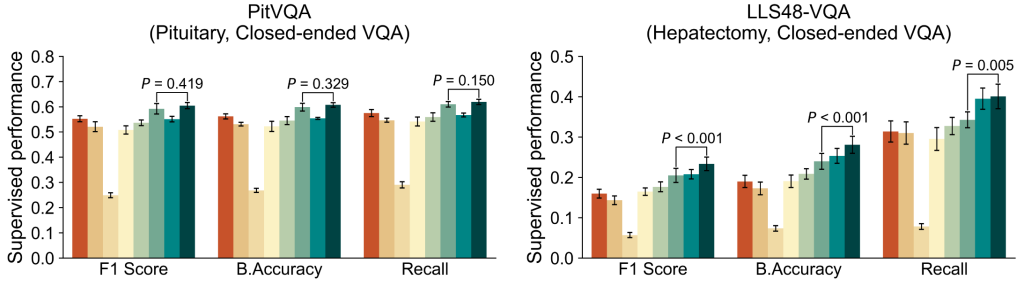
Interpreting complex surgical dynamics requires specialized expertise; however, limited availability of such expertise constrains access for medical trainees and non-expert clinicians [59]. This bottleneck highlights a critical unmet need for automated systems capable of bridging visual data with natural language to provide accessible explanations and precise information retrieval [60, 61]. To assess ZEN’s potential to address these clinical challenges, we evaluated its multimodal capabilities in two distinct domains. First, we assessed vision–language reasoning via Visual Question Answering (VQA) [62–64]. This task evaluates the model’s ability to interpret surgical scenes in response to clinical language queries. Second, we evaluated vision–language alignment through zero-shot cross-modal retrieval and zero-shot phase recognition [26, 65, 66]. These tasks measure how well the model aligns surgical video representations with natural language in a shared embedding space, enabling generalization without task-specific training.

Visual question answering

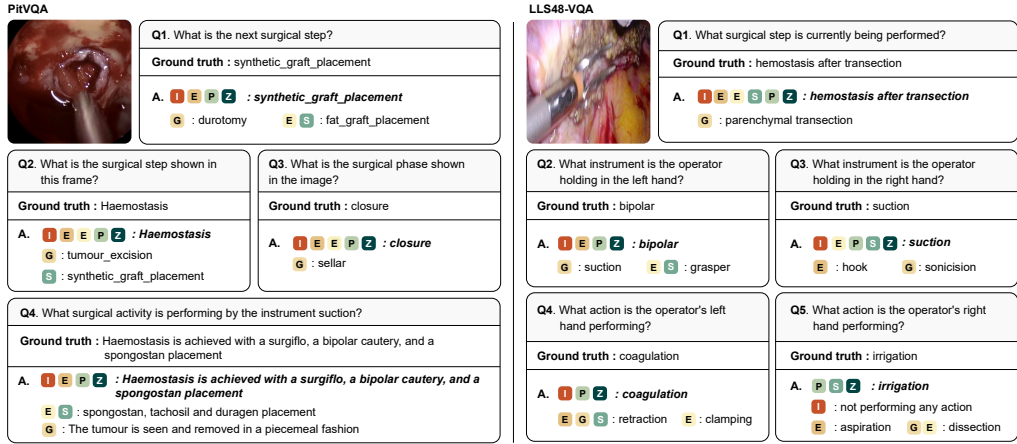
We assessed ZEN’s VQA performance using two datasets: PitVQA [63], which contains closed-ended VQA for endoscopic pituitary surgery, and LLS48-VQA, which includes both closed- and open-ended



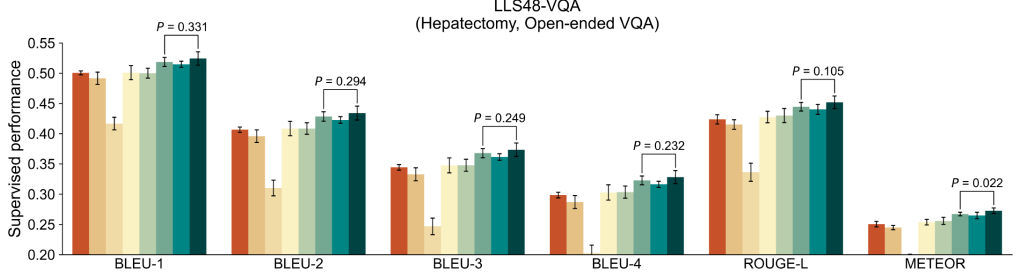
a. Visual question answering (Closed-ended VQA)



b. Closed-ended VQA examples



c. Visual question answering (Open-ended VQA)



d. Cross-modal retrieval

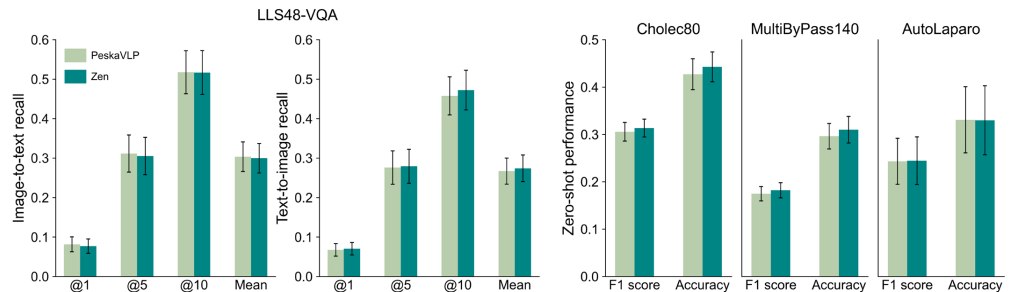


Fig. 5 Performance comparison for vision–language understanding. **a.** Closed-ended VQA performance in the fine-tuned backbone setting. Evaluation metrics include macro F1 score, balanced accuracy (B.Accuracy), and recall, measured by exact match criteria. **b.** Representative closed-ended VQA examples from two datasets. **c.** Open-ended VQA performance in the fine-tuned backbone setting, evaluated using BLEU-1–4, ROUGE-L, and METEOR. **d.** Cross-modal retrieval performance of ZEN compared with PeskaVLP. Metrics include Recall@K ($K = \{1, 5, 10\}$) and mean recall for both image-to-text and text-to-image retrieval tasks. **e.** Zero-shot surgical phase recognition performance on three datasets. Performance is measured by video-level F1 score and accuracy. For **a** and **c**, error bars represent 95% confidence intervals (CIs) over five independent runs ($n = 5$). P values were computed using two-sided paired t -tests. For **d** and **e**, error bars represent 95% CIs across test videos.

VQA for laparoscopic hepatectomy. Closed-ended VQA addressed categorical, clinically grounded questions—such as tool counts, instrument types, and surgical phases—and was evaluated using exact-match metrics (macro F1 score, balanced accuracy, and recall). Open-ended VQA, defined only on LLS48-VQA, targeted non-categorical questions related to surgical scene description, procedural intent, and planning. Performance was evaluated using standard text-generation metrics (BLEU-1 to BLEU-4, ROUGE-L, and METEOR). Under full fine-tuning setting, ZEN achieved the best performance on closed-ended VQA across both datasets (Fig. 5a and Supplementary Tables 39, 40). On PitVQA, ZEN achieved the highest scores across all metrics, although differences were not statistically significant. For closed-ended VQA on LLS48-VQA, ZEN achieved significantly higher macro F1 and balanced accuracy than the second-best model, with performance gains of 2.9% ($P < 0.001$) and 4.1% ($P < 0.001$), respectively, and also showed higher recall with an improvement of 5.8% ($P = 0.005$). In the frozen-backbone setting, ZEN significantly outperformed the second-best model on both datasets ($P < 0.05$) (Extended Data Fig. 6a and Supplementary Tables 39, 40). For open-ended VQA on LLS48-VQA, ZEN achieved the highest scores across all text-generation metrics under both full fine-tuning (Fig. 5c and Supplementary Tables 41) and frozen-backbone settings (Extended Data Fig. 6b and Supplementary Tables 42). Representative qualitative examples for both closed- and open-ended VQA, including input questions, corresponding images, and model predictions, are shown in Fig. 5b and Extended Data Fig. 7, respectively.

Vision–language alignment

We evaluated ZEN’s vision–language alignment using two zero-shot tasks: cross-modal retrieval and phase recognition. Zero-shot cross-modal retrieval was conducted on the LLS48-VQA dataset and included both text-to-image and image-to-text retrieval, using natural-language descriptions as queries (Fig. 5d and Supplementary Table 43). Zero-shot phase recognition was evaluated on three surgical phase recognition datasets (Cholec80, MultiBypass140, and AutoLaparo) using textual phase descriptions [26] (Fig. 5e and Supplementary Table 44). Because these tasks require a shared image–text embedding space, image-only FMs could not be directly evaluated. Accordingly, we benchmarked ZEN against PeskaVLP, a vision–language foundation model that served as the teacher during multi-teacher distillation. Cross-modal retrieval performance was assessed using Recall@K ($K = 1, 5, 10$). In image-to-text retrieval, ZEN achieved slightly lower recall than PeskaVLP, with a mean recall of 0.300 compared with 0.304, whereas in text-to-image retrieval, ZEN achieved comparable or higher recall, reaching a mean recall of 0.274 relative to 0.267 for PeskaVLP. For zero-shot phase recognition, evaluated using video-level F1 score and accuracy, ZEN outperformed PeskaVLP on two of the three datasets. Together, these results demonstrate that the proposed multi-teacher distillation framework effectively transfers vision–language alignment from PeskaVLP to ZEN, enabling cross-modal alignment between surgical images and textual descriptions.

Effectiveness of multi-teacher distillation

To assess the effectiveness of our proposed multi-teacher distillation framework, we compared ZEN against its two specialized teacher models: MIS-DINOv2 (ViT-Large) and PeskaVLP (ResNet50) (Extended Data Fig. 8). Performance was evaluated across 15 supervised downstream tasks. Although ZEN uses a lighter ViT-Base architecture than MIS-DINOv2 (ViT-Large), it achieved competitive performance across tasks. In the frozen-backbone setting, ZEN showed marginally lower average performance than MIS-DINOv2; however, after backbone fine-tuning, ZEN outperformed MIS-DINOv2, highlighting the effectiveness of knowledge distillation in transferring rich representations from a larger teacher to a more compact student model. This efficiency is particularly important in surgical video understanding, where models must process large volumes of video frames. Compared with PeskaVLP, ZEN outperformed the teacher across most tasks and metrics under both frozen and fine-tuned settings. For tasks involving vision–language alignment, ZEN exhibited performance comparable to PeskaVLP, despite the absence of direct vision–language supervision during training (Fig. 5d,e). Overall, these results show that multi-teacher distillation enables ZEN to inherit both rich visual representations and vision–language alignment from specialized teacher models, allowing a compact architecture to achieve strong performance across diverse surgical tasks.

Discussion

In this study, we introduce ZEN, a generalizable FM for MIS video analysis, trained using a self-supervised multi-teacher distillation. We curated a large-scale surgical video dataset comprising over 4

million frames covering more than 21 surgical procedures for pretraining. We then evaluated its performance against existing surgical FMs across 20 downstream tasks covering surgical workflow, dense spatial, and vision–language understanding under full fine-tuning, frozen-backbone, few-shot and zero-shot settings. Across supervised tasks, ZEN achieved the strongest overall performance under both full fine-tuning and frozen-backbone settings. Notably, ZEN maintained competitive or superior performance even when the backbone was frozen, outperforming fully fine-tuned models on several tasks. ZEN also exhibited strong few-shot performance, indicating effective generalization with minimal labeled data. On zero-shot cross-modal alignment tasks, ZEN achieved strong performance without direct vision–language supervision, approaching that of its vision–language teacher, PeskaVLP [26]. Together, these results show ZEN not only performs strongly across a wide range of surgical tasks but also learns highly transferable representations that remain effective when labeled data or computational resources are constrained.

Despite recent progress, robust surgical video analysis remains particularly challenging. Surgical videos exhibit substantial visual variability due to differences in anatomy, technique, image conditions, and surgeon expertise [67]. In addition, procedures are inherently long and complex, with temporally evolving scenes and subtle visual cues that are often difficult to annotate consistently, even for experts. As a result, large-scale labeled datasets are expensive to obtain. In such data-constrained settings, task-specific supervised models are prone to overfitting to narrow data distributions, which often limits their ability to generalize across institutions, surgeons, and procedures. In this context, the strong performance of ZEN under frozen-backbone and few-shot settings is particularly meaningful. Frozen-backbone evaluations provide a stringent test of representation quality by assessing whether pretrained features remain general and transferable when the backbone is fixed. ZEN’s ability to outperform or match fully fine-tuned models in this setting suggests that it learns semantically rich and stable representations that capture fundamental aspects of surgical scenes, rather than overfitting to narrow task-specific cues. Similarly, strong few-shot performance indicates that ZEN can adapt to new tasks with minimal labeled data, which is critical in surgical domains with limited annotation. Importantly, ZEN demonstrated robust generalization to surgical procedures not seen during pretraining. Although the pretraining dataset was predominantly composed of abdominal laparoscopic surgeries, ZEN achieved strong performance not only on external abdominal surgical datasets but also on pituitary surgery videos, where it outperformed existing surgical FMs despite the substantial anatomical and procedural differences. Such robust generalization is essential for real-world deployment, where surgical AI systems are frequently applied to new procedures, institutions, or devices. These results underscore the potential of ZEN as a practical FM for surgical video analysis, capable of maintaining strong performance under data scarcity, domain shift.

Existing surgical FMs [23–28] have typically relied on heterogeneous combinations of open-access datasets and institution-specific private data, trained using a single pretraining strategy. As a result, such heterogeneity has obscured which approaches are most effective for surgical video understanding. Moreover, most previous work has focused primarily on workflow analysis, with comparatively less attention paid to dense spatial and geometric understanding or vision–language reasoning. Consequently, it remains unclear whether these models generalize across the wide range of complex surgical tasks encountered in real clinical practice. To address these limitations, we pretrained and evaluated multiple self-supervised learning strategies using a unified pretraining dataset and benchmark, and compared them with existing surgical FMs across a broad range of downstream tasks. This analysis revealed that different pretraining strategies offer complementary strengths. Vision-only self-supervised approaches, exemplified by MIS-DINOv2 pretrained on our dataset using SimDINOv2 with a ViT-Large backbone, showed strong performance across a broad range of downstream tasks. In contrast, models pretrained with vision–language contrastive objectives, such as PeskaVLP, demonstrated clear advantages in tasks requiring explicit zero-shot cross-modal alignment. Motivated by these observations, we integrated both forms of supervision via multi-teacher distillation, resulting in ZEN, which achieved strong and balanced performance across diverse surgical tasks. This approach highlights the potential of multi-teacher distillation as an effective strategy for building versatile medical FMs in settings where large-scale data sharing is constrained by privacy considerations, yet pretrained model weights can be shared.

Unlike many other medical domains, surgery involves substantial human intervention and limited experimental control. This makes rigorous clinical validation of individual AI methods particularly challenging and requires a gradual and exploratory approach to assessing clinical benefit [68]. In this context, recent research has begun to introduce surgical AI systems into the operating room to evaluate their real-world clinical impact. Most current deployments focus on perceptual assistance, such as real-time anatomical segmentation to support intraoperative awareness. Although these systems are starting to enter clinical practice, their deployment remains limited, and their impact on patient outcomes is still

under active investigation [69]. In parallel, recent research has increasingly explored surgical AI systems that engage more directly with the physical and cognitive processes of surgery. These efforts include multimodal and interactive interfaces [70, 71], as well as physically grounded AI systems [72, 73] that integrate perception, spatial reasoning, and surgeon interaction. A central bottleneck in this line of work lies in accurately modeling the surgeon’s intraoperative interactions with instruments and anatomy in a manner that generalizes across procedures and settings. Addressing this challenge requires coordinated automated capabilities spanning surgical workflow understanding, dense spatial and semantic perception of anatomy and instruments, and language-based interaction with the surgeon. Across these approaches, a robust and generalizable visual representation is a critical prerequisite. Together, these requirements highlight the need for generalizable foundation models that perform reliably across diverse perceptual tasks. By demonstrating strong and balanced performance across surgical workflow, dense spatial, and vision–language understanding, ZEN may provide a useful foundation for future surgical AI systems, supporting both rigorous clinical impact analysis and the development of more interactive and treatment-relevant applications.

Several limitations of this study should be acknowledged. First, although our pretraining dataset spans a wide range of procedures, it is predominantly composed of abdominal laparoscopic surgeries and may not fully capture the variability of robotic-assisted or non-abdominal endoscopic interventions. While our results show encouraging generalization to anatomically and procedurally distinct settings, incorporating a broader range of non-abdominal and robotic surgical videos during pretraining will be important to further improve coverage and robustness. Second, while our benchmark is broader than those used in previous studies, the 20 downstream tasks are derived from datasets covering nine surgical procedures, which still represent a relatively limited procedural scope. As a result, certain surgical specialties and rarer interventions are underrepresented. Third, the tasks considered in this study focus primarily on surgical video analysis and therefore provide limited insight into direct clinical impact, such as effects on patient outcomes or therapeutic decision-making. Future work could address these limitations by expanding data collection through collaboration with multiple institutions and surgical specialties. Beyond video analysis, an important next step is to link visual understanding models with clinically meaningful endpoints, including patient outcomes and intraoperative decision support. Integrating such models into intervention-oriented systems, including robotic-assisted surgery and emerging physical AI frameworks, may help translate advances in surgical video understanding into direct benefits for patient care.

Methods

Pretraining dataset

Developing a generalizable surgical FM requires a large-scale and diverse pretraining dataset. We curated a dataset comprising over 4,780 videos spanning more than 21 surgical procedures across 10 organ systems, including porcine procedures used for surgical training. The dataset consists of 100 in-house hepatectomy cases and 14 publicly available open-access surgical video datasets, with detailed statistics on the number of videos and frames provided in Supplementary Table 45. The in-house hepatectomy videos were collected under institutional review board approval (IRB No. SMC2024-08-027). The raw videos were processed using a standardized preprocessing pipeline consisting of frame sampling and data filtering. Video frames were uniformly sampled at 1 frame per second using FFmpeg. To ensure data quality and remove irrelevant content common in raw surgical videos, such as out-of-body views or blank frames, all sampled frames underwent a two-stage filtering process. First, a deep learning–based detector was applied to automatically remove frames in which the surgical field was not visible [74]. This automated filtering was followed by manual verification to exclude any remaining irrelevant frames, including blank frames or segments depicting non–minimally invasive procedures. The resulting pretraining dataset comprised a total of 4,316,410 frames.

Comparative benchmarking of self-supervised learning methods

To systematically compare different pretraining strategies for surgical video representation learning, we conducted a comparative study of five self-supervised learning methods spanning diverse paradigms: masked autoencoders (MAE [75]), contrastive learning (MoCoV3 [76]), masked siamese networks (MSN [77]), and two distillation approaches (SimDINO and SimDINOv2 [30]). All methods were evaluated using a consistent ViT-Base backbone (13 transformer blocks, 768-dimensional embeddings) with

a 224×224 input resolution and initialized with publicly available ImageNet-pretrained weights. Implementations were based on official code, with MAE adapted from the EndoViT [25] repository. For MAE, checkpoint selection was based on validation performance on Cholec80 (8 videos) and MultiByPass140 (10 videos), with the checkpoint achieving the lowest reconstruction error selected. These validation videos were excluded from the upstream pretraining corpus and downstream test sets, but included in the downstream training set. For the other SSL methods, default configurations were used, with checkpoint selection guided by validation performance on two downstream tasks: semantic segmentation (CholecSeg8k) and surgical action triplet recognition (CholecT50). Among all evaluated methods, SimDINOv2 achieved the strongest performance in the frozen-backbone setting across most downstream tasks (Extended Data Fig. 1a,b). Motivated by this result, we selected SimDINOv2 as the pretraining strategy and applied it to a ViT-Large architecture (24 transformer blocks, 1,024-dimensional embeddings, 224×224 input resolution), resulting in the higher-capacity model, MIS-DINOv2. All models were trained using three NVIDIA H100 GPUs (80 GB each). Batch size and other hardware-dependent parameters were adjusted to fit the available resources, while all remaining hyperparameters followed the original implementations; links to the code are provided in the Computing hardware and software setting section.

Pretraining with the multi-teacher distillation

ZEN was trained using a multi-teacher distillation strategy that integrates the unique properties of different expert models into a single model. Specifically, we distilled knowledge from two surgical-domain expert teachers into a ViT-Base student model with an input resolution of 224×224 pixels. The teachers were: (1) our MIS-DINOv2 (ViT-Large) model, serving as the vision expert for high-fidelity spatial representations, and (2) PeskaVLP, a ResNet50-based vision–language model pretrained with CLIP-style contrastive learning on approximately 26,000 surgical video–narration pairs, providing robust zero-shot recognition and cross-modal retrieval capabilities. To transfer knowledge from the teachers to the student, we adopted a feature-level distillation scheme that aligns the final-stage representations of each teacher with those of the student. For the vision expert teacher (MIS-DINOv2, ViT-Large), distillation was performed by matching both [CLS] token and the patch token embeddings with those of the student. For the vision–language expert teacher (PeskaVLP, ResNet50), we distilled knowledge by aligning the mean of the student’s patch tokens with the teacher’s final feature representation obtained through global average pooling (GAP).

To facilitate this alignment, we introduced three separate adaptors, each ensuring compatibility between the student and teacher feature spaces. Each adaptor consisted of two linear layers with a LayerNorm [78] and GELU [79] activation in between, following the adaptor design used in AM-RADIO [32]. The adaptor input dimension matched the student’s embedding dimension. The intermediate dimension was set to 2,048, and the output dimension matched that of the corresponding teacher. The distillation loss was defined at the feature level and then aggregated across feature types and teachers. For each student feature $z_{s,f}$ distilled from teacher t , the loss was formulated as:

$$L_{t,f}(x) = \alpha L^{\cos}(h_t(z_{s,f}), y_{t,f}) + \beta L^{\text{smooth-L1}}(h_t(z_{s,f}), y_{t,f}), \quad (1)$$

where f denotes the feature type ([CLS] token or patch tokens), $h_t(z_{s,f})$ is the student feature after passing through the adaptor for teacher t , and $y_{t,f}$ is the corresponding teacher feature. We set $\alpha = 0.9$ and $\beta = 0.1$, assigning greater weight to cosine similarity while retaining the contribution of the smooth-L1 term. This loss formulation follows the feature-level distillation objective used in AM-RADIO. To mitigate inconsistencies in feature statistics between teachers that could degrade performance, all teacher features were standardized to zero mean and unit variance before loss computation. These statistics were estimated on-the-fly during training using an exponential moving average, following the feature standardization strategy introduced in UNIC [33].

For the vision teacher (MIS-DINOv2, ViT-Large), the final teacher loss was obtained by averaging the [CLS] and patch token losses:

$$L_{\text{DINOv2}}(x) = \frac{1}{2} \left(L_{\text{DINOv2,CLS}}(x) + L_{\text{DINOv2,patch}}(x) \right). \quad (2)$$

For the vision–language teacher (PeskaVLP, ResNet50), the loss was defined by aligning the mean of the student’s patch tokens with the teacher’s global average pooling feature representation:

$$L_{\text{PeskaVLP}}(x) = L_{\text{PeskaVLP,pooled}}(x). \quad (3)$$

The final distillation loss was defined as the sum of the individual teacher losses, with stochastic teacher dropping applied during training. Formally,

$$L_{\text{distill}}(x) = \sum_{t \in \{\text{DINOv2, PeskaVLP}\}} m_t L_t(x), \quad (4)$$

where $m_t \in \{0, 1\}$ is a stochastic mask indicating whether teacher t contributes to the loss. To prevent the student from becoming biased toward a single teacher, the teacher with the smaller loss magnitude was dropped with probability $p_{\text{drop}} = 0.25$. This probabilistic masking ensures that both teachers provide balanced supervision during training, following the stochastic teacher dropping strategy introduced in UNIC. During training, the parameters of both teacher models were kept frozen, and only the student network and adaptors were updated. Multi-teacher distillation pretraining was conducted for 200 epochs on three NVIDIA H100 (80 GB each) GPUs, with a per-GPU batch size of 512 and an input resolution of 224×224 pixels. All experimental results reported in this study are based on the checkpoint obtained in the final pretraining epoch.

Baselines

To comprehensively benchmark the performance of ZEN, we compared it against baseline models, including publicly available surgical FMs with vision-only architectures (GSViT [23], EndoFM [24], EndoViT [25], and SurgeNet [27]) and a vision–language model (PeskaVLP [26]). We additionally included an ImageNet-pretrained ViT-Base model as a general-purpose visual baseline. All models were evaluated using a 224×224 input resolution across all downstream tasks. Detailed model configurations and training details for all evaluated models are provided in Supplementary Table 46.

Statistical analysis

For all supervised downstream tasks, except visual question answering (VQA), experiments were repeated over five independent runs using identical training protocols and hyperparameter settings. The test set was fixed, whereas the training and validation sets were independently sampled for each run. Performance is reported as the mean across runs. Variability was quantified using the standard deviation and the standard error, computed as the standard deviation divided by the square root of the number of runs. The 95% confidence interval was computed as 1.96 times the standard error. For VQA tasks, no separate validation set was used. Instead, experiments were conducted over five independent runs with independently sampled train–test splits. Performance metrics were averaged across runs using the same statistical reporting procedure described above. Statistical significance for task-specific comparisons across repeated runs was assessed using two-sided paired t-tests comparing ZEN with each corresponding baseline model. To evaluate overall performance differences aggregated across tasks, we performed two-sided Wilcoxon signed-rank tests on task-level average metrics (Fig.2c,e).

For cross-modal retrieval and zero-shot phase recognition, which do not involve task-specific training, statistical analysis was performed at the video level. We computed the mean and standard deviation of performance across videos, calculated the standard error by dividing the standard deviation by the square root of the number of videos, and computed the 95% confidence interval as 1.96 times the standard error.

Downstream evaluation details

In this section, we describe the experimental settings for evaluating model performance across downstream tasks. Detailed descriptions of the training protocols and evaluation metrics for each task are provided in the corresponding subsections below.

Surgical phase recognition

We followed the two-stage evaluation protocol introduced in TeCNO [11], consisting of frame-level feature extraction followed by temporal aggregation using a multi-stage temporal convolutional network [80]. Models were evaluated under three settings: (1) frozen-backbone: The pretrained encoder was kept fixed, and frame-level features were directly extracted from videos. These features were then used to train the temporal aggregation network; (2) fine-tuning: The pretrained encoder was first fine-tuned alongside a linear classifier using frame-wise supervision. After fine-tuning, the encoder was used to extract frame-level features, which were then used to train the temporal aggregation network for temporal modeling; (3)

Few-shot learning (1–5 videos; limited training data): Similar to the frozen setting, the encoder remained fixed. The temporal aggregation network was trained using features extracted from only 1 to 5 training videos to evaluate performance under limited data conditions. For fine-tuning, the encoder and linear classifier were trained for 15 epochs using cross-entropy loss, the AdamW [81] optimizer (learning rate: 1×10^{-5} , weight decay: 0.01), and a batch size of 128, with data augmentations including flipping, shift-scale-rotate, HSV adjustments, and Gaussian noise. The temporal aggregation network was trained for 100 epochs using the Adam [82] optimizer (initial learning rate: 7×10^{-4} , weight decay: 1×10^{-5}), with a step scheduler that halved the learning rate every 30 epochs. Performance was evaluated using video-level F1 score and accuracy, as well as phase-level recall, precision, and Jaccard index [83].

Surgical action triplet recognition

For this task, we appended a linear classifier to the pretrained encoder and followed the Self-Distillation [37], formulating the problem as multi-label classification. The model was trained to jointly predict the composite triplet class (instrument–verb–target, IVT) as well as the individual instrument (I), verb (V), and target (T) components. We evaluated performance under two settings: (1) frozen-backbone, where the encoder was fixed and only the classifier was trained; and (2) fine-tuning, where both the encoder and classifier were trained. All experiments used the AdamW optimizer (weight decay: 0.01), binary cross-entropy loss, and a cosine annealing scheduler with a 3-epoch warm-up. Input images were resized to 224×224 pixels and augmented with horizontal flipping, shift-scale-rotate, hue-saturation-value adjustments, and Gaussian noise. Training configurations varied by dataset and setting: On CholecT50, models were trained for 15 epochs (frozen) and 20 epochs (fine-tuning). The frozen setting used a base learning rate of 2×10^{-4} and minimum learning rate of 1×10^{-5} , while the fine-tuning setting used 1×10^{-4} and 1×10^{-6} . On LLS48, models were trained for 20 epochs (frozen) and 30 epochs (fine-tuning), with base and minimum learning rates of $5 \times 10^{-4}/1 \times 10^{-5}$ (frozen) and $2 \times 10^{-4}/1 \times 10^{-6}$ (fine-tuning), respectively. Performance was evaluated using mAP, computed for individual components (I, V, T), component pairs (IV, IT), and the full triplet (IVT).

Skill assessment

Skill assessment was performed based on Strasberg’s criteria for achieving the critical view of safety (CVS) during laparoscopic cholecystectomy [45]. Following COLENET [46], we appended a linear classifier to the pretrained encoder and trained the model to predict whether each CVS criterion was satisfied in a multi-label setting. We evaluated performance under two settings: (1) a frozen-backbone setting, in which the encoder was kept fixed and only the classifier was trained; and (2) a fine-tuning setting, in which both the encoder and classifier were jointly optimized. All models were trained for 10 epochs using the AdamW optimizer (learning rate: 1×10^{-5} , weight decay: 0.01) with binary cross-entropy loss. Input images were resized to 224×224 pixels and augmented using horizontal flipping, shift-scale-rotate transformations, hue-saturation-value adjustments, and Gaussian noise. Performance was evaluated using mAP and macro F1 score.

Semantic segmentation

We employed the UperNet [84] architecture from the mmSegmentation toolbox to perform semantic segmentation of surgical instruments and anatomy. Models were evaluated under three settings: (1) frozen-backbone, where only UperNet was trained to assess the quality of the pretrained features; (2) fine-tuning, where all parameters, including the encoder, were updated end-to-end; (3) Few-shot learning (1–5 videos; limited training data), which followed the same training strategy as the frozen setting but used a small training set. We applied a strict video-wise split to ensure that training, validation, and test sets did not share any overlapping frames from the same video. All models were trained for 20 epochs using the AdamW optimizer (weight decay: 0.01), a batch size of 64, and a cosine annealing learning rate scheduler with a 1-epoch linear warm-up. Input images were resized to 224×224 pixels and augmented with horizontal and vertical flipping. For the fine-tuning setting, the base and minimum learning rates were set to 5×10^{-4} and 1×10^{-6} , respectively. For the frozen and few-shot settings, they were set to 5×10^{-3} and 1×10^{-5} . Performance was evaluated using the Dice score and 95% Hausdorff distance.

Instance segmentation

For instance segmentation of surgical instruments, we used the Mask R-CNN [85] architecture from the Torchvision library. To isolate the effect of different pretrained backbones, all other components were kept identical across experiments, including the feature pyramid network [86], box head, and mask head.

Models were evaluated under two settings: (1) frozen-backbone, where only the non-backbone components (FPN and heads) were trained to assess the quality of the pretrained features; (2) Full fine-tuning, where all network parameters, including the encoder backbone, were updated. All models were trained for 100 epochs using the AdamW optimizer, a batch size of 16, and a cosine annealing learning rate scheduler with a 5-epoch linear warm-up. Input images were resized to 224×224 pixels and augmented with horizontal and vertical flipping. In the frozen setting, the base and minimum learning rates were set to 5×10^{-3} and 1×10^{-5} , respectively. In the fine-tuning setting, they were set to 3×10^{-4} and 1×10^{-6} . Standard Mask R-CNN loss functions were used. Performance was evaluated using mAP, computed by averaging precision across intersection-over-union thresholds ranging from 0.5 to 0.95, for both bounding box detection and segmentation masks. All models were evaluated on the GraSP dataset using the same train, validation, and test splits as those employed for semantic segmentation.

Depth estimation

We adopted the supervised evaluation protocol from Surgical-DINO [87] for monocular depth estimation. This protocol uses a lightweight decoder composed of a single linear layer, which takes as input the concatenated features from four intermediate stages of the encoder. For ViT backbones, we concatenated the [CLS] token with the patch tokens; for other architectures, intermediate feature maps were used directly. Models were evaluated under two settings: (1) frozen-backbone, where only the decoder was trained; (2) fine-tuning, where both the encoder and decoder were trained. During evaluation, predicted depth maps were rescaled using a median scaling method. All models were trained using scale-invariant log loss [88], the AdamW optimizer (learning rate: 1×10^{-5} , weight decay: 1×10^{-4}), and a batch size of 8. Input images were resized to 224×224 pixels, and data augmentation included color jittering and random horizontal flipping. Following prior works [53, 87], performance was evaluated using five standard depth estimation metrics: absolute relative error (Abs-Rel), square relative error (Sq-Rel), root mean square error (RMSE), log-scale RMSE (RMSE log), and accuracy under threshold (δ).

Visual question answering (VQA)

We adapted the nanoVLM-450M [89] framework for visual question answering by replacing its default vision encoder with each pretrained models. Input images were resized to 224×224 pixels before being fed into the vision encoder. We evaluated two training settings: a frozen-backbone setting and a fine-tuning setting. In the frozen-backbone setting, the vision encoder was kept fixed, and only two components were updated during training: (1) a linear projection layer that mapped the final spatial features from the vision encoder to the language model input space, and (2) Low-rank adaptation [90] (LORA) modules applied to the query and value projections of the language model. The LORA modules were configured with rank 8, alpha 8, and a dropout rate of 0.1. Models were trained for 5 epochs using the AdamW optimizer with a batch size of 16 and a cosine learning rate schedule with a linear warm-up over the first 3% of training steps. Learning rates were set to 1×10^{-3} for the projection layer and 1×10^{-4} for the LORA modules. In the fine-tuning setting, the vision encoder was jointly optimized together with the projection layer and LORA modules, enabling end-to-end adaptation of the visual representations. In this setting, the vision encoder was trained with a learning rate of 1×10^{-5} , while the projection layer and LORA modules used the same learning rates as in the frozen-backbone setting. Models were trained for 3 epochs using the same optimization strategy. For both settings, evaluation was performed on the test set using the checkpoint from the final training epoch. We evaluated both closed-ended and open-ended VQA tasks. Closed-ended VQA required selecting an answer from a predefined set of labels and was evaluated using exact match-based metrics, including macro F1 score, balanced accuracy, and recall. Open-ended VQA required generating free-form natural language responses and was evaluated using text-generation metrics, including BLEU-1–BLEU-4, ROUGE-L, and METEOR.

Cross-modal retrieval

We evaluated cross-modal retrieval performance under a zero-shot inference setting, without any additional task-specific training. This evaluation was restricted to vision–language aligned models (ZEN and PeskaVLP), as image-only FMs do not provide a shared image–text embedding space. All experiments were conducted on the LLS48 dataset, which is organized at the clip level, with each clip consisting of five consecutive frames. During inference, all frames were resized to 224×224 pixels. Following the PeskaVLP protocol, visual features were first extracted at the frame level and then aggregated into a clip-level representation via average pooling. Text embeddings were obtained using the ClinicalBERT [91] language encoder of PeskaVLP. Cross-modal similarity was computed as the dot product between image and text

embeddings. For PeskaVLP, image embeddings were obtained directly from the visual encoder. For ZEN, visual features were passed through the adaptor introduced during distillation from the PeskaVLP teacher to ensure alignment with the text embedding space. We evaluated two retrieval tasks: (1) image-to-text retrieval, which retrieves the correct textual description given an image clip; and (2) text-to-image retrieval, which retrieves the corresponding image clip given a textual prompt. In both tasks, the textual descriptions were the open-ended answers to the question “Describe the current surgical scene” from the LLS48-VQA dataset. Performance was measured using recall@ k ($k = 1, 5, 10$), defined as the proportion of queries for which the correct match appears among the top- k retrieved results. We additionally report mean recall, computed as the average of recall@1, recall@5, and recall@10.

Zero-shot phase recognition

We evaluated zero-shot retrieval performance following the protocol and text prompts provided in the PeskaVLP. This evaluation was restricted to vision–language aligned models (ZEN and PeskaVLP), as image-only FMs do not provide a shared image–text embedding space. Experiments were conducted on the hold-out test sets of the Cholec80, MultiByPass140, and AutoLaparo datasets, using the same splits described in the surgical phase recognition experiments. During inference, all images were resized to 224×224 pixels. Text embeddings corresponding to each surgical phase were generated using the language encoder provided in the PeskaVLP framework. Zero-shot phase prediction was performed by computing the dot product similarity between image embeddings and all phase text embeddings, and assigning the phase with the highest similarity score. For PeskaVLP, image embeddings were extracted directly from the visual encoder. For ZEN, visual features were passed through the adaptor module introduced during distillation from the PeskaVLP teacher to ensure alignment with the text embedding space. Performance was evaluated using video-level macro F1 score and accuracy.

Downstream datasets

This section details the datasets used for downstream tasks, including the surgical procedures and dataset statistics (number of videos and frames), as well as the dataset splits for each training protocol. An overview of the datasets and tasks is provided in Supplementary Table 47.

Cholec80 (7 classes)

The Cholec80 [10] dataset contains 80 laparoscopic cholecystectomy videos, totaling 184,578 frames. Each frame is labeled with one of 7 surgical phases. To prevent data leakage, 32 videos were held out as a test set and excluded from all pretraining stages. The remaining 48 videos were used for training and validation. For frozen and fine-tuning experiments, we split the 48 videos into 40 for training and 8 for validation (5:1 ratio). In the few-shot setting, the test set (32 videos) and validation set (8 videos) were fixed, while k videos (1 to 5) were sampled from the 40 training videos for each of five runs.

MultiByPass140 (12 classes)

The MultiByPass140 [41] dataset contains 140 videos of laparoscopic Roux-en-Y gastric bypass surgeries, totaling 770,617 frames. Each frame is labeled with one of 12 surgical phases. We held out 40 videos as a test set, strictly excluding them from all pretraining stages. The remaining 100 videos were used for training and validation. For frozen and fine-tuning experiments, the 100 videos were split into 80 for training and 20 for validation (4:1 ratio). In the few-shot setting, the test set (40 videos) and validation set (20 videos) were fixed, while k videos (1 to 5) were sampled from the 80 training videos across five runs.

AutoLaparo (7 classes)

The AutoLaparo [42] contains 21 videos of laparoscopic hysterectomy, with a total of 83,243 frames annotated across 7 surgical phases. It was not included in the pretraining corpus and was used as an external test set. Among the 21 videos, 6 were held out as a test set, and the remaining 15 were used for training and validation. For frozen and fine-tuning experiments, the 15 videos were split into 10 for training and 5 for validation (2:1 ratio). In the few-shot setting, the test set (6 videos) and validation set (5 videos) were fixed, while k videos (1 to 5) were sampled from the 10 training videos over five runs.

CholecT50 (100 classes)

This CholecT50 [43] dataset was developed for surgical action triplet recognition and includes 50 videos, totaling 100,863 frames. Of these, 45 videos are sourced from Cholec80, with 5 additional cases included

to complete the set. CholecT50 features 100 unique triplet classes, derived from 6 instruments, 10 verbs, and 15 targets. To avoid data leakage, the 40 videos overlapping with the pretraining data were used for training and validation, while the 10 non-overlapping videos served as a hold-out test set. For evaluation, the training split consisted of 35 training and 5 validation videos (7:1 ratio).

LLS48 (195 classes)

The LLS48 [44] dataset is an in-house collection of 48 laparoscopic hepatectomy videos, specifically laparoscopic left lateral sectionectomy procedures, acquired at Samsung Medical Center, totaling 9,560 frames. The videos were segmented into 1,912 five-second clips, sampled every 90 seconds across full procedures. All annotations were performed by experienced clinicians, following SAGES consensus guidelines [92]. Each clip was labeled with 17 instruments, 16 verbs, and 38 targets, resulting in 195 unique triplet classes. This dataset was excluded from the pretraining corpus. We reserved 8 videos as a hold-out test set and used the remaining 40 for training and validation. For evaluation, the 40 videos were divided into 35 training and 5 validation videos (7:1 ratio).

Cholec80-CVS (3 classes)

The Cholec80-CVS [46] dataset comprises 62,760 frames annotated with the critical view of safety (CVS) criteria for laparoscopic cholecystectomy. Each frame is labeled with three CVS criteria, scored on a scale from 0 to 2. Following the COLENET, we binarized these annotations by converting the scores into binary labels indicating whether each criterion was satisfied or not. The Cholec80-CVS dataset is derived from the same videos as the Cholec80 dataset. Accordingly, the dataset was split using the same video-level partitions as those used for surgical phase recognition on Cholec80, ensuring identical training, validation, and test splits.

CholecSeg8k (7 classes)

This CholecSeg8k [54] dataset consists of 8,080 frames with pixel-level annotations for surgical instruments and anatomical structures in laparoscopic cholecystectomy. The dataset was constructed from 17 video clips, each corresponding to a different patient in the Cholec80 dataset. Following prior work, the original 13 classes were merged into 7 classes: abdominal wall, liver, gastrointestinal tract, fat, gallbladder, miscellaneous, and instrument. To prevent data leakage, we used 4 clips that do not overlap with our pretraining data as a hold-out test set. Due to this strict split, the ‘miscellaneous’ class was absent in the test set, though present in training. The remaining 13 clips, which include overlaps with the pretraining corpus, were used for training and validation. For frozen and fine-tuning settings, they were split into 11 for training and 2 for validation (6:1 ratio). In the few-shot setting, the 4 video test set and 2 video validation set were fixed, while k videos (1–5) were sampled from the 11 training clips across five runs.

DSAD (7 classes)

The DSAD [55] dataset contains videos of robot-assisted anterior rectal resections and rectal extirpations with pixel-level semantic segmentation masks for surgical anatomy. It includes both binary and multi-class annotations; we used the multi-class subset to better reflect real-world surgical scenes. This subset consists of 23 videos with 1,430 annotated frames across 8 classes: abdominal wall, colon, liver, pancreas, small intestine, spleen, and stomach. As the dataset was not part of the pretraining corpus, it was used as an external test set. We used 5 videos as a hold-out test set, and the remaining 18 videos were used for training and validation. For frozen and fine-tuning settings, these 18 videos were divided into 14 training and 4 validation videos (7:2 ratio). In the few-shot setting, the 5 video test set and 4 video validation set were fixed, while k videos (1–5) were sampled from the 14 training videos over five runs.

GraSP (7 classes)

The GraSP [56] dataset contains 3,449 annotated frames from 13 videos of robotic-assisted radical prostatectomy. It provides labels for 7 instrument classes: bipolar forceps, prograsp forceps, large needle driver, monopolar curved scissors, suction instrument, clip applier, and laparoscopic instrument (which includes laparoscopic retraction forceps, laparoscopic suture scissors, and laparoscopic needle holder). The dataset supports both semantic and instance segmentation tasks and was used for external evaluation, as it was not included in the pretraining data. We used 3 videos as a fixed hold-out test set and the remaining 10 videos for training and validation, applying the same split across both segmentation tasks. For frozen and fine-tuning settings, these were divided into 8 training and 2 validation videos (4:1 ratio). In the few-shot

setting, the 3 video test set and 2 video validation set were fixed, while k videos (1–5) were sampled from the 8 training videos over five runs.

SCARED

The SCARED [57] dataset contains 35 endoscopic video clips (22,950 frames) collected from porcine cadaver surgeries. The SCARED dataset was not included in our pretraining corpus and was used as an external test set. We used 7 clips as a hold-out test set, with the remaining 28 for training and validation. For five runs, we created five distinct random splits of the 28 clips at approximately an 11:3 ratio. The same split was applied to both the frozen and fine-tuning settings.

Hamlyn

The Hamlyn [58] dataset consists of 21 video clips (91,866 frames) capturing in vivo scenes from laparoscopic and endoscopic surgeries. We used 6 video clips as a fixed hold-out test set, and the remaining 15 were used for training and validation. For five independent runs, we randomly partitioned these 15 clips into 12 for training and 3 for validation (4:1 ratio). The same split was applied to both the frozen and fine-tuning settings.

PitVQA

The PitVQA [63] dataset contains 25 videos of endoscopic pituitary surgeries, comprising 109,173 frames and 884,242 question–answer pairs. It includes only closed-ended questions, each requiring a selection from predefined answer classes. Annotations span 59 distinct classes, including 4 surgical phases, 15 procedural steps, 18 instruments, 3 instrument presence categories, 5 instrument positions, and 14 types of operation notes. We evaluated closed-ended VQA performance across all 59 classes. The 25 videos were split into 20 training and 5 test videos, and experiments were repeated over five runs.

LLS48-VQA

The LLS48-VQA dataset comprises 22 question–answer pairs per video clip and was derived from the in-house LLS48 action triplet recognition dataset. It includes two types of questions: closed-ended and open-ended. Closed-ended questions cover tool count (5 classes), instrument classification (18), action recognition (16), target identification (38), triplet (IVT) classification (196), anatomical structure recognition (115), and surgical phase classification (5), resulting in a total of 393 classes. Open-ended questions consist of free-form queries related to scene description, current task objectives, and subsequent surgical actions. Answer generation protocols differed by question type. Closed-ended answers were manually constructed using consistent sentence templates based on action triplet recognition annotations. For open-ended VQA, answers were generated using structured prompting with GPT-4.1 [93] under predefined guidelines. An experienced surgeon first provided clip-level descriptions detailing the visible anatomy, ongoing surgical actions, and expected subsequent steps, informed by the underlying action triplet annotations. Based on these expert descriptions, GPT-4.1 was prompted to generate responses to the questions “Describe the current surgical scene”, “What is the purpose of the current actions?”, and “What should be done next?”. Closed-ended VQA performance was evaluated across all 393 classes, while open-ended VQA was evaluated on the three open-ended question types. The 48 videos were split into 40 for training and 8 for testing (5:1 ratio) across five runs.

Computing hardware and software

Video-to-frame sampling during data preprocessing was performed using FFmpeg (v6.1.1). Self-supervised pretraining was conducted on a single node equipped with 3×80 GB NVIDIA H100 GPUs, using multi-GPU training implemented via PyTorch DistributedDataParallel (DDP). Pretraining experiments were implemented in Python (v3.9.13) with PyTorch (v2.2.1, CUDA 11.8) and Torchvision (v0.17.1). Our foundation model was developed using the UNIC codebase, which is publicly available at <https://github.com/naver/unic>. Self-supervised learning methods were trained using their official implementations. Only the batch size was adjusted to accommodate the available hardware. Specifically, we used MAE (EndoViT; <https://github.com/DominikBatic/EndoViT>), MoCoV3 (<https://github.com/facebookresearch/moco-v3>), MSN (<https://github.com/facebookresearch/msn>), and SimDINO/SimDINOv2 (<https://github.com/RobinWu218/SimDINO>). All downstream task evaluations were conducted on 4×24 GB NVIDIA RTX4090 GPUs. These experiments were implemented in Python (v3.9.19) using PyTorch (v2.2.2, CUDA 11.8) and Torchvision (v0.17.2). Task-specific implementations were adapted from publicly available repositories: surgical phase recognition

(<https://github.com/tobiascz/TeCNO>), action triplet recognition (<https://github.com/IMSY-DKFZ/self-distilled-swin>), action triplet recognition metric (<https://github.com/CAMMA-public/ivtmetrics>), skill assessment (<https://github.com/ManuelRios18/CHOLEC80-CVS-PUBLIC>), semantic segmentation (<https://github.com/open-mmlab/mmsegmentation>), instance segmentation (<https://github.com/pytorch/vision/tree/main/torchvision/models/detection>), depth estimation (<https://github.com/BeileiCui/SurgicalDINO>), and visual question answering (<https://github.com/huggingface/nanoVLM>). Implementations of other pretrained baseline models followed the official configurations provided in their respective repositories, including EndoFM (<https://github.com/med-air/Endo-FM>), GSViT (<https://github.com/SamuelSchmidgall/GSViT>), EndoViT (<https://github.com/DominikBatic/EndoViT>), PeskaVLP (<https://github.com/CAMMA-public/SurgVLP>), and SurgeNet (<https://github.com/TimJaspers0801/SurgeNet>). The ImageNet-pretrained ViT-Base model was obtained from Hugging Face (https://huggingface.co/timm/vit_base_patch16_224.augreg_in1k). Statistical analyses were performed using SciPy (v1.15.3).

Data availability. Most of datasets used in this study are publicly available: Cholec80 (<https://camma.unistra.fr/datasets/>), CholecT50 (<https://github.com/CAMMA-public/cholect50>), CholecSeg8k (<https://www.kaggle.com/datasets/newslab/cholecseg8k>), Cholec80-CVS (<https://github.com/ManuelRios18/CHOLEC80-CVS-PUBLIC>), hSBD-instrument (<https://hsdb-instrument.github.io/>), Sisvse (<https://sisvse.github.io/>), HeiChole (<https://www.synapse.org/Synapse:syn18824884/wiki/591922>), Endoscapes (<https://github.com/CAMMA-public/Endoscapes>), ART-Net (<https://github.com/kamruleee51/ART-Net>), ESAD (<https://saras-esad.grand-challenge.org/>), AutoLaparo (<https://autolaparo.github.io/>), MultiByPass140 (<https://github.com/CAMMA-public/MultiBypass140>), LapGyn4 (<https://ftp.itec.aau.at/datasets/LapGyn4>), SurgicalAction160 (<https://ftp.itec.aau.at/datasets/SurgicalActions160>), GLENDa (<https://ftp.itec.aau.at/datasets/GLENDa>), HeiCo (<https://www.synapse.org/Synapse:syn21903917/wiki/601992>), SurgToolLoc2022 (<https://surgtoolloc23.grand-challenge.org/surgtoolloc-2022-resources/>), DSAD (<https://www.kaggle.com/datasets/anindyamajumder/the-dresden-surgical-anatomy-dataset>), GraSP (<https://github.com/BCV-Uniandes/GraSP>), SCARED (<https://endovissub2019-scared.grand-challenge.org/>), Hamlyn (<https://hamlyn.doc.ic.ac.uk/vision/>), PitVQA (<https://github.com/mobarakol/PitVQA>) and SurgicalYoutube (<https://github.com/TimJaspers0801/SurgeNet>). Links to publicly available datasets are also provided in Supplementary Table 48. Access to in-house datasets is restricted due to patient privacy and data protection regulations. Access requests may be directed to the corresponding author and will be evaluated subject to institutional approval and applicable regulations.

Code availability. The code and pretrained weights for ZEN will be made publicly available upon acceptance of this manuscript on GitHub.

Acknowledgements. This work was supported by a grant of the Korean ARPA-H Project through the Korea Health Industry Development Institute (KHIDI), funded by the Ministry of Health & Welfare, Republic of Korea (RS-2025-25424639); by the National Research Foundation of Korea (NRF) grant funded by the Korean government (Ministry of Science and ICT) (RS-2024-00392495); by the Future Medicine 2030 Project of Samsung Medical Center (SMX1230771); and by a grant from Samsung Medical Center (SMO1250271).

Author contributions. K.P., N.O. and K.H.J. conceived the study and designed the experiments. K.P., S.P., J.S. and J.Y.K. collected the data for self-supervised learning. K.P. developed the models and conducted downstream task evaluation. K.P., Y.J. and S.L. conducted result summarization and visualization. K.P., S.P. and J.S. organized the datasets for VQA tasks. K.P., Y.J., J.S. and S.A. carried out analysis of surgical action triplet recognition and semantic segmentation. J.R., J.K., G.S.C. and N.O. provided in-house surgical videos and domain expertise. N.O. and K.H.J. supervised the study. All authors contributed to the drafting and revising of the paper.

Competing interests. The authors declare no competing interests.

References

- [1] Surya SAY Biere, Mark I van Berge Henegouwen, Kirsten W Maas, Luigi Bonavina, Camiel Rosman, Josep Roig Garcia, Suzanne S Gisbertz, Jean HG Klinkenbijl, Markus W Hollmann, Elly SM de Lange, et al. Minimally invasive versus open oesophagectomy for patients with oesophageal cancer: a multicentre, open-label, randomised controlled trial. *The Lancet*, 379(9829):1887–1892, 2012.

- [2] Martijn HGM van der Pas, Eva Haglind, Miguel A Cuesta, Alois Fürst, Antonio M Lacy, Wim CJ Hop, and Hendrik Jaap Bonjer. Laparoscopic versus open surgery for rectal cancer (color ii): short-term outcomes of a randomised, phase 3 trial. *The lancet oncology*, 14(3):210–218, 2013.
- [3] H Jaap Bonjer, Charlotte L Deijen, Gabor A Abis, Miguel A Cuesta, Martijn HGM Van Der Pas, Elly SM De Lange-De Klerk, Antonio M Lacy, Willem A Bemelman, John Andersson, Eva Angenete, et al. A randomized trial of laparoscopic versus open surgery for rectal cancer. *New England Journal of Medicine*, 372(14):1324–1332, 2015.
- [4] Tina Vajsbauer, Holger Schultheis, and Nader K Francis. Spatial cognition in minimally invasive surgery: a systematic review. *BMC surgery*, 18(1):94, 2018.
- [5] Robin Julia Trute, Afshin Aljani, and Mustafa Suphi Erden. Visual cues of soft-tissue behaviour in minimal-invasive and robotic surgery. *Journal of Robotic Surgery*, 18(1):401, 2024.
- [6] Keryn Pauley, Rhona Flin, Steven Yule, and George Youngson. Surgeons’ intraoperative decision making and risk management. *The American journal of surgery*, 202(4):375–381, 2011.
- [7] Selwyn O Rogers Jr, Atul A Gawande, Mary Kwaan, Ann Louise Puopolo, Catherine Yoon, Troyen A Brennan, and David M Studdert. Analysis of surgical errors in closed malpractice claims at 4 liability insurers. *Surgery*, 140(1):25–33, 2006.
- [8] D Kiyasseh, R Ma, TF Haque, BJ Miles, C Wagner, DA Donoho, A Anandkumar, and AJ Hung. A vision transformer for decoding surgeon activity from surgical videos. *nat biomed eng*, 2023.
- [9] Lena Maier-Hein, Matthias Eisenmann, Duygu Sarikaya, Keno März, Toby Collins, Anand Malpani, Johannes Fallert, Hubertus Feussner, Stamatia Giannarou, Pietro Mascagni, et al. Surgical data science—from concepts toward clinical translation. *Medical image analysis*, 76:102306, 2022.
- [10] Andru P Twinanda, Sherif Shehata, Didier Mutter, Jacques Marescaux, Michel De Mathelin, and Nicolas Padoy. Endonet: a deep architecture for recognition tasks on laparoscopic videos. *IEEE transactions on medical imaging*, 36(1):86–97, 2016.
- [11] Tobias Czempiel, Magdalini Paschali, Matthias Keicher, Walter Simson, Hubertus Feussner, Seong Tae Kim, and Nassir Navab. Tecno: Surgical phase recognition with multi-stage temporal convolutional networks. In *International conference on medical image computing and computer-assisted intervention*, pages 343–352. Springer, 2020.
- [12] Yueming Jin, Yonghao Long, Cheng Chen, Zixu Zhao, Qi Dou, and Pheng-Ann Heng. Temporal memory relation network for workflow recognition from surgical video. *IEEE Transactions on Medical Imaging*, 40(7):1911–1923, 2021.
- [13] Xinpeng Ding and Xiaomeng Li. Exploring segment-level semantics for online phase recognition from surgical videos. *IEEE Transactions on Medical Imaging*, 41(11):3309–3319, 2022.
- [14] Yang Liu, Maxence Boels, Luis C Garcia-Peraza-Herrera, Tom Vercauteren, Prokar Dasgupta, Alejandro Granados, and Sebastien Ourselin. Lovit: Long video transformer for surgical phase recognition. *Medical Image Analysis*, 99:103366, 2025.
- [15] Matthias Carstens, Shubha Vasisht, Zheyuan Zhang, Iulia Barbur, Annika Reinke, Lena Maier-Hein, Daniel A Hashimoto, and Fiona R Kolbinger. Artificial intelligence for surgical scene understanding: a systematic review and reporting quality meta-analysis. *npj Digital Medicine*, 2025.
- [16] Xinpeng Ding, Xinjian Yan, Zixun Wang, Wei Zhao, Jian Zhuang, Xiaowei Xu, and Xiaomeng Li. Less is more: Surgical phase recognition from timestamp supervision. *IEEE Transactions on Medical Imaging*, 42(6):1897–1910, 2023.
- [17] Muhammad Awais, Muzammal Naseer, Salman Khan, Rao Muhammad Anwer, Hisham Cholakkal, Mubarak Shah, Ming-Hsuan Yang, and Fahad Shahbaz Khan. Foundation models defining a new era in vision: a survey and outlook. *IEEE Transactions on Pattern Analysis and Machine Intelligence*,

2025.

- [18] Yukun Zhou, Mark A Chia, Siegfried K Wagner, Murat S Ayhan, Dominic J Williamson, Robbert R Struyven, Timing Liu, Moucheng Xu, Mateo G Lozano, Peter Woodward-Court, et al. A foundation model for generalizable disease detection from retinal images. *Nature*, 622(7981):156–163, 2023.
- [19] DongAo Ma, Jiaxuan Pang, Michael B Gotway, and Jianming Liang. A fully open ai foundation model applied to chest radiography. *Nature*, pages 1–11, 2025.
- [20] Richard J Chen, Tong Ding, Ming Y Lu, Drew FK Williamson, Guillaume Jaume, Andrew H Song, Bowen Chen, Andrew Zhang, Daniel Shao, Muhammad Shaban, et al. Towards a general-purpose foundation model for computational pathology. *Nature medicine*, 30(3):850–862, 2024.
- [21] Jiabo Ma, Zhengrui Guo, Fengtao Zhou, Yihui Wang, Yingxue Xu, Jinbang Li, Fang Yan, Yu Cai, Zhengjie Zhu, Cheng Jin, et al. A generalizable pathology foundation model using a unified knowledge distillation pretraining framework. *Nature Biomedical Engineering*, pages 1–20, 2025.
- [22] Siyuan Yan, Zhen Yu, Clare Primiero, Cristina Vico-Alonso, Zhonghua Wang, Litao Yang, Philipp Tschandl, Ming Hu, Lie Ju, Gin Tan, et al. A multimodal vision foundation model for clinical dermatology. *Nature Medicine*, pages 1–12, 2025.
- [23] Samuel Schmidgall, Ji Woong Kim, Jeffrey Jopling, and Axel Krieger. General surgery vision transformer: A video pre-trained foundation model for general surgery. *arXiv preprint arXiv:2403.05949*, 2024.
- [24] Zhao Wang, Chang Liu, Shaoting Zhang, and Qi Dou. Foundation model for endoscopy video analysis via large-scale self-supervised pre-train. In *International Conference on Medical Image Computing and Computer-Assisted Intervention*, pages 101–111. Springer, 2023.
- [25] Dominik Batić, Felix Holm, Ege Özsoy, Tobias Czempiel, and Nassir Navab. Endovit: pretraining vision transformers on a large collection of endoscopic images. *International Journal of Computer Assisted Radiology and Surgery*, 19(6):1085–1091, 2024.
- [26] Kun Yuan, Nassir Navab, Nicolas Padoy, et al. Procedure-aware surgical video-language pretraining with hierarchical knowledge augmentation. *Advances in Neural Information Processing Systems*, 37: 122952–122983, 2024.
- [27] Tim J.M. Jaspers, Ronald L.P.D. de Jong, Yiping Li, Carolus H.J. Kusters, Franciscus H.A. Bakker, Romy C. van Jaarsveld, Gino M. Kuiper, Richard van Hillegersberg, Jelle P. Ruurda, Willem M. Brinkman, Josien P.W. Pluim, Peter H.N. de With, Marcel Breeuwer, Yasmina Al Khalil, and Fons van der Sommen. Scaling up self-supervised learning for improved surgical foundation models. *Medical Image Analysis*, 108:103873, 2026. ISSN 1361-8415. doi: <https://doi.org/10.1016/j.media.2025.103873>.
- [28] Shu Yang, Fengtao Zhou, Leon Mayer, Fuxiang Huang, Yiliang Chen, Yihui Wang, Sunan He, Yuxiang Nie, Xi Wang, Ömer Sümer, et al. Large-scale self-supervised video foundation model for intelligent surgery. *arXiv preprint arXiv:2506.02692*, 2025.
- [29] Alexey Dosovitskiy. An image is worth 16x16 words: Transformers for image recognition at scale. *arXiv preprint arXiv:2010.11929*, 2020.
- [30] Ziyang Wu, Jingyuan Zhang, Druv Pai, XuDong Wang, Chandan Singh, Jianwei Yang, Jianfeng Gao, and Yi Ma. Simplifying dino via coding rate regularization. *arXiv preprint arXiv:2502.10385*, 2025.
- [31] Alec Radford, Jong Wook Kim, Chris Hallacy, Aditya Ramesh, Gabriel Goh, Sandhini Agarwal, Girish Sastry, Amanda Askell, Pamela Mishkin, Jack Clark, et al. Learning transferable visual models from natural language supervision. In *International conference on machine learning*, pages 8748–8763. PMLR, 2021.

[32] Mike Ranzinger, Greg Heinrich, Jan Kautz, and Pavlo Molchanov. Am-radio: Agglomerative vision foundation model reduce all domains into one. In *Proceedings of the IEEE/CVF conference on computer vision and pattern recognition*, pages 12490–12500, 2024.

[33] Mert Bülent Sarıyıldız, Philippe Weinzaepfel, Thomas Lucas, Diane Larlus, and Yannis Kalantidis. Unic: Universal classification models via multi-teacher distillation. In *European Conference on Computer Vision*, pages 353–371. Springer, 2024.

[34] Greg Heinrich, Mike Ranzinger, Hongxu Yin, Yao Lu, Jan Kautz, Andrew Tao, Bryan Catanzaro, and Pavlo Molchanov. Radiov2. 5: Improved baselines for agglomerative vision foundation models. In *Proceedings of the Computer Vision and Pattern Recognition Conference*, pages 22487–22497, 2025.

[35] Mert Bülent Sarıyıldız, Philippe Weinzaepfel, Thomas Lucas, Pau de Jorge, Diane Larlus, and Yannis Kalantidis. Dune: Distilling a universal encoder from heterogeneous 2d and 3d teachers. In *Proceedings of the Computer Vision and Pattern Recognition Conference*, pages 30084–30094, 2025.

[36] Saurav Sharma, Chinedu Innocent Nwoye, Didier Mutter, and Nicolas Padoy. Rendezvous in time: an attention-based temporal fusion approach for surgical triplet recognition. *International Journal of Computer Assisted Radiology and Surgery*, 18(6):1053–1059, 2023.

[37] Amine Yamlahi, Thuy Nuong Tran, Patrick Godau, Melanie Schellenberg, Dominik Michael, Finn-Henri Smidt, Jan-Hinrich Nölke, Tim J Adler, Minu Dietlinde Tizabi, Chinedu Innocent Nwoye, et al. Self-distillation for surgical action recognition. In *International Conference on Medical Image Computing and Computer-Assisted Intervention*, pages 637–646. Springer, 2023.

[38] Shuangchun Gui and Zhenkun Wang. Tail-enhanced representation learning for surgical triplet recognition. In *International Conference on Medical Image Computing and Computer-Assisted Intervention*, pages 689–699. Springer, 2024.

[39] Yongjun Jeon, Jongmin Shin, Seonmin Park, Bogeun Kim, Kanggil Park, Namkee Oh, and Kyu-Hwan Jung. Curconmix: A curriculum contrastive learning framework for enhancing surgical action triplet recognition. In *International Conference on Medical Image Computing and Computer-Assisted Intervention*, pages 149–158. Springer, 2025.

[40] Pietro Mascagni, Armine Vardazaryan, Deepak Alapatt, Takeshi Urade, Taha Emre, Claudio Fiorillo, Patrick Pessaux, Didier Mutter, Jacques Marescaux, Guido Costamagna, et al. Artificial intelligence for surgical safety: automatic assessment of the critical view of safety in laparoscopic cholecystectomy using deep learning. *Annals of surgery*, 275(5):955–961, 2022.

[41] Joël L Lavanchy, Sanat Ramesh, Diego Dall’Alba, Cristians Gonzalez, Paolo Fiorini, Beat P Müller-Stich, Philipp C Nett, Jacques Marescaux, Didier Mutter, and Nicolas Padoy. Challenges in multi-centric generalization: phase and step recognition in roux-en-y gastric bypass surgery. *International journal of computer assisted radiology and surgery*, 19(11):2249–2257, 2024.

[42] Ziyi Wang, Bo Lu, Yonghao Long, Fangxun Zhong, Tak-Hong Cheung, Qi Dou, and Yunhui Liu. Autolaparo: A new dataset of integrated multi-tasks for image-guided surgical automation in laparoscopic hysterectomy. In *International Conference on Medical Image Computing and Computer-Assisted Intervention*, pages 486–496. Springer, 2022.

[43] Chinedu Innocent Nwoye and Nicolas Padoy. Data splits and metrics for method benchmarking on surgical action triplet datasets. *arXiv preprint arXiv:2204.05235*, 2022.

[44] Yongjun Jeon, Jongmin Shin, Kanggil Park, Seonmin Park, Soyoung Lim, Jung Yong Kim, Jinsoo Rhu, Jongman Kim, Gyu-Seong Choi, Namkee Oh, et al. Curconmix+: A unified spatio-temporal framework for hierarchical surgical workflow understanding. *arXiv preprint arXiv:2601.12312*, 2026.

[45] Steven M Strasberg, Martin Hertl, and Nathaniel J Soper. An analysis of the problem of biliary injury during laparoscopic cholecystectomy. *Journal of the American College of Surgeons*, 180(1):101–125, 1995.

[46] Manuel Sebastián Ríos, María Alejandra Molina-Rodriguez, Daniella Londoño, Camilo Andrés Guillén, Sebastián Sierra, Felipe Zapata, and Luis Felipe Giraldo. Cholec80-cvs: An open dataset with an evaluation of strasberg’s critical view of safety for ai. *Scientific Data*, 10(1):194, 2023.

[47] Namkee Oh, Bogeun Kim, Taeyoung Kim, Jinsoo Rhu, Jongman Kim, and Gyu-Seong Choi. Real-time segmentation of biliary structure in pure laparoscopic donor hepatectomy. *Scientific Reports*, 14(1):22508, 2024.

[48] RB Den Boer, TJM Jaspers, C De Jongh, JPW Pluim, F Van Der Sommen, T Boers, R Van Hillegersberg, MAJM Van Eijnatten, and JP Ruurda. Deep learning-based recognition of key anatomical structures during robot-assisted minimally invasive esophagectomy. *Surgical endoscopy*, 37(7):5164–5175, 2023.

[49] Yanwen Sun, Bo Pan, and Yili Fu. Lightweight deep neural network for real-time instrument semantic segmentation in robot assisted minimally invasive surgery. *IEEE Robotics and Automation Letters*, 6(2):3870–3877, 2021.

[50] Chinedu Innocent Nwoye, Kareem Elgohary, Anvita Srinivas, Fauzan Zaid, Joël L Lavanchy, and Nicolas Padoy. Cholectrack20: A multi-perspective tracking dataset for surgical tools. In *Proceedings of the Computer Vision and Pattern Recognition Conference*, pages 8942–8952, 2025.

[51] Shuwei Shao, Zhongcai Pei, Weihai Chen, Baochang Zhang, Xingming Wu, Dianmin Sun, and David Doermann. Self-supervised learning for monocular depth estimation on minimally invasive surgery scenes. In *2021 IEEE International Conference on Robotics and Automation (ICRA)*, pages 7159–7165. IEEE, 2021.

[52] Xue Li, Wenxin Chen, Xingguang Duan, Xiaoyi Gu, and Changsheng Li. Collaborative surgical instrument segmentation for monocular depth estimation in minimally invasive surgery. *Medical Image Analysis*, page 103765, 2025.

[53] Shuwei Shao, Zhongcai Pei, Weihai Chen, Wentao Zhu, Xingming Wu, Dianmin Sun, and Baochang Zhang. Self-supervised monocular depth and ego-motion estimation in endoscopy: Appearance flow to the rescue. *Medical image analysis*, 77:102338, 2022.

[54] W-Y Hong, C-L Kao, Y-H Kuo, J-R Wang, W-L Chang, and C-S Shih. Cholecseg8k: a semantic segmentation dataset for laparoscopic cholecystectomy based on cholec80. *arXiv preprint arXiv:2012.12453*, 2020.

[55] Matthias Carstens, Franziska M Rinner, Sebastian Bodenstedt, Alexander C Jenke, Jürgen Weitz, Marius Distler, Stefanie Speidel, and Fiona R Kolbinger. The dresden surgical anatomy dataset for abdominal organ segmentation in surgical data science. *Scientific Data*, 10(1):1–8, 2023.

[56] Nicolás Ayobi, Santiago Rodríguez, Alejandra Pérez, Isabela Hernández, Nicolás Aparicio, Eugénie Dessevres, Sebastián Peña, Jessica Santander, Juan Ignacio Caicedo, Nicolás Fernández, et al. Pixel-wise recognition for holistic surgical scene understanding. *Medical Image Analysis*, page 103726, 2025.

[57] Max Allan, Jonathan Mcleod, Congcong Wang, Jean Claude Rosenthal, Zhenglei Hu, Niklas Gard, Peter Eisert, Ke Xue Fu, Trevor Zeffiro, Wenyao Xia, et al. Stereo correspondence and reconstruction of endoscopic data challenge. *arXiv preprint arXiv:2101.01133*, 2021.

[58] Hamlyn Centre for Robotic Surgery. Surgical vision group. URL <http://hamlyn.doc.ic.ac.uk/vision/>. accessed 8 March 2025.

[59] Lena Maier-Hein, Swaroop S Vedula, Stefanie Speidel, Nassir Navab, Ron Kikinis, Adrian Park, Matthias Eisenmann, Hubertus Feussner, Germain Forestier, Stamatia Giannarou, et al. Surgical data science for next-generation interventions. *Nature Biomedical Engineering*, 1(9):691–696, 2017.

[60] Kai Sun, Siyan Xue, Fuchun Sun, Haoran Sun, Yu Luo, Ling Wang, Siyuan Wang, Na Guo, Lei Liu, Tian Zhao, et al. Medical multimodal foundation models in clinical diagnosis and treatment:

Applications, challenges, and future directions. *Artificial Intelligence in Medicine*, page 103265, 2025.

[61] Sheng Zhang, Yanbo Xu, Naoto Usuyama, Hanwen Xu, Jaspreet Bagga, Robert Tinn, Sam Preston, Rajesh Rao, Mu Wei, Naveen Valluri, et al. A multimodal biomedical foundation model trained from fifteen million image–text pairs. *NEJM AI*, 2(1):A1oa2400640, 2025.

[62] Lalithkumar Seenivasan, Mobarakol Islam, Adithya K Krishna, and Hongliang Ren. Surgical-vqa: Visual question answering in surgical scenes using transformer. In *International Conference on Medical Image Computing and Computer-Assisted Intervention*, pages 33–43. Springer, 2022.

[63] Runlong He, Mengya Xu, Adrito Das, Danyal Z Khan, Sophia Bano, Hani J Marcus, Danail Stoyanov, Matthew J Clarkson, and Mobarakol Islam. Pitvqa: Image-grounded text embedding llm for visual question answering in pituitary surgery. In *International Conference on Medical Image Computing and Computer-Assisted Intervention*, pages 488–498. Springer, 2024.

[64] Yongjun Jeon, Seonmin Park, Jongmin Shin, Kanggil Park, Bogeun Kim, Namkee Oh, and Kyu-Hwan Jung. Surgen-net: A generative approach for surgical vqa with structured text generation. In *Proceedings of the IEEE/CVF International Conference on Computer Vision*, pages 1292–1299, 2025.

[65] Kun Yuan, Vinkle Srivastav, Tong Yu, Joel L Lavanchy, Jacques Marescaux, Pietro Mascagni, Nassir Navab, and Nicolas Padoy. Learning multi-modal representations by watching hundreds of surgical video lectures. *Medical Image Analysis*, page 103644, 2025.

[66] Kun Yuan, Vinkle Srivastav, Nassir Navab, and Nicolas Padoy. Hecvl: Hierarchical video-language pretraining for zero-shot surgical phase recognition. In *International Conference on Medical Image Computing and Computer-Assisted Intervention*, pages 306–316. Springer, 2024.

[67] Thomas M Ward, Danyal M Fer, Yutong Ban, Guy Rosman, Ozanan R Meireles, and Daniel A Hashimoto. Challenges in surgical video annotation. *Computer Assisted Surgery*, 26(1):58–68, 2021.

[68] Melissa Thornton, Benjamin AY Cher, Cameron Macdonald, Jocelyn G Baker, Elisa L Marten, Don Mai, Ganesh Sankaranarayanan, and Courtney J Balentine. Expectations vs reality of an intraoperative artificial intelligence intervention. *JAMA surgery*, 2026.

[69] Daichi Kitaguchi, Norihito Kosugi, Yuto Ishikawa, Satoshi Narihiro, Tsuyoshi Enomoto, Tatsuya Oda, Nobuyoshi Takeshita, and Masaaki Ito. A multicentre randomized controlled trial exploring the clinical usefulness of the intraoperative use of an artificial intelligence–based anatomical navigation system. *British Journal of Surgery*, 112(6):znaf121, 2025.

[70] Guankun Wang, Long Bai, Junyi Wang, Kun Yuan, Zhen Li, Tianxu Jiang, Xiting He, Jinlin Wu, Zhen Chen, Zhen Lei, et al. Endochat: Grounded multimodal large language model for endoscopic surgery. *arXiv preprint arXiv:2501.11347*, 2025.

[71] Zhitao Zeng, Zhu Zhuo, Xiaojun Jia, Erli Zhang, Junde Wu, Jiaan Zhang, Yuxuan Wang, Chang Han Low, Jian Jiang, Zilong Zheng, et al. Surgvlm: A large vision-language model and systematic evaluation benchmark for surgical intelligence. *arXiv preprint arXiv:2506.02555*, 2025.

[72] Shunlei Li, Jin Wang, Rui Dai, Wanyu Ma, Wing Yin Ng, Yingbai Hu, and Zheng Li. Robonurse-vla: Robotic scrub nurse system based on vision-language-action model. In *2025 IEEE/RSJ International Conference on Intelligent Robots and Systems (IROS)*, pages 3986–3993. IEEE, 2025.

[73] Ji Woong Kim, Juo-Tung Chen, Pascal Hansen, Lucy Xiaoyang Shi, Antony Goldenberg, Samuel Schmidgall, Paul Maria Scheikl, Anton Deguet, Brandon M White, De Ru Tsai, et al. Srt-h: A hierarchical framework for autonomous surgery via language-conditioned imitation learning. *Science robotics*, 10(104):eadt5254, 2025.

[74] Joël L Lavanchy, Armine Vardazaryan, Pietro Mascagni, Didier Mutter, and Nicolas Padoy. Preserving privacy in surgical video analysis using a deep learning classifier to identify out-of-body scenes in endoscopic videos. *Scientific reports*, 13(1):9235, 2023.

[75] Kaiming He, Xinlei Chen, Saining Xie, Yanghao Li, Piotr Dollár, and Ross Girshick. Masked autoencoders are scalable vision learners. In *Proceedings of the IEEE/CVF conference on computer vision and pattern recognition*, pages 16000–16009, 2022.

[76] Xinlei Chen, Saining Xie, and Kaiming He. An empirical study of training self-supervised vision transformers. In *Proceedings of the IEEE/CVF international conference on computer vision*, pages 9640–9649, 2021.

[77] Mahmoud Assran, Mathilde Caron, Ishan Misra, Piotr Bojanowski, Florian Bordes, Pascal Vincent, Armand Joulin, Mike Rabbat, and Nicolas Ballas. Masked siamese networks for label-efficient learning. In *European conference on computer vision*, pages 456–473. Springer, 2022.

[78] Jimmy Lei Ba, Jamie Ryan Kiros, and Geoffrey E Hinton. Layer normalization. *arXiv preprint arXiv:1607.06450*, 2016.

[79] D Hendrycks. Gaussian error linear units (gelus). *arXiv preprint arXiv:1606.08415*, 2016.

[80] Yazan Abu Farha and Jurgen Gall. Ms-tcn: Multi-stage temporal convolutional network for action segmentation. In *Proceedings of the IEEE/CVF conference on computer vision and pattern recognition*, pages 3575–3584, 2019.

[81] Ilya Loshchilov and Frank Hutter. Decoupled weight decay regularization. *arXiv preprint arXiv:1711.05101*, 2017.

[82] Diederik P Kingma. Adam: A method for stochastic optimization. *arXiv preprint arXiv:1412.6980*, 2014.

[83] Isabel Funke, Dominik Rivoir, and Stefanie Speidel. Metrics matter in surgical phase recognition. *arXiv preprint arXiv:2305.13961*, 2023.

[84] Tete Xiao, Yingcheng Liu, Bolei Zhou, Yuning Jiang, and Jian Sun. Unified perceptual parsing for scene understanding. In *Proceedings of the European conference on computer vision (ECCV)*, pages 418–434, 2018.

[85] Kaiming He, Georgia Gkioxari, Piotr Dollár, and Ross Girshick. Mask r-cnn. In *Proceedings of the IEEE international conference on computer vision*, pages 2961–2969, 2017.

[86] Tsung-Yi Lin, Piotr Dollár, Ross Girshick, Kaiming He, Bharath Hariharan, and Serge Belongie. Feature pyramid networks for object detection. In *Proceedings of the IEEE conference on computer vision and pattern recognition*, pages 2117–2125, 2017.

[87] Beilei Cui, Mobarakol Islam, Long Bai, and Hongliang Ren. Surgical-dino: adapter learning of foundation models for depth estimation in endoscopic surgery. *International Journal of Computer Assisted Radiology and Surgery*, 19(6):1013–1020, 2024.

[88] David Eigen, Christian Puhrsch, and Rob Fergus. Depth map prediction from a single image using a multi-scale deep network. *Advances in neural information processing systems*, 27, 2014.

[89] Luis Wiedmann, Aritra Roy Gosthipaty, and Andrés Marafioti. nanovlm. <https://github.com/huggingface/nanoVLM>, 2025.

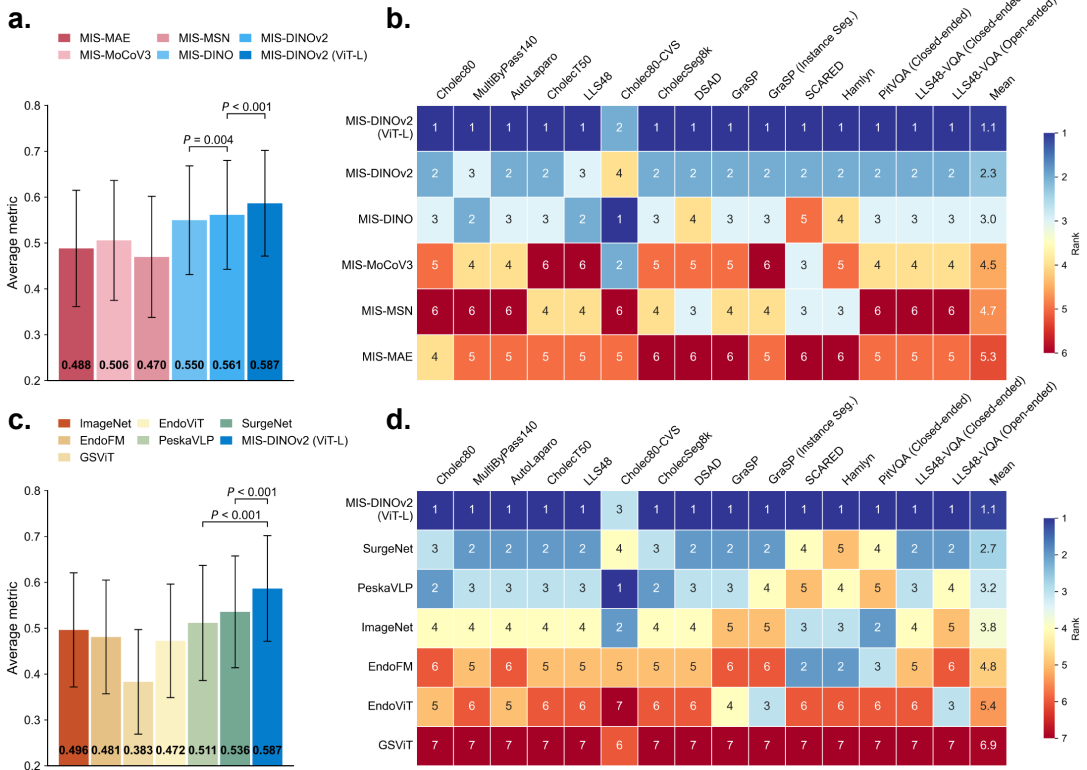
[90] Edward J Hu, Yelong Shen, Phillip Wallis, Zeyuan Allen-Zhu, Yuanzhi Li, Shean Wang, Lu Wang, Weizhu Chen, et al. Lora: Low-rank adaptation of large language models. *ICLR*, 1(2):3, 2022.

[91] Kexin Huang, Jaan Altosaar, and Rajesh Ranganath. Clinicalbert: Modeling clinical notes and predicting hospital readmission. *arXiv preprint arXiv:1904.05342*, 2019.

[92] Ozanan R Meireles, Guy Rosman, Maria S Altieri, Lawrence Carin, Gregory Hager, Amin Madani, Nicolas Padoy, Carla M Pugh, Patricia Sylla, Thomas M Ward, et al. Sages consensus recommendations on an annotation framework for surgical video. *Surgical endoscopy*, 35(9):4918–4929,

2021.

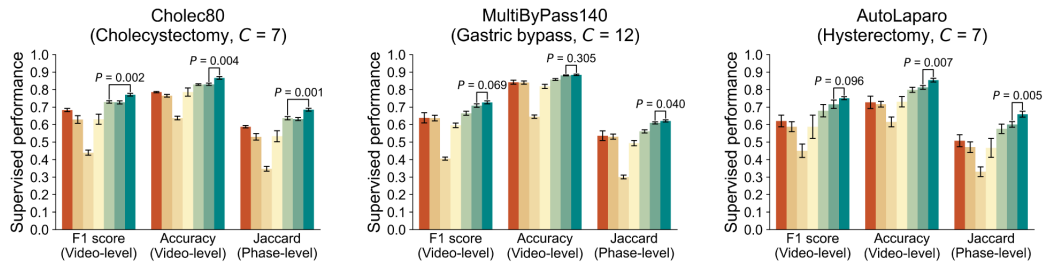
[93] OpenAI. Chatgpt (gpt-4.1), 2025. URL <https://openai.com>.



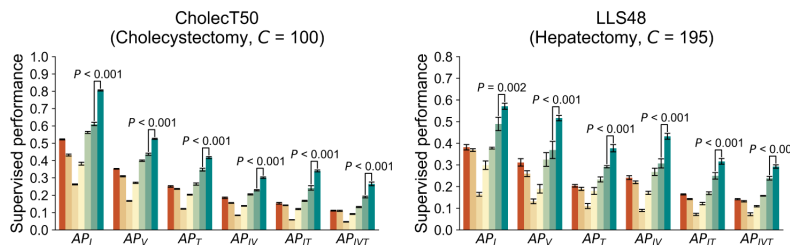
Extended Data Fig. 1 Comprehensive comparison of self-supervised and existing pretrained models. **a.** Average performance in the frozen-backbone setting across 15 supervised downstream tasks for self-supervised pretrained models trained on minimally invasive surgical videos. Task-specific representative metrics are used, including the average of video-level macro F1 score and accuracy for surgical phase recognition; mean average precision (mAP) for surgical action triplet recognition; mAP for skill assessment; Dice score for semantic segmentation; the average of detection and segmentation mAP for instance segmentation; 1 – absolute relative error for depth estimation; the average of macro F1 score and balanced accuracy for closed-ended visual question answering (VQA); and the average of BLEU, ROUGE-L, and METEOR scores for open-ended VQA. **b.** Ranking heatmap of self-supervised pretrained models across the same 15 supervised tasks in the frozen-backbone setting, based on the corresponding representative task-level metrics. **c.** Average performance in the frozen-backbone setting across the 15 supervised tasks for MIS-DINOv2 (ViT-L) and existing pretrained models, computed using the representative metrics as in **a**. **d.** Ranking heatmap comparing MIS-DINOv2 (ViT-L) and existing pretrained models across the 15 supervised tasks in the frozen-backbone setting. For **a** and **c**, error bars indicate 95% confidence intervals. P values were calculated using a two-sided Wilcoxon signed-rank test.

ImageNet (Frozen) EndoFM (Frozen) GSViT (Frozen) EndoViT (Frozen) PeskaVLP (Frozen) SurgeNet (Frozen) Zen (Frozen)

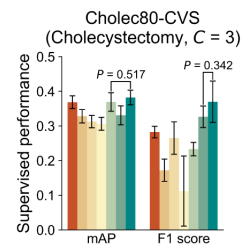
a. Surgical phase recognition



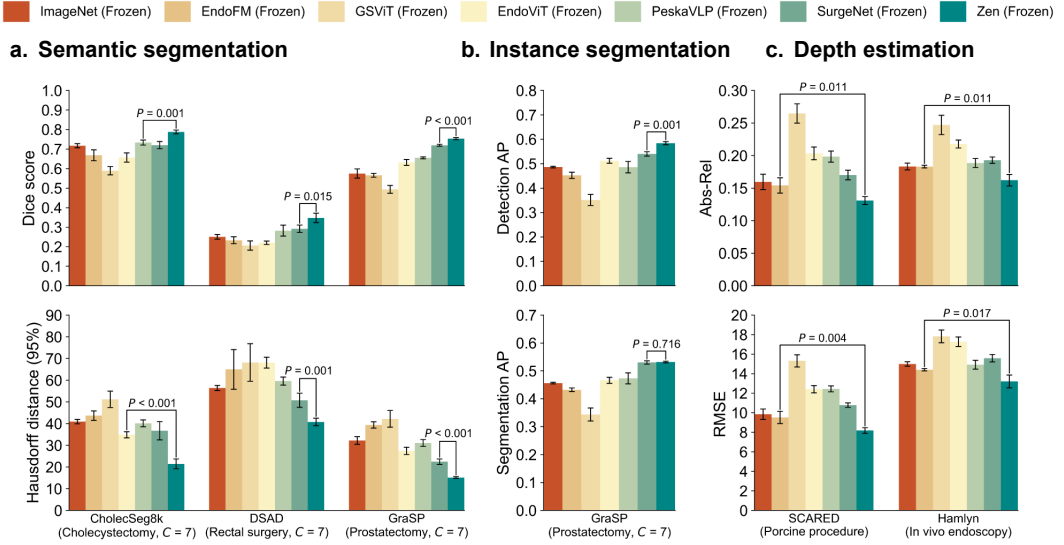
b. Surgical action triplet recognition



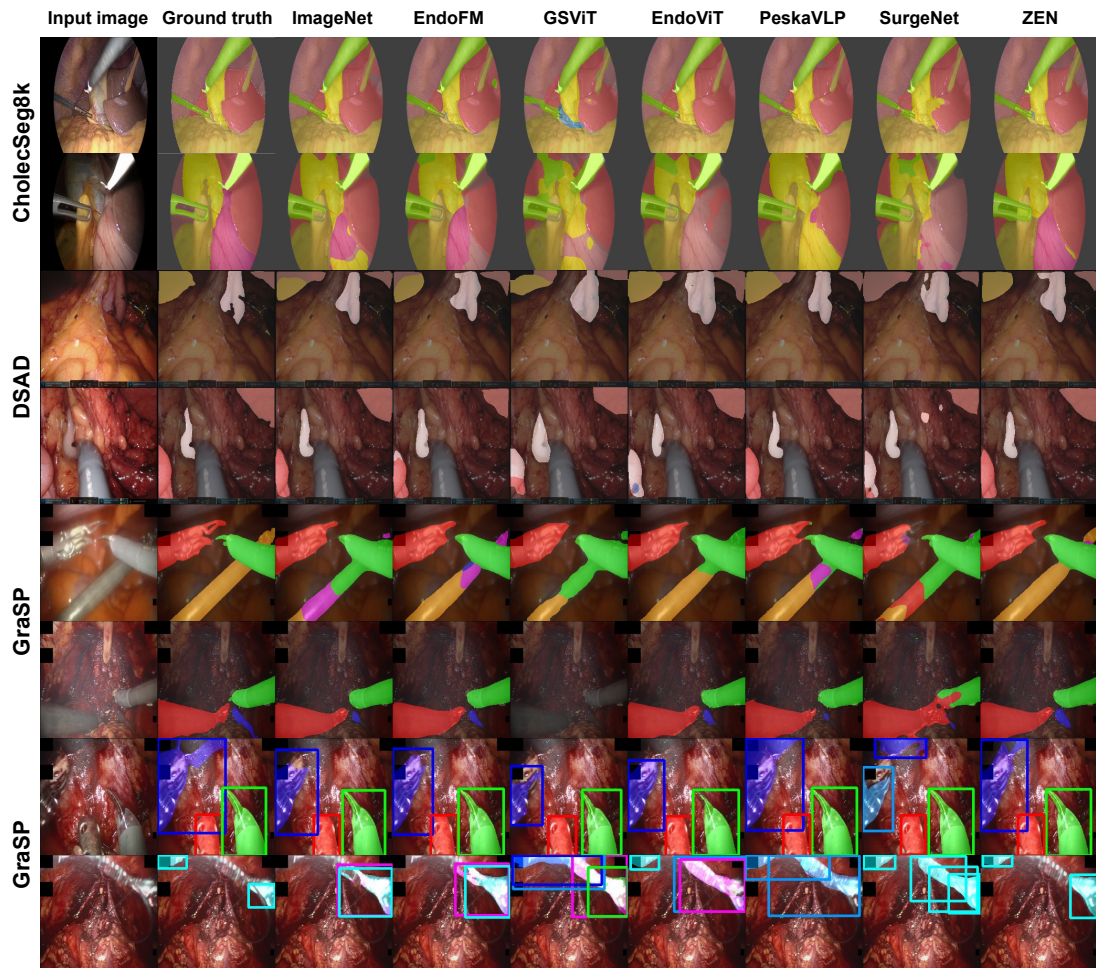
c. Skill assessment



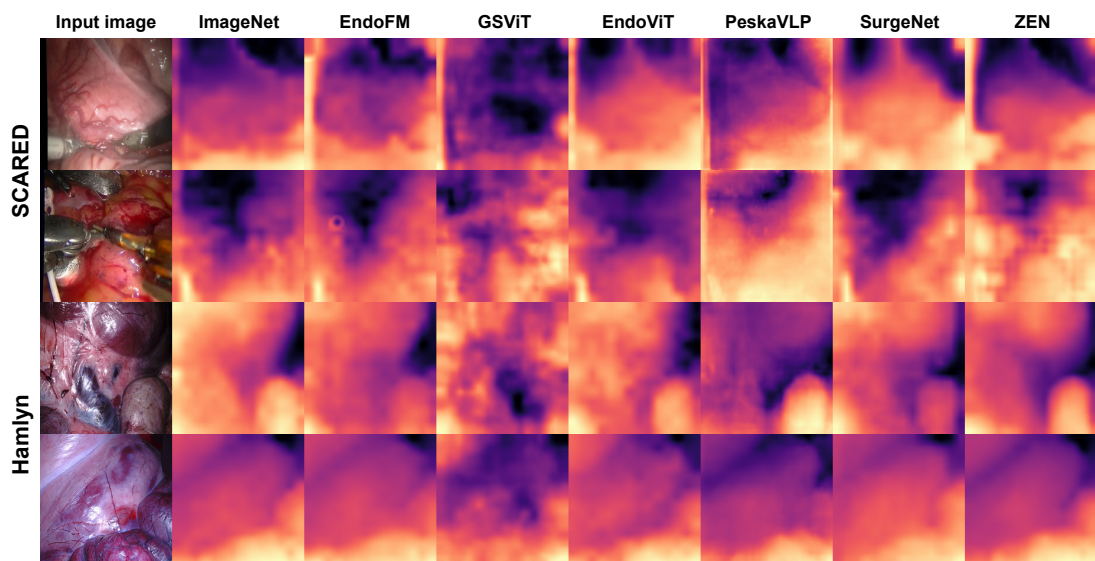
Extended Data Fig. 2 Performance comparison for surgical workflow understanding. **a**, Performance of ZEN and other pretrained models on surgical phase recognition across three datasets in the frozen-backbone setting. Metrics include video-level macro F1 score, accuracy, and phase-level Jaccard index. C denotes the number of phases. **b**, Surgical action triplet recognition performance across two datasets in the frozen-backbone setting. Performance is evaluated using mean Average Precision (mAP) for instrument (I), verb (V), and target (T) components, as well as their combinations. C denotes the number of triplet (IVT) classes. **c**, Skill assessment performance using mAP and macro F1 score in the frozen-backbone setting. C denotes the number of safety criteria. Error bars represent 95% confidence intervals over five independent runs ($n = 5$). P values were calculated using two-sided paired t -test.



Extended Data Fig. 3 Performance comparison for dense spatial understanding. **a**, Semantic segmentation performance across three datasets in the frozen-backbone setting. Performance is measured using Dice score and 95% Hausdorff distance. C denotes the number of classes. **b**, Instance segmentation performance in the frozen-backbone setting. Performance is evaluated using mean Average Precision (mAP), averaged over Intersection over Union thresholds from 0.5 to 0.95. Results are reported for bounding box detection (Detection AP) and segmentation masks (Segmentation AP). C denotes the number of classes. **c**, Depth estimation performance across two datasets in the frozen-backbone setting. Metrics include Absolute Relative Error (Abs-Rel) and Root Mean Squared Error (RMSE). Error bars represent 95% confidence intervals over five independent runs ($n = 5$). P values were calculated using two-sided paired t -tests.



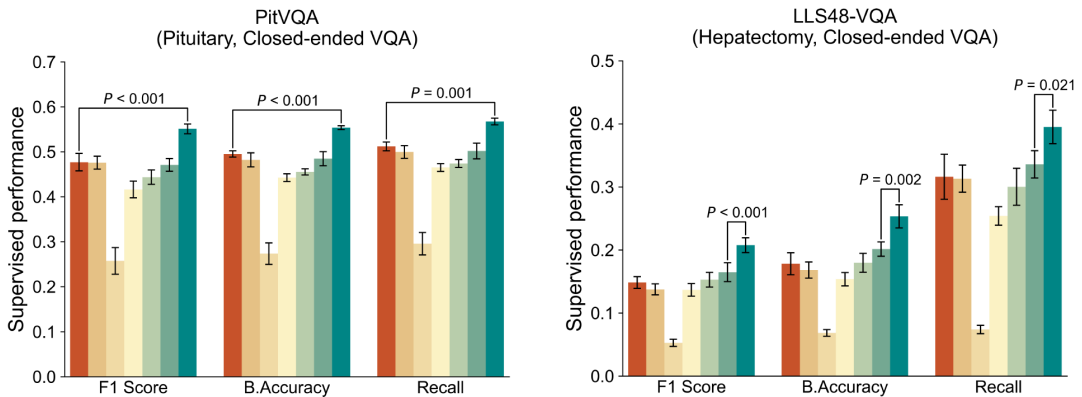
Extended Data Fig. 4 Qualitative comparison of semantic and instance segmentation. Visual examples comparing ZEN with other pretrained models across multiple surgical datasets.



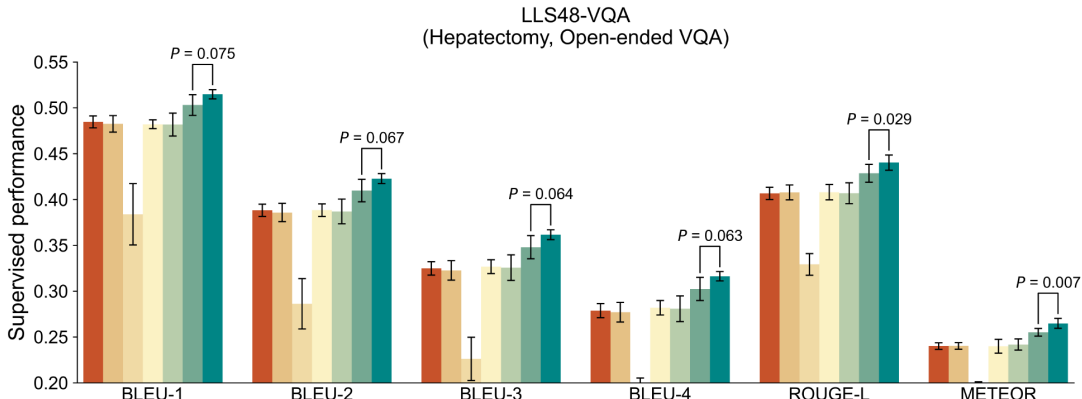
Extended Data Fig. 5 Qualitative comparison of depth estimation. Visual examples comparing ZEN with other pretrained models across two surgical datasets.

■ ImageNet (Frozen) ■ EndoFM (Frozen) ■ GSViT (Frozen) ■ EndoViT (Frozen) ■ PeskaVLP (Frozen) ■ SurgeNet (Frozen) ■ Zen (Frozen)

a. Visual question answering (Closed-ended VQA)



b. Visual question answering (Open-ended VQA)



Extended Data Fig. 6 Performance comparison for visual question answering. **a**, Closed-ended VQA performance in the frozen-backbone setting. Evaluation metrics include macro F1 score, balanced accuracy (B.Accuracy), and recall, measured by exact match. **b**, Open-ended VQA performance in the frozen-backbone setting, evaluated using BLEU-1–4, ROUGE-L, and METEOR. Error bars represent 95% confidence intervals over five independent runs ($n = 5$). P values were calculated using two-sided paired t -tests.



ImageNet (Finetuned) EndoFM (Finetuned) GSViT (Finetuned) EndoViT (Finetuned) PeskaVLP (Finetuned) SurgeNet (Finetuned) Zen (Finetuned)

LLS48-VQA

Q1. Describe the current surgical scene.

Ground truth : The surgeon is performing hemostasis on the transected surface of the liver. The left hand is using a bipolar instrument to coagulate bleeding points on the liver parenchyma, while the right hand is using suction and irrigation to clear blood and fluids from the liver surface. The assistant is not actively using any instruments. The background shows the exposed liver surface, and hemostatic agents are being prepared for placement.

A. **I** : The surgeon is performing hemostasis on the transected surface of the liver using a bipolar instrument to coagulate bleeding points, while also using suction to clear blood and maintain control of the area. The assistant is not actively using any instruments.

E : The surgeon is performing hemostasis on the perihepatic tissue after liver transection, using a bipolar instrument to coagulate the liver parenchyma.

G : The surgeon is performing parenchymal transection of the liver, using suction and retraction with the left hand and a sonication device to dissect the liver parenchyma with the right hand. The assistant is not actively involved at this moment.

E : The surgeon is performing hemostasis on the transected surface of the liver, using a bipolar instrument to coagulate bleeding points. The assistant is not actively using any instruments. The background indicates that the liver parenchyma has been exposed and is being coagulated with a grasper.

P : The surgeon is performing hemostasis on the transected surface of the liver using a bipolar instrument to coagulate bleeding points, while also using suction to clear blood and fluid from the area. The assistant is not actively involved at this moment.

S : The surgeon is performing hemostasis on the transected surface of the liver using a bipolar instrument to coagulate bleeding points, while also using suction to aspirate blood and a hook to coagulate bleeding sites. The assistant is not actively using any instruments. The background includes the liver parenchyma and the insertion of a trocar.

Z : The surgeon is performing hemostasis on the transected surface of the liver using a bipolar instrument to coagulate bleeding points, while also using suction to clear blood and fluids. The assistant is not actively using any instruments. The background shows the surgical field and the use of a suture to control bleeding.

Q2. What is the purpose of the current actions?

Ground truth : The purpose is to achieve hemostasis by stopping bleeding from the transected liver surface using coagulation and to maintain a clear surgical field with suction and irrigation.

A. **I** : The purpose is to control bleeding from the liver surface after transection, ensuring hemostasis and clear surgical fields.

E : The purpose is to achieve hemostasis by controlling bleeding from the liver parenchyma after transection, ensuring a clear surgical field and preventing postoperative bleeding.

G : The purpose is to carefully divide the liver parenchyma, likely as part of a liver resection procedure, while maintaining hemostasis and clear visualization.

E : The purpose is to achieve hemostasis by controlling bleeding from the liver parenchyma after transection.

P : The purpose is to achieve hemostasis by coagulating bleeding points on the liver surface to prevent further blood loss.

S : The purpose is to achieve hemostasis by controlling bleeding from the liver surface after transection.

Z : The purpose is to control bleeding from the cut surface of the liver after transection, ensuring a clear and stable operative field.

Q3. What should be done next?

Ground truth : Hemostatic agents should be placed on the liver surface, followed by the application of anti-adhesive agents and then insertion of a drainage tube.

A. **I** : After controlling inflow, the next step is to divide the inflow structures using a stapler.

E : Placement of anti-adhesive agents and then insertion of a drain.

G : After completing the dissection of the left triangular ligament, the next step is to identify the hepatoduodenal ligament and perform the Pringle's maneuver.

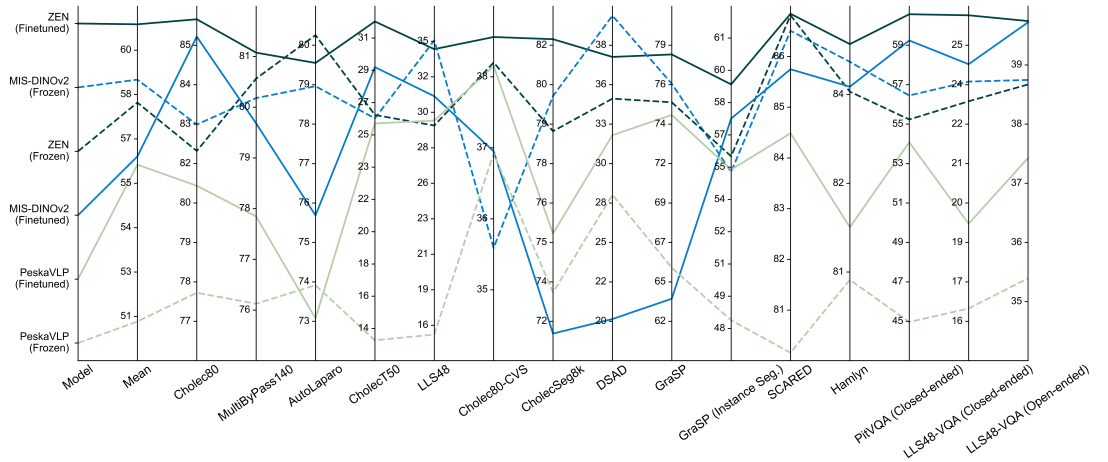
E : Placement of hemostatic agents and anti-adhesive agents, followed by insertion of a drain.

P : After bleeding control, hemostatic agents should be placed on the liver surface, and then the next step is to identify the target area for drainage.

S : After bleeding is controlled, hemostatic agents and anti-adhesive agents should be placed.

Z : After achieving hemostasis, the next step is to apply hemostatic agents to the liver surface.

Extended Data Fig. 7 Examples of Open-ended VQA.



Extended Data Fig. 8 Downstream performance comparison of ZEN and its teacher models. Performance of ZEN and its teacher models, MIS-DINOv2 and PeskaVLP, are shown across 15 supervised downstream tasks, under frozen and fine-tuned backbone settings. Each axis represents a dataset, and values correspond to task-specific representative evaluation metrics (higher is better).

Table 1 Surgical phase recognition performance comparison on the Cholec80 dataset using fine-tuned backbones. The upper block reports results for self-supervised learning pretrained models, and the lower block reports results for existing pretrained models. Best-performing models for each metric are highlighted in bold. Values are reported as mean \pm standard deviation over five independent runs.

Method	Backbone	Video-level			Phase-level		
		F1 score	Accuracy	Precision	Recall	Jaccard	
MIS-MAE	ViT-B	0.7732 \pm 0.0246	0.8680 \pm 0.0163	0.7924 \pm 0.0215	0.8249 \pm 0.0212	0.6802 \pm 0.0285	
MIS-MoCoV3	ViT-B	0.7398 \pm 0.0138	0.8509 \pm 0.0104	0.7727 \pm 0.0119	0.7891 \pm 0.0118	0.6435 \pm 0.0151	
MIS-MSN	ViT-B	0.7455 \pm 0.0189	0.8566 \pm 0.0077	0.7745 \pm 0.0156	0.8058 \pm 0.0246	0.6603 \pm 0.0183	
MIS-DINO	ViT-B	0.7939 \pm 0.0156	0.8756 \pm 0.0102	0.7921 \pm 0.0208	0.8647 \pm 0.0115	0.7040 \pm 0.0172	
MIS-DINOv2	ViT-B	0.7901 \pm 0.0146	0.8774 \pm 0.0111	0.7924 \pm 0.0159	0.8526 \pm 0.0099	0.7005 \pm 0.0160	
MIS-DINOv2	ViT-L	0.8065 \pm 0.0119	0.8961 \pm 0.0072	0.8146 \pm 0.0101	0.8622 \pm 0.0106	0.7169 \pm 0.0144	
ImageNet	ViT-B	0.7324 \pm 0.0086	0.8346 \pm 0.0043	0.7526 \pm 0.0065	0.7941 \pm 0.0153	0.6244 \pm 0.0128	
EndoFM	ViT-B	0.7175 \pm 0.0190	0.8293 \pm 0.0094	0.7519 \pm 0.0109	0.7747 \pm 0.0217	0.6113 \pm 0.0181	
GSViT	EfficientViT	0.4248 \pm 0.0268	0.6322 \pm 0.0146	0.5454 \pm 0.0149	0.4704 \pm 0.0327	0.3356 \pm 0.0224	
EndoViT	ViT-B	0.7401 \pm 0.0067	0.8416 \pm 0.0086	0.7690 \pm 0.0086	0.7959 \pm 0.0167	0.6414 \pm 0.0074	
PeskaVLP	ResNet50	0.7622 \pm 0.0090	0.8564 \pm 0.0069	0.7852 \pm 0.0072	0.8195 \pm 0.0163	0.6611 \pm 0.0088	
SurgeNet	CAFormer18	0.7742 \pm 0.0298	0.8746 \pm 0.0135	0.7922 \pm 0.0130	0.8353 \pm 0.0372	0.6822 \pm 0.0324	
ZEN	ViT-B	0.8120 \pm 0.0089	0.9004 \pm 0.0055	0.8203 \pm 0.0086	0.8690 \pm 0.0129	0.7267 \pm 0.0124	

Table 2 Surgical phase recognition performance comparison on the MultiByPass140 dataset using fine-tuned backbones. The upper block reports results for self-supervised learning pretrained models, and the lower block reports results for existing pretrained models. Best-performing models for each metric are highlighted in bold. Values are reported as mean \pm standard deviation over five independent runs.

Method	Backbone	Video-level			Phase-level		
		F1 score	Accuracy	Precision	Recall	Jaccard	
MIS-MAE	ViT-B	0.6901 \pm 0.0292	0.8707 \pm 0.0088	0.6991 \pm 0.0299	0.7473 \pm 0.0114	0.5829 \pm 0.0247	
MIS-MoCoV3	ViT-B	0.6889 \pm 0.0227	0.8718 \pm 0.0074	0.7010 \pm 0.0240	0.7346 \pm 0.0131	0.5820 \pm 0.0154	
MIS-MSN	ViT-B	0.7048 \pm 0.0083	0.8833 \pm 0.0017	0.7099 \pm 0.0157	0.7737 \pm 0.0220	0.6047 \pm 0.0058	
MIS-DINO	ViT-B	0.7195 \pm 0.0193	0.8846 \pm 0.0036	0.7418 \pm 0.0309	0.7705 \pm 0.0192	0.6158 \pm 0.0085	
MIS-DINOv2	ViT-B	0.6845 \pm 0.0142	0.8744 \pm 0.0079	0.6958 \pm 0.0211	0.7551 \pm 0.0234	0.5805 \pm 0.0127	
MIS-DINOv2	ViT-L	0.7038 \pm 0.0179	0.8898 \pm 0.0050	0.7029 \pm 0.0192	0.7831 \pm 0.0134	0.6068 \pm 0.0202	
ImageNet	ViT-B	0.6760 \pm 0.0303	0.8672 \pm 0.0097	0.6999 \pm 0.0274	0.7230 \pm 0.0252	0.5690 \pm 0.0197	
EndoFM	ViT-B	0.6655 \pm 0.0124	0.8587 \pm 0.0076	0.6891 \pm 0.0142	0.7385 \pm 0.0108	0.5670 \pm 0.0132	
GSViT	EfficientViT	0.4470 \pm 0.0160	0.6835 \pm 0.0196	0.5015 \pm 0.0356	0.4799 \pm 0.0229	0.3404 \pm 0.0156	
EndoViT	ViT-B	0.6705 \pm 0.0160	0.8581 \pm 0.0052	0.6887 \pm 0.0218	0.7262 \pm 0.0116	0.5631 \pm 0.0111	
PeskaVLP	ResNet50	0.6821 \pm 0.0183	0.8748 \pm 0.0084	0.6955 \pm 0.0114	0.7521 \pm 0.0213	0.5821 \pm 0.0175	
SurgeNet	CAFormer18	0.7278 \pm 0.0245	0.8851 \pm 0.0035	0.7347 \pm 0.0196	0.7714 \pm 0.0210	0.6246 \pm 0.0227	
ZEN	ViT-B	0.7273 \pm 0.0261	0.8942 \pm 0.0042	0.7381 \pm 0.0319	0.7737 \pm 0.0116	0.6236 \pm 0.0163	

Table 3 Surgical phase recognition performance comparison on the AutoLaparo dataset using fine-tuned backbones. The upper block reports results for self-supervised learning pretrained models, and the lower block reports results for existing pretrained models. Best-performing models for each metric are highlighted in bold. Values are reported as mean \pm standard deviation over five independent runs.

Method	Backbone	Video-level			Phase-level		
		F1 score	Accuracy	Precision	Recall	Jaccard	
MIS-MoCoV3	ViT-B	0.6878 \pm 0.0205	0.7889 \pm 0.0122	0.7279 \pm 0.0245	0.7093 \pm 0.0259	0.5783 \pm 0.0298	
MIS-MSN	ViT-B	0.7232 \pm 0.0191	0.8325 \pm 0.0137	0.7533 \pm 0.0213	0.7474 \pm 0.0338	0.6300 \pm 0.0229	
MIS-DINO	ViT-B	0.7417 \pm 0.0157	0.8362 \pm 0.0116	0.7911 \pm 0.0181	0.7605 \pm 0.0041	0.6488 \pm 0.0156	
MIS-DINOv2	ViT-B	0.6982 \pm 0.0259	0.8009 \pm 0.0258	0.7659 \pm 0.0171	0.7294 \pm 0.0286	0.6085 \pm 0.0288	
MIS-DINOv2	ViT-L	0.7058 \pm 0.0441	0.8079 \pm 0.0258	0.7636 \pm 0.0164	0.7367 \pm 0.0433	0.6101 \pm 0.0471	
ImageNet	ViT-B	0.6679 \pm 0.0401	0.7673 \pm 0.0360	0.7118 \pm 0.0315	0.6907 \pm 0.0304	0.5646 \pm 0.0373	
EndoFM	ViT-B	0.6391 \pm 0.0523	0.7429 \pm 0.0383	0.7095 \pm 0.0138	0.6794 \pm 0.0460	0.5330 \pm 0.0512	
GSViT	EfficientViT	0.4206 \pm 0.0609	0.5876 \pm 0.0474	0.6707 \pm 0.0426	0.4403 \pm 0.0607	0.3109 \pm 0.0506	
EndoViT	ViT-B	0.6358 \pm 0.0232	0.7285 \pm 0.0277	0.6953 \pm 0.0136	0.6651 \pm 0.0169	0.5284 \pm 0.0248	
PeskaVLP	ResNet50	0.6737 \pm 0.0248	0.7878 \pm 0.0166	0.7308 \pm 0.0175	0.6876 \pm 0.0270	0.5672 \pm 0.0231	
SurgeNet	CAFormer18	0.7277 \pm 0.0209	0.8341 \pm 0.0107	0.7702 \pm 0.0172	0.7362 \pm 0.0267	0.6356 \pm 0.0242	
ZEN	ViT-B	0.7603 \pm 0.0218	0.8307 \pm 0.0222	0.7826 \pm 0.0136	0.7597 \pm 0.0220	0.6576 \pm 0.0248	

Table 4 Surgical phase recognition performance comparison on the Cholec80 dataset using frozen backbones. The upper block reports results for self-supervised learning pretrained models, and the lower block reports results for existing pretrained models. Best-performing models for each metric are highlighted in bold. Values are reported as mean \pm standard deviation over five independent runs.

Method	Backbone	Video-level			Phase-level		
		F1 score	Accuracy	Precision	Recall	Jaccard	
MIS-MAE	ViT-B	0.7015 \pm 0.0196	0.8293 \pm 0.0107	0.7543 \pm 0.0130	0.7468 \pm 0.0324	0.6093 \pm 0.0216	
MIS-MoCoV3	ViT-B	0.6790 \pm 0.0152	0.8077 \pm 0.0108	0.7329 \pm 0.0126	0.7342 \pm 0.0220	0.5833 \pm 0.0169	
MIS-MSN	ViT-B	0.5714 \pm 0.0354	0.7573 \pm 0.0091	0.6833 \pm 0.0121	0.6199 \pm 0.0460	0.4790 \pm 0.0328	
MIS-DINO	ViT-B	0.7261 \pm 0.0137	0.8306 \pm 0.0134	0.7483 \pm 0.0209	0.7935 \pm 0.0121	0.6297 \pm 0.0166	
MIS-DINOv2	ViT-B	0.7448 \pm 0.0080	0.8421 \pm 0.0057	0.7788 \pm 0.0147	0.7957 \pm 0.0164	0.6508 \pm 0.0073	
MIS-DINOv2	ViT-L	0.7796 \pm 0.0120	0.8735 \pm 0.0059	0.7814 \pm 0.0136	0.8499 \pm 0.0105	0.6921 \pm 0.0127	
ImageNet	ViT-B	0.6832 \pm 0.0102	0.7855 \pm 0.0039	0.7396 \pm 0.0094	0.7278 \pm 0.0149	0.5878 \pm 0.0081	
EndoFM	ViT-B	0.6291 \pm 0.0250	0.7647 \pm 0.0090	0.7210 \pm 0.0069	0.6579 \pm 0.0287	0.5300 \pm 0.0214	
GSViT	EfficientViT	0.4396 \pm 0.0167	0.6374 \pm 0.0120	0.5466 \pm 0.0291	0.4936 \pm 0.0162	0.3470 \pm 0.0159	
EndoViT	ViT-B	0.6308 \pm 0.0325	0.7860 \pm 0.0267	0.7377 \pm 0.0183	0.6671 \pm 0.0296	0.5336 \pm 0.0357	
PeskaVLP	ResNet50	0.7296 \pm 0.0080	0.8287 \pm 0.0054	0.7526 \pm 0.0109	0.7923 \pm 0.0044	0.6364 \pm 0.0107	
SurgeNet	CAFormer18	0.7270 \pm 0.0102	0.8304 \pm 0.0071	0.7645 \pm 0.0146	0.7807 \pm 0.0106	0.6319 \pm 0.0101	
ZEN	ViT-B	0.7710 \pm 0.0083	0.8672 \pm 0.0082	0.7870 \pm 0.0140	0.8339 \pm 0.0171	0.6853 \pm 0.0098	

Table 5 Surgical phase recognition performance comparison on the MultiByPass140 dataset using frozen backbones. The upper block reports results for self-supervised learning pretrained models, and the lower block reports results for existing pretrained models. Best-performing models for each metric are highlighted in bold. Values are reported as mean \pm standard deviation over five independent runs.

Method	Backbone	Video-level			Phase-level		
		F1 score	Accuracy	Precision	Recall	Jaccard	
MIS-MAE	ViT-B	0.6614 \pm 0.0076	0.8537 \pm 0.0076	0.6746 \pm 0.0095	0.7133 \pm 0.0181	0.5629 \pm 0.0058	
MIS-MoCoV3	ViT-B	0.6610 \pm 0.0100	0.8598 \pm 0.0060	0.6779 \pm 0.0081	0.7351 \pm 0.0224	0.5642 \pm 0.0110	
MIS-MSN	ViT-B	0.6183 \pm 0.0119	0.8316 \pm 0.0036	0.6333 \pm 0.0077	0.6627 \pm 0.0113	0.5134 \pm 0.0071	
MIS-DINO	ViT-B	0.7076 \pm 0.0166	0.8781 \pm 0.0057	0.7097 \pm 0.0122	0.7592 \pm 0.0268	0.5985 \pm 0.0159	
MIS-DINOv2	ViT-B	0.7043 \pm 0.0155	0.8740 \pm 0.0059	0.7143 \pm 0.0184	0.7508 \pm 0.0078	0.5973 \pm 0.0147	
MIS-DINOv2	ViT-L	0.7221 \pm 0.0181	0.8815 \pm 0.0085	0.7256 \pm 0.0171	0.7574 \pm 0.0209	0.6156 \pm 0.0171	
ImageNet	ViT-B	0.6387 \pm 0.0333	0.8425 \pm 0.0133	0.6531 \pm 0.0168	0.6940 \pm 0.0257	0.5365 \pm 0.0314	
EndoFM	ViT-B	0.6373 \pm 0.0183	0.8403 \pm 0.0109	0.6561 \pm 0.0089	0.6835 \pm 0.0244	0.5310 \pm 0.0165	
GSViT	EfficientViT	0.4053 \pm 0.0103	0.6451 \pm 0.0106	0.4612 \pm 0.0256	0.4296 \pm 0.0210	0.3005 \pm 0.0121	
EndoViT	ViT-B	0.5959 \pm 0.0150	0.8185 \pm 0.0133	0.6160 \pm 0.0202	0.6481 \pm 0.0145	0.4940 \pm 0.0168	
PeskaVLP	ResNet50	0.6648 \pm 0.0132	0.8577 \pm 0.0061	0.6758 \pm 0.0084	0.7020 \pm 0.0194	0.5615 \pm 0.0108	
SurgeNet	CAFormer18	0.7082 \pm 0.0115	0.8812 \pm 0.0028	0.7175 \pm 0.0094	0.7619 \pm 0.0128	0.6096 \pm 0.0069	
ZEN	ViT-B	0.7268 \pm 0.0096	0.8845 \pm 0.0049	0.7260 \pm 0.0116	0.7697 \pm 0.0148	0.6212 \pm 0.0071	

Table 6 Surgical phase recognition performance comparison on the AutoLaparo dataset using frozen backbones. The upper block reports results for self-supervised learning pretrained models, and the lower block reports results for existing pretrained models. Best-performing models for each metric are highlighted in bold. Values are reported as mean \pm standard deviation over five independent runs.

Method	Backbone	Video-level			Phase-level		
		F1 score	Accuracy	Precision	Recall	Jaccard	
MIS-MAE	ViT-B	0.6483 \pm 0.0305	0.7452 \pm 0.0220	0.7280 \pm 0.0358	0.6572 \pm 0.0398	0.5290 \pm 0.0387	
MIS-MoCoV3	ViT-B	0.6755 \pm 0.0233	0.7928 \pm 0.0224	0.7167 \pm 0.0346	0.6973 \pm 0.0204	0.5752 \pm 0.0195	
MIS-MSN	ViT-B	0.5196 \pm 0.0480	0.6716 \pm 0.0374	0.6965 \pm 0.0454	0.5241 \pm 0.0406	0.3934 \pm 0.0405	
MIS-DINO	ViT-B	0.7023 \pm 0.0431	0.8088 \pm 0.0430	0.7534 \pm 0.0244	0.7328 \pm 0.0440	0.6158 \pm 0.0453	
MIS-DINOv2	ViT-B	0.7148 \pm 0.0511	0.8230 \pm 0.0173	0.7863 \pm 0.0280	0.7275 \pm 0.0608	0.6157 \pm 0.0547	
MIS-DINOv2	ViT-L	0.7410 \pm 0.0179	0.8382 \pm 0.0143	0.7845 \pm 0.0361	0.7429 \pm 0.0176	0.6376 \pm 0.0205	
ImageNet	ViT-B	0.6208 \pm 0.0382	0.7273 \pm 0.0408	0.6747 \pm 0.0528	0.6402 \pm 0.0304	0.5075 \pm 0.0391	
EndoFM	ViT-B	0.5876 \pm 0.0325	0.7167 \pm 0.0182	0.6501 \pm 0.0166	0.6040 \pm 0.0385	0.4710 \pm 0.0350	
GSViT	EfficientViT	0.4503 \pm 0.0440	0.6155 \pm 0.0319	0.6636 \pm 0.0437	0.4639 \pm 0.0333	0.3306 \pm 0.0318	
EndoViT	ViT-B	0.5875 \pm 0.0761	0.7307 \pm 0.0335	0.7043 \pm 0.0753	0.5991 \pm 0.0649	0.4668 \pm 0.0615	
PeskaVLP	ResNet50	0.6792 \pm 0.0405	0.7991 \pm 0.0164	0.7293 \pm 0.0463	0.6844 \pm 0.0299	0.5758 \pm 0.0309	
SurgeNet	CAFormer18	0.7160 \pm 0.0271	0.8124 \pm 0.0123	0.7734 \pm 0.0525	0.7169 \pm 0.0250	0.6008 \pm 0.0186	
ZEN	ViT-B	0.7509 \pm 0.0096	0.8542 \pm 0.0121	0.7853 \pm 0.0182	0.7626 \pm 0.0191	0.6593 \pm 0.0191	

Table 7 Few-shot evaluation on the Cholec80 dataset for surgical phase recognition (1-shot). The upper block reports results for self-supervised learning pretrained models, and the lower block reports results for existing pretrained models. Best-performing models for each metric are highlighted in bold. Values are reported as mean \pm standard deviation over five independent runs.

Method	Backbone	Video-level			Phase-level		
		F1 score	Accuracy	Precision	Recall	Jaccard	
MIS-MAE	ViT-B	0.2087 \pm 0.0476	0.5363 \pm 0.0852	0.4899 \pm 0.1419	0.2625 \pm 0.0379	0.1605 \pm 0.0384	
MIS-MoCoV3	ViT-B	0.2096 \pm 0.0461	0.5233 \pm 0.0560	0.4983 \pm 0.0778	0.2613 \pm 0.0402	0.1596 \pm 0.0361	
MIS-MSN	ViT-B	0.2055 \pm 0.0450	0.5008 \pm 0.0755	0.4989 \pm 0.1138	0.2571 \pm 0.0423	0.1554 \pm 0.0364	
MIS-DINO	ViT-B	0.3168 \pm 0.1103	0.5698 \pm 0.0540	0.4477 \pm 0.0751	0.3911 \pm 0.1110	0.2452 \pm 0.0927	
MIS-DINOv2	ViT-B	0.2307 \pm 0.0768	0.5397 \pm 0.0740	0.5256 \pm 0.0863	0.2885 \pm 0.0733	0.1776 \pm 0.0627	
MIS-DINOv2	ViT-L	0.2400 \pm 0.0456	0.5553 \pm 0.0914	0.4380 \pm 0.0985	0.3065 \pm 0.0487	0.1868 \pm 0.0414	
ImageNet	ViT-B	0.1871 \pm 0.0268	0.5301 \pm 0.0525	0.5124 \pm 0.1209	0.2416 \pm 0.0403	0.1404 \pm 0.0183	
EndoFM	ViT-B	0.2227 \pm 0.0491	0.5215 \pm 0.0562	0.4467 \pm 0.0976	0.2812 \pm 0.0446	0.1704 \pm 0.0396	
GSViT	EfficientViT	0.2139 \pm 0.0417	0.5198 \pm 0.0622	0.4913 \pm 0.1140	0.2639 \pm 0.0387	0.1625 \pm 0.0329	
EndoViT	ViT-B	0.2082 \pm 0.0543	0.5162 \pm 0.0650	0.4858 \pm 0.0975	0.2683 \pm 0.0546	0.1589 \pm 0.0440	
PeskaVLP	ResNet50	0.2098 \pm 0.0604	0.5147 \pm 0.0584	0.4604 \pm 0.1246	0.2681 \pm 0.0723	0.1592 \pm 0.0471	
SurgeNet	CAFormer18	0.2193 \pm 0.0230	0.5551 \pm 0.0460	0.4690 \pm 0.0271	0.2719 \pm 0.0387	0.1698 \pm 0.0162	
ZEN	ViT-B	0.2269 \pm 0.0341	0.5586 \pm 0.0936	0.4672 \pm 0.0935	0.2895 \pm 0.0446	0.1759 \pm 0.0328	

Table 8 Few-shot evaluation on the Cholec80 dataset for surgical phase recognition (2-shot). The upper block reports results for self-supervised learning pretrained models, and the lower block reports results for existing pretrained models. Best-performing models for each metric are highlighted in bold. Values are reported as mean \pm standard deviation over five independent runs.

Method	Backbone	Video-level			Phase-level		
		F1 score	Accuracy	Precision	Recall	Jaccard	
MIS-MAE	ViT-B	0.3094 \pm 0.0914	0.5685 \pm 0.0424	0.4877 \pm 0.0882	0.3738 \pm 0.0953	0.2417 \pm 0.0765	
MIS-MoCoV3	ViT-B	0.3540 \pm 0.0802	0.5675 \pm 0.0545	0.4608 \pm 0.0949	0.4150 \pm 0.0871	0.2749 \pm 0.0690	
MIS-MSN	ViT-B	0.2490 \pm 0.1093	0.5170 \pm 0.0918	0.4707 \pm 0.1148	0.3114 \pm 0.1153	0.1919 \pm 0.0897	
MIS-DINO	ViT-B	0.4243 \pm 0.0512	0.6456 \pm 0.0361	0.5152 \pm 0.0389	0.4993 \pm 0.0593	0.3346 \pm 0.0394	
MIS-DINOv2	ViT-B	0.3544 \pm 0.0476	0.6230 \pm 0.0203	0.4945 \pm 0.0543	0.4209 \pm 0.0481	0.2782 \pm 0.0404	
MIS-DINOv2	ViT-L	0.4190 \pm 0.0989	0.6579 \pm 0.0556	0.5207 \pm 0.0781	0.4975 \pm 0.0964	0.3362 \pm 0.0869	
ImageNet	ViT-B	0.2765 \pm 0.0649	0.5588 \pm 0.0314	0.4565 \pm 0.0667	0.3300 \pm 0.0645	0.2125 \pm 0.0532	
EndoFM	ViT-B	0.3135 \pm 0.0707	0.5518 \pm 0.0609	0.4167 \pm 0.1123	0.3684 \pm 0.0632	0.2396 \pm 0.0631	
GSViT	EfficientViT	0.2097 \pm 0.0824	0.5046 \pm 0.0852	0.5044 \pm 0.0626	0.2695 \pm 0.0806	0.1607 \pm 0.0667	
EndoViT	ViT-B	0.2818 \pm 0.0916	0.5274 \pm 0.0806	0.4324 \pm 0.1339	0.3449 \pm 0.0961	0.2193 \pm 0.0754	
PeskaVLP	ResNet50	0.2991 \pm 0.1185	0.5521 \pm 0.0754	0.4430 \pm 0.1412	0.3630 \pm 0.1303	0.2322 \pm 0.0981	
SurgeNet	CAFormer18	0.3508 \pm 0.1344	0.6216 \pm 0.0224	0.5849 \pm 0.0708	0.4144 \pm 0.1523	0.2743 \pm 0.1094	
ZEN	ViT-B	0.3635 \pm 0.1223	0.6164 \pm 0.0505	0.4796 \pm 0.0846	0.4399 \pm 0.1321	0.2881 \pm 0.1038	

Table 9 Few-shot evaluation on the Cholec80 dataset for surgical phase recognition (3-shot). The upper block reports results for self-supervised learning pretrained models, and the lower block reports results for existing pretrained models. Best-performing models for each metric are highlighted in bold. Values are reported as mean \pm standard deviation over five independent runs.

Method	Backbone	Video-level			Phase-level		
		F1 score	Accuracy	Precision	Recall	Jaccard	
MIS-MAE	ViT-B	0.3337 \pm 0.0880	0.6059 \pm 0.0450	0.4978 \pm 0.0552	0.3890 \pm 0.0976	0.2643 \pm 0.0770	
MIS-MoCoV3	ViT-B	0.3977 \pm 0.0351	0.6040 \pm 0.0486	0.5248 \pm 0.0529	0.4382 \pm 0.0375	0.3138 \pm 0.0318	
MIS-MSN	ViT-B	0.3070 \pm 0.1053	0.5483 \pm 0.0804	0.4590 \pm 0.1165	0.3712 \pm 0.1132	0.2384 \pm 0.0869	
MIS-DINO	ViT-B	0.4742 \pm 0.0684	0.6862 \pm 0.0124	0.5390 \pm 0.0500	0.5515 \pm 0.0828	0.3852 \pm 0.0571	
MIS-DINOv2	ViT-B	0.4586 \pm 0.0601	0.6737 \pm 0.0231	0.5753 \pm 0.0512	0.5187 \pm 0.0585	0.3687 \pm 0.0517	
MIS-DINOv2	ViT-L	0.5220 \pm 0.0326	0.7331 \pm 0.0152	0.6417 \pm 0.0225	0.5834 \pm 0.0439	0.4298 \pm 0.0240	
ImageNet	ViT-B	0.3647 \pm 0.1054	0.6102 \pm 0.0334	0.5365 \pm 0.0368	0.4151 \pm 0.1081	0.2859 \pm 0.0840	
EndoFM	ViT-B	0.3805 \pm 0.0518	0.5968 \pm 0.0387	0.4982 \pm 0.0505	0.4348 \pm 0.0451	0.2953 \pm 0.0506	
GSViT	EfficientViT	0.2083 \pm 0.0779	0.5566 \pm 0.0803	0.5619 \pm 0.0846	0.2568 \pm 0.0751	0.1617 \pm 0.0647	
EndoViT	ViT-B	0.3299 \pm 0.0779	0.5770 \pm 0.0429	0.4757 \pm 0.0647	0.3898 \pm 0.0845	0.2588 \pm 0.0633	
PeskaVLP	ResNet50	0.4159 \pm 0.0690	0.6277 \pm 0.0464	0.4908 \pm 0.0738	0.4774 \pm 0.0763	0.3343 \pm 0.0632	
SurgeNet	CAFormer18	0.4114 \pm 0.0980	0.6544 \pm 0.0407	0.5406 \pm 0.0487	0.4767 \pm 0.1057	0.3333 \pm 0.0831	
ZEN	ViT-B	0.5338 \pm 0.0387	0.7212 \pm 0.0477	0.5932 \pm 0.0661	0.6084 \pm 0.0246	0.4375 \pm 0.0394	

Table 10 Few-shot evaluation on the Cholec80 dataset for surgical phase recognition (4-shot). The upper block reports results for self-supervised learning pretrained models, and the lower block reports results for existing pretrained models. Best-performing models for each metric are highlighted in bold. Values are reported as mean \pm standard deviation over five independent runs.

Method	Backbone	Video-level			Phase-level		
		F1 score	Accuracy	Precision	Recall	Jaccard	
MIS-MAE	ViT-B	0.4290 \pm 0.0642	0.6521 \pm 0.0276	0.5828 \pm 0.0524	0.4879 \pm 0.0662	0.3458 \pm 0.0548	
MIS-MoCoV3	ViT-B	0.4389 \pm 0.0348	0.6461 \pm 0.0164	0.5613 \pm 0.0173	0.4875 \pm 0.0305	0.3536 \pm 0.0295	
MIS-MSN	ViT-B	0.3747 \pm 0.0743	0.6049 \pm 0.0578	0.5664 \pm 0.0755	0.4347 \pm 0.0565	0.3003 \pm 0.0661	
MIS-DINO	ViT-B	0.5086 \pm 0.0510	0.7105 \pm 0.0134	0.5687 \pm 0.0519	0.5782 \pm 0.0621	0.4139 \pm 0.0395	
MIS-DINOv2	ViT-B	0.4570 \pm 0.0673	0.6991 \pm 0.0143	0.5912 \pm 0.0286	0.5139 \pm 0.0736	0.3775 \pm 0.0522	
MIS-DINOv2	ViT-L	0.6044 \pm 0.0357	0.7710 \pm 0.0149	0.6715 \pm 0.0290	0.6787 \pm 0.0542	0.5072 \pm 0.0345	
ImageNet	ViT-B	0.4033 \pm 0.0261	0.6426 \pm 0.0110	0.5252 \pm 0.0450	0.4496 \pm 0.0274	0.3173 \pm 0.0183	
EndoFM	ViT-B	0.3393 \pm 0.0811	0.6264 \pm 0.0245	0.5632 \pm 0.0209	0.3892 \pm 0.0825	0.2702 \pm 0.0664	
GSViT	EfficientViT	0.2439 \pm 0.0463	0.5940 \pm 0.0063	0.6138 \pm 0.0537	0.2857 \pm 0.0478	0.1897 \pm 0.0350	
EndoViT	ViT-B	0.4129 \pm 0.0368	0.6134 \pm 0.0345	0.5020 \pm 0.0436	0.4703 \pm 0.0245	0.3300 \pm 0.0378	
PeskaVLP	ResNet50	0.4682 \pm 0.0577	0.6567 \pm 0.0211	0.5680 \pm 0.0670	0.5204 \pm 0.0590	0.3800 \pm 0.0505	
SurgeNet	CAFormer18	0.5474 \pm 0.0317	0.7030 \pm 0.0128	0.6140 \pm 0.0149	0.6229 \pm 0.0555	0.4471 \pm 0.0285	
ZEN	ViT-B	0.5489 \pm 0.0834	0.7483 \pm 0.0467	0.6199 \pm 0.0890	0.6170 \pm 0.0734	0.4593 \pm 0.0721	

Table 11 Few-shot evaluation on the Cholec80 dataset for surgical phase recognition (5-shot). The upper block reports results for self-supervised learning pretrained models, and the lower block reports results for existing pretrained models. Best-performing models for each metric are highlighted in bold. Values are reported as mean \pm standard deviation over five independent runs.

Method	Backbone	Video-level			Phase-level		
		F1 score	Accuracy	Precision	Recall	Jaccard	
MIS-MAE	ViT-B	0.4564 \pm 0.0624	0.6589 \pm 0.0415	0.5355 \pm 0.0613	0.5170 \pm 0.0631	0.3726 \pm 0.0564	
MIS-MoCoV3	ViT-B	0.4671 \pm 0.0472	0.6684 \pm 0.0118	0.5550 \pm 0.0490	0.5178 \pm 0.0518	0.3831 \pm 0.0402	
MIS-MSN	ViT-B	0.3900 \pm 0.1066	0.6216 \pm 0.0360	0.5560 \pm 0.0746	0.4439 \pm 0.1082	0.3099 \pm 0.0881	
MIS-SimDINO	ViT-B	0.5645 \pm 0.0730	0.7463 \pm 0.0202	0.6224 \pm 0.0494	0.6280 \pm 0.0824	0.4705 \pm 0.0645	
MIS-DINOv2	ViT-B	0.5416 \pm 0.0095	0.7277 \pm 0.0242	0.6129 \pm 0.0228	0.6028 \pm 0.0136	0.4494 \pm 0.0121	
MIS-DINOv2	ViT-L	0.6055 \pm 0.0649	0.7847 \pm 0.0313	0.6540 \pm 0.0329	0.6778 \pm 0.0833	0.5110 \pm 0.0559	
ImageNet	ViT-B	0.4153 \pm 0.0711	0.6398 \pm 0.0230	0.5544 \pm 0.0543	0.4618 \pm 0.0640	0.3320 \pm 0.0579	
EndoFM	ViT-B	0.3748 \pm 0.0997	0.6323 \pm 0.0269	0.5438 \pm 0.0393	0.4181 \pm 0.0999	0.2982 \pm 0.0796	
GSViT	EfficientViT	0.2637 \pm 0.0397	0.5941 \pm 0.0150	0.6092 \pm 0.0995	0.3038 \pm 0.0403	0.2051 \pm 0.0314	
EndoViT	ViT-B	0.3482 \pm 0.0891	0.6394 \pm 0.0260	0.5828 \pm 0.0796	0.3951 \pm 0.0920	0.2827 \pm 0.0778	
PeskaVLP	ResNet50	0.4626 \pm 0.1362	0.6776 \pm 0.0419	0.6040 \pm 0.0170	0.5198 \pm 0.1476	0.3817 \pm 0.1161	
SurgeNet	CAFormer18	0.5626 \pm 0.0242	0.7234 \pm 0.0213	0.6302 \pm 0.0283	0.6306 \pm 0.0192	0.4613 \pm 0.0232	
ZEN	ViT-B	0.5837 \pm 0.0502	0.7523 \pm 0.0200	0.6320 \pm 0.0182	0.6628 \pm 0.0691	0.4858 \pm 0.0423	

Table 12 Few-shot evaluation on the MultiByPass140 dataset for surgical phase recognition (1-shot). The upper block reports results for self-supervised learning pretrained models, and the lower block reports results for existing pretrained models. Best-performing models for each metric are highlighted in bold. Values are reported as mean \pm standard deviation over five independent runs.

Method	Backbone	Video-level			Phase-level		
		F1 score	Accuracy	Precision	Recall	Jaccard	
MIS-MAE	ViT-B	0.1669 \pm 0.0211	0.4056 \pm 0.0338	0.3892 \pm 0.0571	0.1777 \pm 0.0272	0.0957 \pm 0.0215	
MIS-MoCoV3	ViT-B	0.1889 \pm 0.0208	0.4238 \pm 0.0191	0.4308 \pm 0.0831	0.1935 \pm 0.0242	0.1091 \pm 0.0180	
MIS-MSN	ViT-B	0.1459 \pm 0.0369	0.3708 \pm 0.0314	0.3701 \pm 0.0780	0.1636 \pm 0.0387	0.0852 \pm 0.0290	
MIS-DINO	ViT-B	0.2240 \pm 0.0424	0.5061 \pm 0.0355	0.4760 \pm 0.0756	0.2259 \pm 0.0435	0.1353 \pm 0.0293	
MIS-DINOv2	ViT-B	0.2199 \pm 0.0423	0.5018 \pm 0.0396	0.5138 \pm 0.0962	0.2112 \pm 0.0391	0.1299 \pm 0.0299	
MIS-DINOv2	ViT-L	0.2282 \pm 0.0325	0.5358 \pm 0.0326	0.4221 \pm 0.0970	0.2304 \pm 0.0252	0.1432 \pm 0.0170	
ImageNet	ViT-B	0.1619 \pm 0.0089	0.4081 \pm 0.0442	0.4188 \pm 0.0996	0.1714 \pm 0.0195	0.0910 \pm 0.0068	
EndoFM	ViT-B	0.1841 \pm 0.0178	0.4320 \pm 0.0320	0.4324 \pm 0.0761	0.1851 \pm 0.0296	0.1029 \pm 0.0141	
GSViT	EfficientViT	0.1401 \pm 0.0372	0.3600 \pm 0.0417	0.3859 \pm 0.0688	0.1595 \pm 0.0359	0.0818 \pm 0.0290	
EndoViT	ViT-B	0.1442 \pm 0.0371	0.3592 \pm 0.0369	0.3754 \pm 0.0738	0.1607 \pm 0.0376	0.0822 \pm 0.0279	
PeskaVLP	ResNet50	0.1952 \pm 0.0483	0.4526 \pm 0.0454	0.3761 \pm 0.0833	0.2084 \pm 0.0611	0.1207 \pm 0.0408	
SurgeNet	CAFormer18	0.2252 \pm 0.0360	0.5064 \pm 0.0178	0.4417 \pm 0.0790	0.2214 \pm 0.0371	0.1350 \pm 0.0262	
ZEN	ViT-B	0.2359 \pm 0.0470	0.5348 \pm 0.0433	0.5018 \pm 0.0624	0.2307 \pm 0.0529	0.1440 \pm 0.0326	

Table 13 Few-shot evaluation on the MultiByPass140 dataset for surgical phase recognition (2-shot). The upper block reports results for self-supervised learning pretrained models, and the lower block reports results for existing pretrained models. Best-performing models for each metric are highlighted in bold. Values are reported as mean \pm standard deviation over five independent runs.

Method	Backbone	Video-level			Phase-level		
		F1 score	Accuracy	Precision	Recall	Jaccard	
MIS-MAE	ViT-B	0.2592 \pm 0.0266	0.5032 \pm 0.0517	0.4363 \pm 0.0813	0.2501 \pm 0.0341	0.1583 \pm 0.0214	
MIS-MoCoV3	ViT-B	0.2616 \pm 0.0426	0.4893 \pm 0.0721	0.4597 \pm 0.1196	0.2589 \pm 0.0528	0.1643 \pm 0.0347	
MIS-MSN	ViT-B	0.2429 \pm 0.0297	0.4602 \pm 0.0333	0.4147 \pm 0.1343	0.2362 \pm 0.0154	0.1478 \pm 0.0206	
MIS-DINO	ViT-B	0.3515 \pm 0.0747	0.6439 \pm 0.0616	0.4614 \pm 0.0595	0.3499 \pm 0.0818	0.2458 \pm 0.0658	
MIS-DINOv2	ViT-B	0.3241 \pm 0.0309	0.6032 \pm 0.0571	0.3953 \pm 0.0405	0.3140 \pm 0.0336	0.2129 \pm 0.0235	
MIS-DINOv2	ViT-L	0.3361 \pm 0.0704	0.6456 \pm 0.0378	0.4384 \pm 0.0750	0.3215 \pm 0.0742	0.2261 \pm 0.0626	
ImageNet	ViT-B	0.2303 \pm 0.0455	0.4964 \pm 0.0371	0.4786 \pm 0.1190	0.2204 \pm 0.0501	0.1364 \pm 0.0336	
EndoFM	ViT-B	0.2250 \pm 0.0256	0.4854 \pm 0.0287	0.4425 \pm 0.0934	0.2369 \pm 0.0232	0.1394 \pm 0.0136	
GSViT	EfficientViT	0.2031 \pm 0.0428	0.4242 \pm 0.0449	0.4512 \pm 0.0795	0.2029 \pm 0.0358	0.1210 \pm 0.0306	
EndoViT	ViT-B	0.2067 \pm 0.0542	0.4382 \pm 0.0551	0.3969 \pm 0.0787	0.2151 \pm 0.0424	0.1266 \pm 0.0362	
PeskaVLP	ResNet50	0.2759 \pm 0.0357	0.5609 \pm 0.0409	0.4183 \pm 0.0637	0.2696 \pm 0.0445	0.1719 \pm 0.0279	
SurgeNet	CAFormer18	0.3217 \pm 0.0733	0.6053 \pm 0.0477	0.4505 \pm 0.0467	0.3058 \pm 0.0678	0.2053 \pm 0.0554	
ZEN	ViT-B	0.3574 \pm 0.0484	0.6320 \pm 0.0647	0.4622 \pm 0.0859	0.3395 \pm 0.0585	0.2390 \pm 0.0479	

Table 14 Few-shot evaluation on the MultiByPass140 dataset for surgical phase recognition (3-shot). The upper block reports results for self-supervised learning pretrained models, and the lower block reports results for existing pretrained models. Best-performing models for each metric are highlighted in bold. Values are reported as mean \pm standard deviation over five independent runs.

Method	Backbone	Video-level			Phase-level		
		F1 score	Accuracy	Precision	Recall	Jaccard	
MIS-MAE	ViT-B	0.2930 \pm 0.0238	0.5341 \pm 0.0427	0.4250 \pm 0.0779	0.2770 \pm 0.0232	0.1835 \pm 0.0236	
MIS-MoCoV3	ViT-B	0.2819 \pm 0.0341	0.5223 \pm 0.0564	0.4136 \pm 0.0487	0.2697 \pm 0.0322	0.1789 \pm 0.0292	
MIS-MSN	ViT-B	0.2668 \pm 0.0369	0.4950 \pm 0.0412	0.4447 \pm 0.0918	0.2550 \pm 0.0276	0.1664 \pm 0.0274	
MIS-DINO	ViT-B	0.3742 \pm 0.0330	0.6530 \pm 0.0537	0.5093 \pm 0.1004	0.3577 \pm 0.0546	0.2548 \pm 0.0387	
MIS-DINOv2	ViT-B	0.3175 \pm 0.0192	0.6202 \pm 0.0560	0.4560 \pm 0.0881	0.3182 \pm 0.0129	0.2179 \pm 0.0100	
MIS-DINOv2	ViT-L	0.3635 \pm 0.0509	0.6617 \pm 0.0411	0.5072 \pm 0.0512	0.3467 \pm 0.0513	0.2438 \pm 0.0494	
ImageNet	ViT-B	0.2693 \pm 0.0154	0.5222 \pm 0.0277	0.5353 \pm 0.1212	0.2486 \pm 0.0139	0.1647 \pm 0.0171	
EndoFM	ViT-B	0.2596 \pm 0.0137	0.5024 \pm 0.0321	0.4575 \pm 0.0870	0.2469 \pm 0.0148	0.1625 \pm 0.0107	
GSViT	EfficientViT	0.2191 \pm 0.0204	0.4335 \pm 0.0362	0.4833 \pm 0.0661	0.2167 \pm 0.0154	0.1333 \pm 0.0192	
EndoViT	ViT-B	0.2222 \pm 0.0558	0.4565 \pm 0.0640	0.4340 \pm 0.1051	0.2200 \pm 0.0443	0.1359 \pm 0.0372	
PeskaVLP	ResNet50	0.2858 \pm 0.0110	0.5489 \pm 0.0627	0.4682 \pm 0.1204	0.2868 \pm 0.0201	0.1923 \pm 0.0097	
SurgeNet	CAFormer18	0.3330 \pm 0.0393	0.6285 \pm 0.0476	0.4837 \pm 0.1330	0.3251 \pm 0.0412	0.2261 \pm 0.0385	
ZEN	ViT-B	0.3560 \pm 0.0432	0.6442 \pm 0.0585	0.4653 \pm 0.0824	0.3595 \pm 0.0625	0.2538 \pm 0.0493	

Table 15 Few-shot evaluation on the MultiByPass140 dataset for surgical phase recognition (4-shot). The upper block reports results for self-supervised learning pretrained models, and the lower block reports results for existing pretrained models. Best-performing models for each metric are highlighted in bold. Values are reported as mean \pm standard deviation over five independent runs.

Method	Backbone	Video-level			Phase-level		
		F1 score	Accuracy	Precision	Recall	Jaccard	
MIS-MAE	ViT-B	0.3247 \pm 0.0337	0.5797 \pm 0.0399	0.4512 \pm 0.1184	0.3129 \pm 0.0304	0.2127 \pm 0.0252	
MIS-MoCoV3	ViT-B	0.2867 \pm 0.0226	0.5691 \pm 0.0314	0.5146 \pm 0.1060	0.2775 \pm 0.0403	0.1831 \pm 0.0319	
MIS-MSN	ViT-B	0.2949 \pm 0.0391	0.5274 \pm 0.0317	0.4106 \pm 0.0501	0.2826 \pm 0.0273	0.1856 \pm 0.0302	
MIS-DINO	ViT-B	0.3762 \pm 0.0346	0.6685 \pm 0.0197	0.4945 \pm 0.0982	0.3636 \pm 0.0464	0.2584 \pm 0.0352	
MIS-DINOv2	ViT-B	0.3472 \pm 0.0331	0.6702 \pm 0.0179	0.4664 \pm 0.0620	0.3239 \pm 0.0266	0.2333 \pm 0.0221	
MIS-DINOv2	ViT-L	0.3808 \pm 0.0321	0.6917 \pm 0.0154	0.4734 \pm 0.0731	0.3612 \pm 0.0334	0.2620 \pm 0.0337	
ImageNet	ViT-B	0.2815 \pm 0.0173	0.5422 \pm 0.0278	0.4597 \pm 0.1174	0.2683 \pm 0.0252	0.1782 \pm 0.0118	
EndoFM	ViT-B	0.2729 \pm 0.0198	0.5282 \pm 0.0236	0.5308 \pm 0.1132	0.2602 \pm 0.0404	0.1679 \pm 0.0273	
GSViT	EfficientViT	0.2345 \pm 0.0122	0.4536 \pm 0.0166	0.5173 \pm 0.0600	0.2233 \pm 0.0058	0.1392 \pm 0.0101	
EndoViT	ViT-B	0.2453 \pm 0.0153	0.4817 \pm 0.0196	0.4781 \pm 0.0970	0.2268 \pm 0.0104	0.1418 \pm 0.0123	
PeskaVLP	ResNet50	0.3309 \pm 0.0245	0.6221 \pm 0.0197	0.4456 \pm 0.0886	0.3202 \pm 0.0469	0.2209 \pm 0.0300	
SurgeNet	CAFormer18	0.3703 \pm 0.0410	0.6664 \pm 0.0298	0.4546 \pm 0.0932	0.3688 \pm 0.0538	0.2619 \pm 0.0413	
ZEN	ViT-B	0.3951 \pm 0.0405	0.6789 \pm 0.0265	0.4596 \pm 0.0558	0.3879 \pm 0.0532	0.2758 \pm 0.0471	

Table 16 Few-shot evaluation on the MultiByPass140 dataset for surgical phase recognition (5-shot). The upper block reports results for self-supervised learning pretrained models, and the lower block reports results for existing pretrained models. Best-performing models for each metric are highlighted in bold. Values are reported as mean \pm standard deviation over five independent runs.

Method	Backbone	Video-level			Phase-level		
		F1 score	Accuracy	Precision	Recall	Jaccard	
MIS-MAE	ViT-B	0.3392 \pm 0.0115	0.5824 \pm 0.0269	0.3855 \pm 0.0402	0.3298 \pm 0.0266	0.2281 \pm 0.0161	
MIS-MoCoV3	ViT-B	0.3214 \pm 0.0235	0.5870 \pm 0.0351	0.3984 \pm 0.0870	0.3085 \pm 0.0310	0.2101 \pm 0.0184	
MIS-MSN	ViT-B	0.3006 \pm 0.0302	0.5487 \pm 0.0223	0.3984 \pm 0.0561	0.2884 \pm 0.0213	0.1934 \pm 0.0200	
MIS-DINO	ViT-B	0.3908 \pm 0.0434	0.6840 \pm 0.0241	0.4573 \pm 0.0456	0.3718 \pm 0.0504	0.2680 \pm 0.0410	
MIS-DINOv2	ViT-B	0.3617 \pm 0.0298	0.6668 \pm 0.0224	0.4557 \pm 0.0599	0.3421 \pm 0.0317	0.2486 \pm 0.0201	
MIS-DINOv2	ViT-L	0.3815 \pm 0.0359	0.6870 \pm 0.0171	0.5315 \pm 0.1548	0.3671 \pm 0.0551	0.2673 \pm 0.0396	
ImageNet	ViT-B	0.2860 \pm 0.0197	0.5470 \pm 0.0218	0.4825 \pm 0.1036	0.2706 \pm 0.0217	0.1790 \pm 0.0192	
EndoFM	ViT-B	0.2821 \pm 0.0171	0.5322 \pm 0.0274	0.4771 \pm 0.1155	0.2652 \pm 0.0292	0.1745 \pm 0.0167	
GSViT	EfficientViT	0.2389 \pm 0.0067	0.4613 \pm 0.0148	0.5000 \pm 0.0569	0.2274 \pm 0.0077	0.1445 \pm 0.0080	
EndoViT	ViT-B	0.2509 \pm 0.0110	0.4877 \pm 0.0231	0.3973 \pm 0.0826	0.2430 \pm 0.0198	0.1532 \pm 0.0106	
PeskaVLP	ResNet50	0.3566 \pm 0.0205	0.6298 \pm 0.0086	0.4302 \pm 0.0242	0.3394 \pm 0.0329	0.2403 \pm 0.0203	
SurgeNet	CAFormer18	0.4084 \pm 0.0116	0.6876 \pm 0.0171	0.4731 \pm 0.0688	0.4039 \pm 0.0502	0.2930 \pm 0.0302	
ZEN	ViT-B	0.3975 \pm 0.0320	0.6883 \pm 0.0211	0.5060 \pm 0.0787	0.3757 \pm 0.0497	0.2764 \pm 0.0407	

Table 17 Few-shot evaluation on the AutoLaparo dataset for surgical phase recognition (1-shot). The upper block reports results for self-supervised learning pretrained models, and the lower block reports results for existing pretrained models. Best-performing models for each metric are highlighted in bold. Values are reported as mean \pm standard deviation over five independent runs.

Method	Backbone	Video-level			Phase-level		
		F1 score	Accuracy	Precision	Recall	Jaccard	
MIS-MAE	ViT-B	0.3066 \pm 0.0520	0.4390 \pm 0.0804	0.4586 \pm 0.0313	0.3449 \pm 0.0516	0.2151 \pm 0.0393	
MIS-MoCoV3	ViT-B	0.3374 \pm 0.0975	0.4482 \pm 0.1191	0.4881 \pm 0.1022	0.3654 \pm 0.0893	0.2399 \pm 0.0741	
MIS-MSN	ViT-B	0.2928 \pm 0.0875	0.4208 \pm 0.1013	0.4423 \pm 0.1284	0.3357 \pm 0.0639	0.2074 \pm 0.0621	
MIS-DINO	ViT-B	0.4508 \pm 0.1098	0.5827 \pm 0.1132	0.6206 \pm 0.0921	0.4813 \pm 0.0711	0.3357 \pm 0.0934	
MIS-DINOv2	ViT-B	0.4244 \pm 0.0809	0.5536 \pm 0.0741	0.5891 \pm 0.0627	0.4528 \pm 0.0617	0.3077 \pm 0.0625	
MIS-DINOv2	ViT-L	0.4838 \pm 0.1104	0.6237 \pm 0.0889	0.6421 \pm 0.0985	0.5165 \pm 0.0762	0.3629 \pm 0.0883	
ImageNet	ViT-B	0.2968 \pm 0.1213	0.4373 \pm 0.0882	0.4745 \pm 0.1188	0.3455 \pm 0.1045	0.2071 \pm 0.0896	
EndoFM	ViT-B	0.2751 \pm 0.0556	0.4003 \pm 0.0409	0.4969 \pm 0.0743	0.3198 \pm 0.0408	0.1905 \pm 0.0359	
GSViT	EfficientViT	0.2863 \pm 0.0965	0.4313 \pm 0.1015	0.4467 \pm 0.1134	0.3313 \pm 0.0761	0.2025 \pm 0.0702	
EndoViT	ViT-B	0.2788 \pm 0.0807	0.4105 \pm 0.0450	0.4860 \pm 0.1202	0.3313 \pm 0.0597	0.1947 \pm 0.0568	
PeskaVLP	ResNet50	0.3439 \pm 0.1467	0.5149 \pm 0.1452	0.5379 \pm 0.1546	0.3783 \pm 0.1198	0.2571 \pm 0.1139	
SurgeNet	CAFormer18	0.3445 \pm 0.1193	0.4972 \pm 0.0942	0.5602 \pm 0.1037	0.3890 \pm 0.0992	0.2517 \pm 0.0936	
ZEN	ViT-B	0.4656 \pm 0.1010	0.6078 \pm 0.1089	0.6321 \pm 0.0965	0.4902 \pm 0.0706	0.3565 \pm 0.0803	

Table 18 Few-shot evaluation on the AutoLaparo dataset for surgical phase recognition (2-shot). The upper block reports results for self-supervised learning pretrained models, and the lower block reports results for existing pretrained models. Best-performing models for each metric are highlighted in bold. Values are reported as mean \pm standard deviation over five independent runs.

Method	Backbone	Video-level			Phase-level		
		F1 score	Accuracy	Precision	Recall	Jaccard	
MIS-MAE	ViT-B	0.3635 \pm 0.0496	0.5118 \pm 0.0647	0.5364 \pm 0.0803	0.4019 \pm 0.0551	0.2641 \pm 0.0415	
MIS-MoCoV3	ViT-B	0.3787 \pm 0.0885	0.5214 \pm 0.1031	0.4629 \pm 0.1145	0.4074 \pm 0.0792	0.2783 \pm 0.0732	
MIS-MSN	ViT-B	0.3304 \pm 0.0427	0.4791 \pm 0.0562	0.4651 \pm 0.0436	0.3632 \pm 0.0381	0.2346 \pm 0.0315	
MIS-DINO	ViT-B	0.5410 \pm 0.0595	0.6846 \pm 0.0670	0.6763 \pm 0.0688	0.5530 \pm 0.0528	0.4235 \pm 0.0588	
MIS-DINOv2	ViT-B	0.4851 \pm 0.0542	0.6409 \pm 0.0706	0.6409 \pm 0.0743	0.4945 \pm 0.0463	0.3678 \pm 0.0462	
MIS-DINOv2	ViT-L	0.5375 \pm 0.0383	0.7081 \pm 0.0458	0.6789 \pm 0.0672	0.5562 \pm 0.0315	0.4293 \pm 0.0345	
ImageNet	ViT-B	0.3409 \pm 0.0621	0.4978 \pm 0.0716	0.4955 \pm 0.0812	0.3795 \pm 0.0464	0.2421 \pm 0.0437	
EndoFM	ViT-B	0.3017 \pm 0.1075	0.4656 \pm 0.1106	0.4548 \pm 0.0483	0.3440 \pm 0.0896	0.2211 \pm 0.0839	
GSViT	EfficientViT	0.3030 \pm 0.0652	0.4577 \pm 0.1011	0.4628 \pm 0.0752	0.3435 \pm 0.0567	0.2158 \pm 0.0494	
EndoViT	ViT-B	0.3205 \pm 0.0564	0.4897 \pm 0.0786	0.4635 \pm 0.0747	0.3529 \pm 0.0609	0.2316 \pm 0.0446	
PeskaVLP	ResNet50	0.4717 \pm 0.0509	0.6200 \pm 0.0858	0.5831 \pm 0.0828	0.4803 \pm 0.0449	0.3552 \pm 0.0434	
SurgeNet	CAFormer18	0.5030 \pm 0.0554	0.6470 \pm 0.0773	0.6148 \pm 0.0686	0.5257 \pm 0.0419	0.3952 \pm 0.0489	
ZEN	ViT-B	0.5330 \pm 0.0660	0.6886 \pm 0.0678	0.6517 \pm 0.0955	0.5462 \pm 0.0436	0.4166 \pm 0.0608	

Table 19 Few-shot evaluation on the AutoLaparo dataset for surgical phase recognition (3-shot). The upper block reports results for self-supervised learning pretrained models, and the lower block reports results for existing pretrained models. Best-performing models for each metric are highlighted in bold. Values are reported as mean \pm standard deviation over five independent runs.

Method	Backbone	Video-level			Phase-level		
		F1 score	Accuracy	Precision	Recall	Jaccard	
MIS-MAE	ViT-B	0.4438 \pm 0.0509	0.5776 \pm 0.0563	0.6240 \pm 0.0327	0.4595 \pm 0.0548	0.3245 \pm 0.0454	
MIS-MoCoV3	ViT-B	0.5150 \pm 0.0386	0.6554 \pm 0.0263	0.6230 \pm 0.0334	0.5284 \pm 0.0402	0.3984 \pm 0.0346	
MIS-MSN	ViT-B	0.3534 \pm 0.0663	0.5115 \pm 0.0740	0.5882 \pm 0.0856	0.3761 \pm 0.0512	0.2529 \pm 0.0482	
MIS-DINO	ViT-B	0.5993 \pm 0.0807	0.7509 \pm 0.0376	0.6972 \pm 0.0580	0.6134 \pm 0.0679	0.4912 \pm 0.0719	
MIS-DINOv2	ViT-B	0.6126 \pm 0.0877	0.7218 \pm 0.0640	0.7125 \pm 0.0654	0.6274 \pm 0.0867	0.4965 \pm 0.0896	
MIS-DINOv2	ViT-L	0.6296 \pm 0.0660	0.7699 \pm 0.0381	0.7098 \pm 0.0528	0.6531 \pm 0.0605	0.5343 \pm 0.0630	
ImageNet	ViT-B	0.3782 \pm 0.0877	0.5082 \pm 0.0358	0.4944 \pm 0.0509	0.4196 \pm 0.0893	0.2717 \pm 0.0708	
EndoFM	ViT-B	0.4120 \pm 0.0439	0.5600 \pm 0.0459	0.5733 \pm 0.0629	0.4378 \pm 0.0467	0.3003 \pm 0.0425	
GSViT	EfficientViT	0.3160 \pm 0.0460	0.4596 \pm 0.0644	0.4662 \pm 0.0749	0.3391 \pm 0.0622	0.2208 \pm 0.0381	
EndoViT	ViT-B	0.4059 \pm 0.0646	0.5454 \pm 0.0909	0.5884 \pm 0.0647	0.4232 \pm 0.0561	0.2984 \pm 0.0456	
PeskaVLP	ResNet50	0.5615 \pm 0.0440	0.7072 \pm 0.0301	0.6846 \pm 0.0494	0.5679 \pm 0.0415	0.4482 \pm 0.0404	
SurgeNet	CAFormer18	0.5810 \pm 0.0988	0.7111 \pm 0.0966	0.6620 \pm 0.0768	0.6141 \pm 0.0951	0.4740 \pm 0.1026	
ZEN	ViT-B	0.6087 \pm 0.0769	0.7542 \pm 0.0412	0.7251 \pm 0.0681	0.6237 \pm 0.0623	0.5024 \pm 0.0684	

Table 20 Few-shot evaluation on the AutoLaparo dataset for surgical phase recognition (4-shot). The upper block reports results for self-supervised learning pretrained models, and the lower block reports results for existing pretrained models. Best-performing models for each metric are highlighted in bold. Values are reported as mean \pm standard deviation over five independent runs.

Method	Backbone	Video-level			Phase-level		
		F1 score	Accuracy	Precision	Recall	Jaccard	
MIS-MAE	ViT-B	0.4672 \pm 0.0590	0.6102 \pm 0.0391	0.6428 \pm 0.0322	0.4886 \pm 0.0592	0.3561 \pm 0.0552	
MIS-MoCoV3	ViT-B	0.5731 \pm 0.0348	0.7057 \pm 0.0272	0.6652 \pm 0.0188	0.5926 \pm 0.0505	0.4481 \pm 0.0447	
MIS-MSN	ViT-B	0.3756 \pm 0.0666	0.5258 \pm 0.0384	0.5899 \pm 0.0767	0.3997 \pm 0.0478	0.2689 \pm 0.0420	
MIS-DINO	ViT-B	0.6656 \pm 0.0572	0.7995 \pm 0.0245	0.7432 \pm 0.0330	0.6832 \pm 0.0575	0.5699 \pm 0.0568	
MIS-DINOv2	ViT-B	0.6138 \pm 0.0603	0.7515 \pm 0.0356	0.7171 \pm 0.0194	0.6339 \pm 0.0558	0.5065 \pm 0.0587	
MIS-DINOv2	ViT-L	0.6677 \pm 0.0510	0.8040 \pm 0.0255	0.7719 \pm 0.0360	0.6759 \pm 0.0498	0.5702 \pm 0.0555	
ImageNet	ViT-B	0.4690 \pm 0.0411	0.5966 \pm 0.0655	0.6072 \pm 0.0334	0.5004 \pm 0.0338	0.3542 \pm 0.0333	
EndoFM	ViT-B	0.4321 \pm 0.0622	0.6000 \pm 0.0298	0.5772 \pm 0.0237	0.4617 \pm 0.0415	0.3233 \pm 0.0463	
GSViT	EfficientViT	0.3766 \pm 0.0678	0.5544 \pm 0.0762	0.5937 \pm 0.0818	0.3985 \pm 0.0686	0.2756 \pm 0.0508	
EndoViT	ViT-B	0.4608 \pm 0.0357	0.5920 \pm 0.0445	0.6049 \pm 0.0639	0.4778 \pm 0.0416	0.3422 \pm 0.0306	
PeskaVLP	ResNet50	0.6103 \pm 0.0325	0.7550 \pm 0.0157	0.7152 \pm 0.0308	0.6174 \pm 0.0332	0.4972 \pm 0.0380	
SurgeNet	CAFormer18	0.6291 \pm 0.0287	0.7594 \pm 0.0104	0.7361 \pm 0.0369	0.6430 \pm 0.0318	0.5118 \pm 0.0308	
ZEN	ViT-B	0.6695 \pm 0.0483	0.8028 \pm 0.0154	0.7817 \pm 0.0404	0.6699 \pm 0.0426	0.5645 \pm 0.0452	

Table 21 Few-shot evaluation on the AutoLaparo dataset for surgical phase recognition (5-shot). The upper block reports results for self-supervised learning pretrained models, and the lower block reports results for existing pretrained models. Best-performing models for each metric are highlighted in bold. Values are reported as mean \pm standard deviation over five independent runs.

Method	Backbone	Video-level			Phase-level		
		F1 score	Accuracy	Precision	Recall	Jaccard	
MIS-MAE	ViT-B	0.5128 \pm 0.0828	0.6455 \pm 0.0529	0.6532 \pm 0.0795	0.5272 \pm 0.0727	0.3902 \pm 0.0738	
MIS-MoCoV3	ViT-B	0.6037 \pm 0.0350	0.7311 \pm 0.0210	0.6914 \pm 0.0359	0.6092 \pm 0.0317	0.4740 \pm 0.0306	
MIS-MSN	ViT-B	0.4568 \pm 0.0889	0.5888 \pm 0.0765	0.6394 \pm 0.0600	0.4531 \pm 0.0780	0.3292 \pm 0.0677	
MIS-DINO	ViT-B	0.6647 \pm 0.0432	0.7927 \pm 0.0182	0.7634 \pm 0.0585	0.6675 \pm 0.0326	0.5520 \pm 0.0339	
MIS-DINOv2	ViT-B	0.6503 \pm 0.0416	0.7737 \pm 0.0182	0.7294 \pm 0.0217	0.6597 \pm 0.0462	0.5386 \pm 0.0408	
MIS-DINOv2	ViT-L	0.7024 \pm 0.0232	0.8113 \pm 0.0138	0.7525 \pm 0.0262	0.7218 \pm 0.0235	0.6088 \pm 0.0174	
ImageNet	ViT-B	0.5429 \pm 0.0215	0.6620 \pm 0.0395	0.6314 \pm 0.0429	0.5628 \pm 0.0181	0.4213 \pm 0.0211	
EndoFM	ViT-B	0.4312 \pm 0.1189	0.5667 \pm 0.0719	0.5798 \pm 0.0885	0.4620 \pm 0.0980	0.3158 \pm 0.0947	
GSViT	EfficientViT	0.3987 \pm 0.0582	0.5505 \pm 0.0324	0.6109 \pm 0.0436	0.4077 \pm 0.0376	0.2865 \pm 0.0418	
EndoViT	ViT-B	0.4792 \pm 0.0909	0.6048 \pm 0.0648	0.5863 \pm 0.0542	0.4972 \pm 0.0885	0.3586 \pm 0.0797	
PeskaVLP	ResNet50	0.6222 \pm 0.0224	0.7520 \pm 0.0147	0.7092 \pm 0.0494	0.6153 \pm 0.0229	0.4997 \pm 0.0251	
SurgeNet	CAFormer18	0.6521 \pm 0.0612	0.7710 \pm 0.0323	0.7651 \pm 0.0607	0.6501 \pm 0.0550	0.5303 \pm 0.0553	
ZEN	ViT-B	0.7069 \pm 0.0345	0.8112 \pm 0.0128	0.7987 \pm 0.0382	0.7122 \pm 0.0477	0.5994 \pm 0.0405	

Table 22 Triplet recognition performance on the CholecT50 dataset using fine-tuned backbones. The upper block reports results for self-supervised learning pretrained models, and the lower block reports results for existing pretrained models. Best-performing models for each metric are highlighted in bold. Values are reported as mean \pm standard deviation over five independent runs.

Method	Backbone	AP _I	AP _V	AP _T	AP _{IV}	AP _{IT}	AP _{IVT}
MIS-MAE	ViT-B	0.7486 \pm 0.0245	0.4897 \pm 0.0123	0.3760 \pm 0.0142	0.2771 \pm 0.0081	0.3144 \pm 0.0202	0.2453 \pm 0.0194
MIS-MoCoV3	ViT-B	0.7920 \pm 0.0075	0.5092 \pm 0.0042	0.3697 \pm 0.0136	0.2959 \pm 0.0041	0.3223 \pm 0.0116	0.2497 \pm 0.0087
MIS-MSN	ViT-B	0.8354 \pm 0.0066	0.5534 \pm 0.0067	0.4000 \pm 0.0095	0.3203 \pm 0.0046	0.3556 \pm 0.0115	0.2789 \pm 0.0104
MIS-DINO	ViT-B	0.8361 \pm 0.0119	0.5559 \pm 0.0085	0.3970 \pm 0.0089	0.3151 \pm 0.0042	0.3308 \pm 0.0141	0.2663 \pm 0.0078
MIS-DINOv2	ViT-B	0.8280 \pm 0.0060	0.5523 \pm 0.0114	0.4243 \pm 0.0243	0.3216 \pm 0.0089	0.3635 \pm 0.0176	0.2813 \pm 0.0125
MIS-DINOv2	ViT-L	0.8540 \pm 0.0051	0.5697 \pm 0.0162	0.4326 \pm 0.0152	0.3352 \pm 0.0128	0.3800 \pm 0.0147	0.2937 \pm 0.0130
ImageNet	ViT-B	0.8091 \pm 0.0131	0.5284 \pm 0.0120	0.3940 \pm 0.0152	0.3026 \pm 0.0112	0.3409 \pm 0.0134	0.2657 \pm 0.0158
EndoFM	ViT-B	0.7818 \pm 0.0178	0.5106 \pm 0.0134	0.3739 \pm 0.0099	0.2897 \pm 0.0066	0.3277 \pm 0.0065	0.2520 \pm 0.0108
GSViT	EfficientViT	0.3227 \pm 0.0113	0.2112 \pm 0.0059	0.1591 \pm 0.0046	0.1108 \pm 0.0051	0.0843 \pm 0.0023	0.0676 \pm 0.0058
EndoViT	ViT-B	0.7324 \pm 0.0205	0.4863 \pm 0.0094	0.3658 \pm 0.0075	0.2730 \pm 0.0069	0.3119 \pm 0.0171	0.2449 \pm 0.0112
PeskaVLP	ResNet50	0.8124 \pm 0.0046	0.5458 \pm 0.0092	0.3858 \pm 0.0113	0.3152 \pm 0.0071	0.3419 \pm 0.0106	0.2604 \pm 0.0123
SurgeNet	CAFormer18	0.8322 \pm 0.0148	0.5461 \pm 0.0197	0.3980 \pm 0.0184	0.3173 \pm 0.0179	0.3383 \pm 0.0242	0.2691 \pm 0.0158
ZEN	ViT-B	0.8611 \pm 0.0043	0.5898 \pm 0.0079	0.4607 \pm 0.0170	0.3515 \pm 0.0033	0.4015 \pm 0.0112	0.3207 \pm 0.0135

Table 23 Triplet recognition performance on the LLS48 dataset using fine-tuned backbones. The upper block reports results for self-supervised learning pretrained models, and the lower block reports results for existing pretrained models. Best-performing models for each metric are highlighted in bold. Values are reported as mean \pm standard deviation over five independent runs.

Method	Backbone	AP _I	AP _V	AP _T	AP _{IV}	AP _{IT}	AP _{IVT}
MIS-MAE	ViT-B	0.4309 \pm 0.0108	0.2895 \pm 0.0166	0.2780 \pm 0.0224	0.2598 \pm 0.0079	0.2337 \pm 0.0205	0.2276 \pm 0.0142
MIS-MoCoV3	ViT-B	0.4640 \pm 0.0139	0.3108 \pm 0.0257	0.2751 \pm 0.0132	0.2701 \pm 0.0132	0.2015 \pm 0.0157	0.1677 \pm 0.0088
MIS-MSN	ViT-B	0.5857 \pm 0.0144	0.4828 \pm 0.0344	0.3760 \pm 0.0201	0.3893 \pm 0.0112	0.3362 \pm 0.0218	0.3138 \pm 0.0085
MIS-DINO	ViT-B	0.5930 \pm 0.0146	0.4555 \pm 0.0084	0.3999 \pm 0.0290	0.3923 \pm 0.0188	0.3417 \pm 0.0239	0.3138 \pm 0.0198
MIS-DINOv2	ViT-B	0.5240 \pm 0.0206	0.4025 \pm 0.0384	0.3348 \pm 0.0298	0.3518 \pm 0.0277	0.2926 \pm 0.0204	0.2727 \pm 0.0107
MIS-DINOv2	ViT-L	0.5978 \pm 0.0305	0.4790 \pm 0.0549	0.3866 \pm 0.0347	0.4029 \pm 0.0328	0.3376 \pm 0.0290	0.3114 \pm 0.0197
ImageNet	ViT-B	0.5422 \pm 0.0280	0.4061 \pm 0.0284	0.3609 \pm 0.0246	0.3599 \pm 0.0138	0.2976 \pm 0.0117	0.2768 \pm 0.0071
EndoFM	ViT-B	0.5222 \pm 0.0243	0.3789 \pm 0.0476	0.3290 \pm 0.0176	0.3439 \pm 0.0225	0.2870 \pm 0.0173	0.2672 \pm 0.0112
GSViT	EfficientViT	0.2310 \pm 0.0314	0.2001 \pm 0.0357	0.1443 \pm 0.0228	0.1470 \pm 0.0220	0.0909 \pm 0.0171	0.0969 \pm 0.0149
EndoViT	ViT-B	0.4374 \pm 0.0131	0.3095 \pm 0.0213	0.2752 \pm 0.0133	0.2772 \pm 0.0134	0.2366 \pm 0.0161	0.2203 \pm 0.0130
PeskaVLP	ResNet50	0.5489 \pm 0.0160	0.4481 \pm 0.0232	0.3929 \pm 0.0218	0.3838 \pm 0.0185	0.3329 \pm 0.0192	0.2956 \pm 0.0134
SurgeNet	CAFormer18	0.5375 \pm 0.0217	0.3932 \pm 0.0385	0.3376 \pm 0.0216	0.3495 \pm 0.0352	0.3035 \pm 0.0162	0.2731 \pm 0.0193
ZEN	ViT-B	0.5979 \pm 0.0283	0.5086 \pm 0.0545	0.4243 \pm 0.0269	0.4388 \pm 0.0345	0.3701 \pm 0.0250	0.3419 \pm 0.0162

Table 24 Triplet recognition performance on the CholecT50 dataset using frozen backbones. The upper block reports results for self-supervised learning pretrained models, and the lower block reports results for existing pretrained models. Best-performing models for each metric are highlighted in bold. Values are reported as mean \pm standard deviation over five independent runs.

Method	Backbone	AP _I	AP _V	AP _T	AP _{IV}	AP _{IT}	AP _{IVT}
MIS-MAE	ViT-B	0.3770 \pm 0.0027	0.2645 \pm 0.0038	0.2178 \pm 0.0061	0.1354 \pm 0.0013	0.1239 \pm 0.0051	0.0927 \pm 0.0042
MIS-MoCoV3	ViT-B	0.4629 \pm 0.0051	0.2993 \pm 0.0037	0.2357 \pm 0.0011	0.1482 \pm 0.0015	0.1219 \pm 0.0009	0.0876 \pm 0.0006
MIS-MSN	ViT-B	0.3869 \pm 0.0081	0.2794 \pm 0.0048	0.2546 \pm 0.0150	0.1417 \pm 0.0046	0.1341 \pm 0.0033	0.1044 \pm 0.0084
MIS-DINO	ViT-B	0.5999 \pm 0.0200	0.4122 \pm 0.0089	0.3590 \pm 0.0025	0.2258 \pm 0.0080	0.2489 \pm 0.0050	0.1986 \pm 0.0059
MIS-DINOv2	ViT-B	0.6980 \pm 0.0098	0.4698 \pm 0.0043	0.3554 \pm 0.0048	0.2571 \pm 0.0030	0.2777 \pm 0.0102	0.2146 \pm 0.0076
MIS-DINOv2	ViT-L	0.8053 \pm 0.0020	0.5348 \pm 0.0053	0.4090 \pm 0.0074	0.3072 \pm 0.0049	0.3348 \pm 0.0081	0.2634 \pm 0.0036
ImageNet	ViT-B	0.5222 \pm 0.0033	0.3520 \pm 0.0025	0.2509 \pm 0.0051	0.1851 \pm 0.0041	0.1536 \pm 0.0049	0.1112 \pm 0.0026
EndoFM	ViT-B	0.4315 \pm 0.0066	0.3095 \pm 0.0033	0.2362 \pm 0.0025	0.1549 \pm 0.0024	0.1419 \pm 0.0018	0.1099 \pm 0.0038
GSViT	EfficientViT	0.2624 \pm 0.0032	0.1668 \pm 0.0022	0.1209 \pm 0.0019	0.0838 \pm 0.0012	0.0581 \pm 0.0010	0.0459 \pm 0.0015
EndoViT	ViT-B	0.3817 \pm 0.0095	0.2712 \pm 0.0037	0.2033 \pm 0.0025	0.1381 \pm 0.0022	0.1197 \pm 0.0034	0.0915 \pm 0.0028
PeskaVLP	ResNet50	0.5624 \pm 0.0067	0.3992 \pm 0.0048	0.2646 \pm 0.0073	0.2045 \pm 0.0032	0.1676 \pm 0.0033	0.1321 \pm 0.0034
SurgeNet	CAFormer18	0.6110 \pm 0.0112	0.4363 \pm 0.0073	0.3472 \pm 0.0094	0.2284 \pm 0.0038	0.2420 \pm 0.0145	0.1897 \pm 0.0060
ZEN	ViT-B	0.8048 \pm 0.0036	0.5253 \pm 0.0037	0.4170 \pm 0.0068	0.3012 \pm 0.0048	0.3401 \pm 0.0063	0.2654 \pm 0.0124

Table 25 Triplet recognition performance on the LLS48 dataset using frozen backbones. The upper block reports results for self-supervised learning pretrained models, and the lower block reports results for existing pretrained models. Best-performing models for each metric are highlighted in bold. Values are reported as mean \pm standard deviation over five independent runs.

Method	Backbone	AP _I	AP _V	AP _T	AP _{IV}	AP _{IT}	AP _{IVT}
MIS-MAE	ViT-B	0.3274 \pm 0.0239	0.1933 \pm 0.0192	0.1913 \pm 0.0167	0.1886 \pm 0.0160	0.1301 \pm 0.0113	0.1308 \pm 0.0119
MIS-MoCoV3	ViT-B	0.3759 \pm 0.0063	0.2176 \pm 0.0081	0.1981 \pm 0.0056	0.1874 \pm 0.0062	0.1238 \pm 0.0049	0.1130 \pm 0.0036
MIS-MSN	ViT-B	0.4419 \pm 0.0503	0.3238 \pm 0.0441	0.2404 \pm 0.0121	0.2623 \pm 0.0295	0.2206 \pm 0.0096	0.1742 \pm 0.0033
MIS-DINO	ViT-B	0.5764 \pm 0.0151	0.4519 \pm 0.0304	0.3621 \pm 0.0184	0.3588 \pm 0.0122	0.3045 \pm 0.0169	0.2834 \pm 0.0109
MIS-DINOv2	ViT-B	0.6014 \pm 0.0209	0.4922 \pm 0.0685	0.3876 \pm 0.0352	0.3948 \pm 0.0266	0.3090 \pm 0.0153	0.2829 \pm 0.0084
MIS-DINOv2	ViT-L	0.6138 \pm 0.0085	0.5678 \pm 0.0350	0.4799 \pm 0.0082	0.4653 \pm 0.0088	0.3716 \pm 0.0113	0.3476 \pm 0.0065
ImageNet	ViT-B	0.3815 \pm 0.0146	0.3114 \pm 0.0194	0.2036 \pm 0.0065	0.2410 \pm 0.0101	0.1636 \pm 0.0027	0.1415 \pm 0.0032
EndoFM	ViT-B	0.3685 \pm 0.0069	0.2596 \pm 0.0155	0.1892 \pm 0.0082	0.2196 \pm 0.0069	0.1423 \pm 0.0024	0.1319 \pm 0.0036
GSViT	EfficientViT	0.1642 \pm 0.0102	0.1315 \pm 0.0121	0.1098 \pm 0.0130	0.0895 \pm 0.0054	0.0712 \pm 0.0059	0.0717 \pm 0.0073
EndoViT	ViT-B	0.2985 \pm 0.0226	0.1896 \pm 0.0226	0.1794 \pm 0.0176	0.1709 \pm 0.0080	0.1213 \pm 0.0063	0.1089 \pm 0.0035
PeskaVLP	ResNet50	0.3775 \pm 0.0048	0.3247 \pm 0.0359	0.2328 \pm 0.0133	0.2677 \pm 0.0190	0.1689 \pm 0.0070	0.1570 \pm 0.0015
SurgeNet	CAFormer18	0.4862 \pm 0.0348	0.3689 \pm 0.0452	0.2915 \pm 0.0060	0.3070 \pm 0.0238	0.2494 \pm 0.0170	0.2383 \pm 0.0094
ZEN	ViT-B	0.5710 \pm 0.0162	0.5163 \pm 0.0141	0.3769 \pm 0.0192	0.4323 \pm 0.0154	0.3161 \pm 0.0147	0.2924 \pm 0.0088

Table 26 Skill assessment performance on the Cholec80-CVS dataset with frozen and fine-tuned backbones. The upper block reports results for self-supervised learning pretrained models, and the lower block reports results for existing pretrained models. Performance is evaluated using mAP and macro F1 score for both frozen and fine-tuned backbone settings. Best-performing models for each metric are highlighted in bold. Values are reported as mean \pm standard deviation over five independent runs.

Method	Backbone	Frozen backbone		Fine-tuned backbone	
		mAP	F1 score	mAP	F1 score
MIS-MAE	ViT-B	0.3251 \pm 0.0183	0.1761 \pm 0.0510	0.3676 \pm 0.0129	0.2453 \pm 0.0837
MIS-MoCoV3	ViT-B	0.3559 \pm 0.0292	0.2280 \pm 0.0106	0.3665 \pm 0.0178	0.3065 \pm 0.0382
MIS-MSN	ViT-B	0.3111 \pm 0.0138	0.2021 \pm 0.0498	0.3509 \pm 0.0135	0.3390 \pm 0.0617
MIS-DINO	ViT-B	0.3606 \pm 0.0361	0.3389 \pm 0.0258	0.3628 \pm 0.0307	0.3346 \pm 0.0220
MIS-DINOv2	ViT-B	0.3526 \pm 0.0088	0.2679 \pm 0.0223	0.3714 \pm 0.0262	0.3062 \pm 0.0221
MIS-DINOv2	ViT-L	0.3557 \pm 0.0101	0.3167 \pm 0.0294	0.3695 \pm 0.0234	0.3038 \pm 0.0477
ImageNet	ViT-B	0.3684 \pm 0.0209	0.2821 \pm 0.0190	0.3722 \pm 0.0303	0.2976 \pm 0.0309
EndoFM	ViT-B	0.3278 \pm 0.0219	0.1721 \pm 0.0366	0.3595 \pm 0.0172	0.2952 \pm 0.0323
GSViT	EfficientViT	0.3126 \pm 0.0203	0.2648 \pm 0.0535	0.3037 \pm 0.0185	0.2088 \pm 0.0487
EndoViT	ViT-B	0.3062 \pm 0.0213	0.1118 \pm 0.1154	0.3568 \pm 0.0134	0.2662 \pm 0.0202
PeskaVLP	ResNet50	0.3692 \pm 0.0306	0.2331 \pm 0.0220	0.3815 \pm 0.0094	0.2748 \pm 0.0172
SurgeNet	CAFormer18	0.3305 \pm 0.0312	0.3265 \pm 0.0354	0.3468 \pm 0.0136	0.2872 \pm 0.0250
ZEN	ViT-B	0.3820 \pm 0.0242	0.3698 \pm 0.0682	0.3856 \pm 0.0230	0.3322 \pm 0.0446

Table 27 Semantic segmentation performance with fine-tuned backbones. Results are reported on CholecSeg8k, DSAD, and GraSP datasets using Dice similarity coefficient (DSC, higher is better) and 95th percentile Hausdorff distance (HD95, lower is better). The upper block reports results for self-supervised learning pretrained models, and the lower block reports results for existing pretrained models. Best-performing models for each metric are highlighted in bold. Values are reported as mean \pm standard deviation over five independent runs.

Method	Backbone	CholecSeg8k		DSAD		GraSP	
		DSC \uparrow	HD95 \downarrow	DSC \uparrow	HD95 \downarrow	DSC \uparrow	HD95 \downarrow
MIS-MAE	ViT-B	0.6916 \pm 0.0280	34.8959 \pm 6.9566	0.2458 \pm 0.0277	62.1893 \pm 5.7180	0.6744 \pm 0.0393	20.2501 \pm 5.0924
MIS-MoCoV3	ViT-B	0.7828 \pm 0.0145	26.8623 \pm 1.6089	0.3217 \pm 0.0206	45.5967 \pm 2.9430	0.7280 \pm 0.0052	16.9154 \pm 0.7323
MIS-MSN	ViT-B	0.7990 \pm 0.0059	23.7916 \pm 1.6266	0.4027 \pm 0.0526	44.9000 \pm 3.5351	0.7380 \pm 0.0072	15.9382 \pm 0.7840
MIS-DINO	ViT-B	0.8020 \pm 0.0095	22.3890 \pm 2.2561	0.4087 \pm 0.0437	40.0732 \pm 3.1323	0.7538 \pm 0.0052	14.2806 \pm 1.0306
MIS-DINO v2	ViT-B	0.8018 \pm 0.0122	21.2345 \pm 1.0944	0.3621 \pm 0.0411	40.9867 \pm 3.2428	0.7743 \pm 0.0057	12.0440 \pm 0.4085
MIS-DINO v2	ViT-L	0.7192 \pm 0.0564	34.5400 \pm 8.2258	0.1982 \pm 0.0422	61.4032 \pm 8.9463	0.6367 \pm 0.1327	24.0193 \pm 11.5118
ImageNet	ViT-B	0.7554 \pm 0.0201	27.7075 \pm 1.9578	0.2739 \pm 0.0276	48.8271 \pm 3.3750	0.7044 \pm 0.0087	17.5523 \pm 1.2971
EndoFM	ViT-B	0.7190 \pm 0.0259	35.1930 \pm 3.1623	0.2542 \pm 0.0269	58.0185 \pm 3.5420	0.6766 \pm 0.0122	22.4027 \pm 1.9139
GSViT	EfficientViT	0.5961 \pm 0.0170	46.4264 \pm 3.5436	0.2167 \pm 0.0259	60.5168 \pm 7.3890	0.4996 \pm 0.0168	37.0787 \pm 2.7134
EndoViT	ViT-B	0.7018 \pm 0.0133	30.8534 \pm 2.4691	0.2546 \pm 0.0330	60.6693 \pm 3.4926	0.6925 \pm 0.0093	19.1756 \pm 1.4426
PeskaVLP	ResNet50	0.7530 \pm 0.0192	29.6100 \pm 1.3554	0.3225 \pm 0.0353	50.9648 \pm 2.6621	0.7454 \pm 0.0110	17.6964 \pm 1.3970
SurgeNet	CAFormer18	0.6585 \pm 0.0290	43.4978 \pm 5.5861	0.2324 \pm 0.0279	67.4836 \pm 7.4230	0.5758 \pm 0.0255	33.1859 \pm 2.4024
ZEN	ViT-B	0.8187 \pm 0.0089	20.4475 \pm 1.4726	0.3754 \pm 0.0205	36.3318 \pm 1.7441	0.7812 \pm 0.0038	11.5334 \pm 0.7093

Table 28 Semantic segmentation performance with frozen backbones. Results are reported on CholecSeg8k, DSAD, and GraSP datasets using Dice similarity coefficient (DSC, higher is better) and 95th percentile Hausdorff distance (HD95, lower is better). The upper block reports results for self-supervised learning pretrained models, and the lower block reports results for existing pretrained models. Best-performing models for each metric are highlighted in bold. Values are reported as mean \pm standard deviation over five independent runs.

Method	Backbone	CholecSeg8k		DSAD		GraSP	
		DSC \uparrow	HD95 \downarrow	DSC \uparrow	HD95 \downarrow	DSC \uparrow	HD95 \downarrow
MIS-MAE	ViT-B	0.6861 \pm 0.0255	38.8152 \pm 2.5011	0.2277 \pm 0.0124	66.1680 \pm 3.1127	0.5938 \pm 0.0212	29.2246 \pm 1.7466
MIS-MoCoV3	ViT-B	0.7348 \pm 0.0239	32.6056 \pm 1.9152	0.2477 \pm 0.0207	54.5426 \pm 4.4232	0.6254 \pm 0.0139	25.2477 \pm 1.4299
MIS-MSN	ViT-B	0.7388 \pm 0.0091	32.6919 \pm 2.6873	0.3109 \pm 0.0420	53.0506 \pm 3.1128	0.6418 \pm 0.0046	25.4631 \pm 0.7746
MIS-DINO	ViT-B	0.7701 \pm 0.0066	26.7690 \pm 1.6323	0.3990 \pm 0.0239	47.0333 \pm 5.1523	0.6833 \pm 0.0108	19.8921 \pm 0.9109
MIS-DINOv2	ViT-B	0.7924 \pm 0.0127	26.9685 \pm 3.6271	0.3571 \pm 0.0428	44.3142 \pm 3.1016	0.7201 \pm 0.0085	18.2404 \pm 1.7884
MIS-DINOv2	ViT-L	0.7995 \pm 0.0106	21.4576 \pm 1.7789	0.4033 \pm 0.0449	41.6426 \pm 2.7067	0.7639 \pm 0.0033	13.9271 \pm 0.5646
ImageNet	ViT-B	0.7166 \pm 0.0120	40.8932 \pm 1.1910	0.2506 \pm 0.0133	56.3714 \pm 1.3337	0.5745 \pm 0.0267	32.1888 \pm 2.0011
EndoFM	ViT-B	0.6679 \pm 0.0318	43.6707 \pm 2.4823	0.2330 \pm 0.0203	64.9675 \pm 10.4080	0.5656 \pm 0.0110	39.3725 \pm 1.6396
GSViT	EfficientViT	0.4996 \pm 0.0172	56.9302 \pm 5.2608	0.1592 \pm 0.0071	68.7672 \pm 2.9062	0.3348 \pm 0.0232	54.9375 \pm 2.7877
EndoViT	ViT-B	0.6564 \pm 0.0269	34.8515 \pm 1.6115	0.2200 \pm 0.0097	68.0728 \pm 2.8587	0.6314 \pm 0.0174	27.3860 \pm 1.9312
PeskaVLP	ResNet50	0.7331 \pm 0.0146	40.1011 \pm 1.7930	0.2822 \pm 0.0319	59.5684 \pm 2.1167	0.6550 \pm 0.0058	31.0452 \pm 1.8067
SurgeNet	CAFormer18	0.7199 \pm 0.0210	36.6993 \pm 4.8076	0.2917 \pm 0.0215	50.7239 \pm 3.7081	0.7193 \pm 0.0057	22.4122 \pm 1.4450
ZEN	ViT-B	0.7876 \pm 0.0109	21.3993 \pm 2.5680	0.3472 \pm 0.0272	40.7567 \pm 1.9581	0.7529 \pm 0.0057	15.1157 \pm 0.5242

Table 29 Few-shot evaluation across three datasets for semantic segmentation (1-shot). Results are reported using the Dice similarity coefficient (DSC; higher is better) and the 95th percentile Hausdorff distance (HD95; lower is better). The upper block reports results for self-supervised learning pretrained models, and the lower block reports results for existing pretrained models. Best-performing models for each metric are highlighted in bold. Values are reported as mean \pm standard deviation over five independent runs.

Method	Backbone	CholecSeg8k		DSAD		GraSP	
		DSC \uparrow	HD95 \downarrow	DSC \uparrow	HD95 \downarrow	DSC \uparrow	HD95 \downarrow
MIS-MAE	ViT-B	0.3792 \pm 0.0791	76.51 \pm 15.2150	0.0955 \pm 0.0429	114.7797 \pm 24.3907	0.2316 \pm 0.0360	67.123 \pm 9.5330
MIS-MoCov3	ViT-B	0.3959 \pm 0.0968	73.9893 \pm 20.7903	0.1270 \pm 0.0504	112.6716 \pm 26.6163	0.2874 \pm 0.0417	52.4048 \pm 15.4301
MSN	ViT-B	0.3913 \pm 0.1132	78.7525 \pm 22.3983	0.1235 \pm 0.0518	107.4917 \pm 25.3223	0.2936 \pm 0.0297	49.9007 \pm 4.3906
MIS-DINO	ViT-B	0.4297 \pm 0.1257	73.8078 \pm 24.3163	0.1357 \pm 0.0555	102.2998 \pm 33.5338	0.3483 \pm 0.0264	38.8752 \pm 6.2540
MIS-DINOv2	ViT-B	0.4384 \pm 0.1211	65.0300 \pm 18.9150	0.1568 \pm 0.0413	85.0391\pm17.1377	0.3760 \pm 0.0459	34.9997 \pm 5.9416
MIS-DINOv2	ViT-L	0.4591\pm0.1409	64.7460\pm20.5177	0.1585\pm0.0534	95.6877 \pm 23.6925	0.3908\pm0.0431	29.7430\pm2.4641
Supervised							
EndoFM	ViT-B	0.3894 \pm 0.1185	77.1273 \pm 21.9425	0.0990 \pm 0.0406	137.6688 \pm 32.7957	0.2538 \pm 0.0259	67.6870 \pm 5.2851
GSViT	EfficientViT	0.3644 \pm 0.0765	83.1372 \pm 14.0706	0.1031 \pm 0.0316	130.1707 \pm 7.9361	0.2082 \pm 0.0598	79.4412 \pm 22.9155
EndoViT	ViT-B	0.2285 \pm 0.0615	96.7734 \pm 20.9503	0.0810 \pm 0.0194	116.2613 \pm 23.4674	0.1698 \pm 0.0295	78.6745 \pm 10.3655
FestaVLP	ResNet50	0.3765 \pm 0.1021	79.1075 \pm 21.9769	0.0994 \pm 0.0314	126.4545 \pm 19.8909	0.2369 \pm 0.0238	65.7764 \pm 14.1126
SurgeNet	CAFormer18	0.4063 \pm 0.0797	77.7464 \pm 11.2262	0.0937 \pm 0.0552	131.3237 \pm 54.3932	0.2984 \pm 0.0517	68.9799 \pm 8.2798
ZEN	ViT-B	0.4541\pm0.1370	62.9728\pm19.2575	0.1373\pm0.0414	106.0836 \pm 34.0479	0.2752 \pm 0.1302	46.1387 \pm 3.6071

Table 30 Few-shot evaluation across three datasets for semantic segmentation (2-shot). Results are reported using the Dice similarity coefficient (DSC; higher is better) and the 95th percentile Hausdorff distance (HD95; lower is better). The upper block reports results for self-supervised learning pretrained models, and the lower block reports results for existing pretrained models. Best-performing models for each metric are highlighted in bold. Values are reported as mean \pm standard deviation over five independent runs.

Method	Backbone	CholecSeg8k		DSAD		GraSP	
		DSC \uparrow	HD95 \downarrow	DSC \uparrow	HD95 \downarrow	DSC \uparrow	HD95 \downarrow
MIS-MAE	ViT-B	0.4866 \pm 0.0683	68.9524 \pm 12.0818	0.1017 \pm 0.0554	117.0918 \pm 50.6241	0.3081 \pm 0.0316	54.2737 \pm 4.1249
MIS-MoCov3	ViT-B	0.5585 \pm 0.0596	59.5376 \pm 12.6458	0.1401 \pm 0.0392	85.1487 \pm 14.8940	0.3919 \pm 0.0333	41.6219 \pm 2.0643
MSN	ViT-B	0.5663 \pm 0.0533	60.3766 \pm 7.4621	0.1357 \pm 0.0454	91.6858 \pm 21.5929	0.3657 \pm 0.0301	41.3406 \pm 3.3496
MIS-DINO	ViT-B	0.6178 \pm 0.0418	47.5757 \pm 5.9662	0.1536 \pm 0.0441	88.5657 \pm 22.8012	0.4268 \pm 0.0491	32.5568 \pm 3.0483
MIS-DINOv2	ViT-B	0.6400 \pm 0.0687	45.6413 \pm 10.6015	0.1836\pm0.0512	81.2450 \pm 21.5940	0.4789 \pm 0.0363	27.6889 \pm 2.2124
MIS-DINOv2	ViT-L	0.6649\pm0.0449	44.5351\pm11.2084	0.1828 \pm 0.0522	80.3261\pm20.3708	0.5241\pm0.0409	21.2048\pm1.6209
ImageNet	ViT-B	0.5389 \pm 0.0839	60.4903 \pm 9.5964	0.1434 \pm 0.0418	106.2664 \pm 21.1179	0.3655 \pm 0.0393	54.3416 \pm 2.3514
EndoFM	ViT-B	0.5119 \pm 0.0895	67.7710 \pm 1.15.2661	0.1245 \pm 0.0389	114.2099 \pm 17.5028	0.3063 \pm 0.0060	62.3997 \pm 9.0828
GSViT	Efficient ViT	0.4048 \pm 0.0410	75.8909 \pm 4.2465	0.0752 \pm 0.0493	106.5556 \pm 20.3083	0.2474 \pm 0.0160	66.5282 \pm 9.9651
EndoViT	ViT-B	0.4977 \pm 0.0492	67.4297 \pm 9.6738	0.0898 \pm 0.0559	113.5676 \pm 20.5245	0.3012 \pm 0.0419	51.4144 \pm 4.9574
PeskaVLP	ResNet50	0.5579 \pm 0.0640	63.7299 \pm 9.7248	0.1279 \pm 0.0482	82.7714\pm11.8551	0.4296 \pm 0.0343	57.4062 \pm 3.4523
SurgeNet	CAFormer18	0.5643 \pm 0.0525	58.0862 \pm 11.8622	0.1190 \pm 0.0755	118.9908 \pm 68.4151	0.4557 \pm 0.0211	35.7468 \pm 2.8892
ZEN	ViT-B	0.6314\pm0.0512	45.2514\pm9.8517	0.1658\pm0.0441	83.1591 \pm 20.1159	0.4815\pm0.0273	25.7157\pm1.6724

Table 31 Few-shot evaluation across three datasets for semantic segmentation (3-shot). Results are reported using the Dice similarity coefficient (DSC; higher is better) and the 95th percentile Hausdorff distance (HD95; lower is better). The upper block reports results for self-supervised learning pretrained models, and the lower block reports results for existing pretrained models. Best-performing models for each metric are highlighted in bold. Values are reported as mean \pm standard deviation over five independent runs.

Method	Backbone	CholecSeg8k			DSAD			GraSP		
		DSC \uparrow	HD95 \downarrow	DSC \uparrow	HD95 \downarrow	DSC \uparrow	HD95 \downarrow	DSC \uparrow	HD95 \downarrow	
MIS-MAE	ViT-B	0.5786 \pm 0.0363	57.7067 \pm 5.6508	0.1351 \pm 0.0349	82.7762 \pm 18.7524	0.4141 \pm 0.0607	42.7034 \pm 5.4854			
MIS-MoCov3	ViT-B	0.6392 \pm 0.0309	45.8050 \pm 8.7912	0.1679 \pm 0.0265	75.6709 \pm 5.5137	0.4610 \pm 0.0305	36.5765 \pm 1.2037			
MSN	ViT-B	0.6489 \pm 0.0431	48.9809 \pm 3.7012	0.1711 \pm 0.0195	71.4510 \pm 9.4944	0.4687 \pm 0.0468	35.7465 \pm 1.6530			
MIS-DINO	ViT-B	0.6844 \pm 0.0378	39.1455 \pm 1.2117	0.1764 \pm 0.0179	66.1154 \pm 5.7820	0.5108 \pm 0.0569	28.2094 \pm 1.2300			
MIS-DINOv2	ViT-B	0.6956 \pm 0.0312	38.6578 \pm 10.2172	0.2060\pm0.0242	62.4711\pm6.7668	0.5889 \pm 0.0458	23.4928 \pm 0.8177			
MIS-DINOv2	ViT-L	0.7278\pm0.0334	35.9219\pm7.3329	0.1995 \pm 0.0295	69.5943 \pm 12.3056	0.6434\pm0.0710	18.4461\pm0.9156			
ImageNet	ViT-B	0.6206 \pm 0.0459	53.5868 \pm 7.4735	0.1663 \pm 0.0227	97.7866 \pm 12.2744	0.4378 \pm 0.0280	49.5688 \pm 3.7807			
EndoFM	ViT-B	0.5889 \pm 0.0282	57.4098 \pm 8.2401	0.1478 \pm 0.0228	97.4356 \pm 13.6616	0.3695 \pm 0.0429	56.9927 \pm 4.8450			
GSViT	EfficientViT	0.4360 \pm 0.0420	71.0993 \pm 2.2085	0.1079 \pm 0.0296	80.6636 \pm 14.3993	0.3067 \pm 0.0292	58.2571 \pm 8.8046			
EndoViT	ViT-B	0.5690 \pm 0.0370	58.0000 \pm 6.3007	0.1401 \pm 0.0349	93.8831 \pm 6.3572	0.4177 \pm 0.0490	39.7205 \pm 2.6880			
PestaVLP	ResNet50	0.6229 \pm 0.0262	58.2219 \pm 7.5270	0.1513 \pm 0.0202	87.2248 \pm 12.4500	0.5003 \pm 0.0412	48.0382 \pm 4.7204			
SurgeNet	CAFormer18	0.6610 \pm 0.0261	49.2176 \pm 4.6224	0.1556 \pm 0.0579	72.2667 \pm 9.7763	0.5578 \pm 0.0536	31.4377 \pm 1.1079			
ZEN	ViT-B	0.7154\pm0.0331	32.1924\pm7.5280	0.2007 \pm 0.0245	65.2202\pm10.1382	0.6047\pm0.0932	20.9223\pm1.6400			

Table 32 Few-shot evaluation across three datasets for semantic segmentation (4-shot). Results are reported using the Dice similarity coefficient (DSC, higher is better) and the 95th percentile Hausdorff distance (HD95; lower is better). The upper block reports results for self-supervised learning pretrained models, and the lower block reports results for existing pretrained models. Best-performing models for each metric are highlighted in bold. Values are reported as mean \pm standard deviation over five independent runs.

Method	Backbone	CholecSeg8k		DSAD		Grasp	
		DSC \uparrow	HD95 \downarrow	DSC \uparrow	HD95 \downarrow	DSC \uparrow	HD95 \downarrow
MIS-MAE	ViT-B	0.5929 \pm 0.0288	53.3101 \pm 5.8728	0.1475 \pm 0.0217	81.8138 \pm 13.1047	0.4349 \pm 0.0452	38.7078 \pm 2.7976
MIS-MoCov3	ViT-B	0.6677 \pm 0.0253	45.0314 \pm 1.5798	0.1811 \pm 0.0117	72.0254 \pm 4.5301	0.5192 \pm 0.0315	33.5958 \pm 3.8141
MSN	ViT-B	0.6734 \pm 0.0381	45.0450 \pm 4.7207	0.1767 \pm 0.0119	68.7937 \pm 9.3974	0.5185 \pm 0.0270	31.3206 \pm 0.5738
MIS-DINO	ViT-B	0.7066 \pm 0.0425	37.2462 \pm 4.8594	0.1889 \pm 0.0161	64.1794 \pm 7.9686	0.5799 \pm 0.0177	26.1727 \pm 1.3549
MIS-DINOv2	ViT-B	0.7278 \pm 0.0498	34.8388 \pm 3.9918	0.2156 \pm 0.0292	61.8369 \pm 8.4555	0.6512 \pm 0.0199	21.7428 \pm 2.0638
MIS-DINOv2	ViT-L	0.7424\pm0.0326	30.4469\pm3.5235	0.2226\pm0.0225	60.7209\pm4.3555	0.6929\pm0.0226	17.6548\pm0.6112
Supervised							
EndoFM	ViT-B	0.6333 \pm 0.0454	51.6669 \pm 5.9001	0.1759 \pm 0.0182	92.2557 \pm 15.0001	0.4734 \pm 0.0120	43.4316 \pm 3.5349
GSViT	EfficientViT	0.6026 \pm 0.0173	55.2072 \pm 3.7543	0.1562 \pm 0.0144	90.6198 \pm 16.5918	0.4302 \pm 0.0113	50.9416 \pm 3.5520
EndoViT	ViT-B	0.4778 \pm 0.0346	65.6504 \pm 4.8604	0.1117 \pm 0.0367	97.8121 \pm 36.7426	0.3406 \pm 0.0228	53.0146 \pm 4.4394
PeskaVLP	ResNet50	0.5958 \pm 0.0299	52.1638 \pm 6.3667	0.1530 \pm 0.0161	78.6007 \pm 6.8572	0.4668 \pm 0.0266	35.9429 \pm 1.7238
SurgeNet	CAFormer18	0.6607 \pm 0.0252	45.7105 \pm 5.4998	0.1764 \pm 0.0056	83.3994 \pm 3.4919	0.5339 \pm 0.0107	43.6190 \pm 3.8169
ZEN	ViT-B	0.7288\pm0.0365	30.3896\pm3.2979	0.2129\pm0.0186	63.4717\pm3.7046	0.6248\pm0.0199	27.5561\pm2.0834

Table 33 Few-shot evaluation across three datasets for semantic segmentation (5-shot). Results are reported using the Dice similarity coefficient (DSC, higher is better) and the 95th percentile Hausdorff distance (HD95; lower is better). The upper block reports results for self-supervised learning pretrained models, and the lower block reports results for existing pretrained models. Best-performing models for each metric are highlighted in bold. Values are reported as mean \pm standard deviation over five independent runs.

Method	Backbone	CholecSeg8k		DSAD		Grasp	
		DSC \uparrow	HD95 \downarrow	DSC \uparrow	HD95 \downarrow	DSC \uparrow	HD95 \downarrow
MIS-MAE	ViT-B	0.6052 \pm 0.0248	54.7292 \pm 5.0447	0.1569 \pm 0.0089	74.8170 \pm 7.4783	0.4976 \pm 0.0167	35.7042 \pm 0.9075
MIS-MoCov3	ViT-B	0.7025 \pm 0.0186	41.8514 \pm 9.7523	0.1762 \pm 0.0061	69.8475 \pm 8.5838	0.5611 \pm 0.0149	30.7770 \pm 1.7680
MSN	ViT-B	0.6874 \pm 0.0262	42.6891 \pm 5.1891	0.1886 \pm 0.0089	66.0214 \pm 5.9567	0.5659 \pm 0.0226	29.8681 \pm 0.8912
MIS-DINO	ViT-B	0.7333 \pm 0.0124	35.1733 \pm 4.2421	0.1991 \pm 0.0182	64.1841 \pm 8.9671	0.6215 \pm 0.0250	24.6398 \pm 1.2782
MIS-DINOv2	ViT-B	0.7561 \pm 0.0128	30.4994 \pm 3.9548	0.2233 \pm 0.0191	57.6411 \pm 6.6478	0.6721 \pm 0.0175	20.7291 \pm 0.8776
MIS-DINOv2	ViT-L	0.7760\pm0.0176	28.0174\pm3.0523	0.2406\pm0.0164	51.6475\pm3.3627	0.7286\pm0.0105	16.2606\pm0.8184
Supervised							
EndoFM	ViT-B	0.6596 \pm 0.0344	48.8830 \pm 7.5070	0.1811 \pm 0.0135	76.4114 \pm 13.2860	0.4953 \pm 0.0231	40.1513 \pm 2.5687
GSViT	EfficientViT	0.6453 \pm 0.0246	52.0217 \pm 7.6721	0.1651 \pm 0.0126	84.5214 \pm 15.0283	0.4685 \pm 0.0275	46.5001 \pm 3.8578
EndoViT	ViT-B	0.5297 \pm 0.0080	61.3753 \pm 3.3816	0.1263 \pm 0.0162	76.0734 \pm 14.3654	0.3921 \pm 0.0252	51.4884 \pm 2.9585
PeskaVLP	ResNet50	0.6464 \pm 0.0320	47.2788 \pm 4.1942	0.1531 \pm 0.0132	81.5460 \pm 9.4837	0.5124 \pm 0.0335	36.2277 \pm 2.2468
SurgeNet	CAFormer18	0.6872 \pm 0.0134	41.8466 \pm 4.7426	0.2137 \pm 0.0182	67.4532 \pm 9.7092	0.5915 \pm 0.0205	37.9177 \pm 1.6946
ZEN	ViT-B	0.7624\pm0.0154	27.7687\pm4.2435	0.2138\pm0.0227	59.6110\pm3.2988	0.7229\pm0.0106	17.3003\pm0.7612

Table 34 Instance segmentation performance on the GraSP dataset. Results are reported in terms of bounding box (BBox) and mask mAP@[0.5:0.95] under frozen and fine-tuned backbone settings. The upper block reports results for self-supervised learning pretrained models, and the lower block reports results for existing pretrained models. Best-performing models for each metric are highlighted in bold. Values are reported as mean \pm standard deviation over five independent runs.

Method	Backbone	Frozen backbone		Fine-tuned backbone	
		BBox	Mask	BBox	Mask
MIS-MAE	ViT-B	0.5008 \pm 0.0165	0.4613 \pm 0.0119	0.5753 \pm 0.0097	0.5204 \pm 0.0067
MIS-MoCoV3	ViT-B	0.4843 \pm 0.0074	0.4486 \pm 0.0093	0.5438 \pm 0.0058	0.5003 \pm 0.0090
MIS-MSN	ViT-B	0.5276 \pm 0.0096	0.4717 \pm 0.0076	0.5582 \pm 0.0053	0.5167 \pm 0.0035
MIS-DINO	ViT-B	0.5478 \pm 0.0120	0.4952 \pm 0.0088	0.5700 \pm 0.0103	0.5231 \pm 0.0075
MIS-DINOv2	ViT-B	0.5504 \pm 0.0076	0.5001 \pm 0.0106	0.5936 \pm 0.0069	0.5282 \pm 0.0062
MIS-DINOv2	ViT-L	0.5746 \pm 0.0071	0.5263 \pm 0.0077	0.6088 \pm 0.0048	0.5432 \pm 0.0053
ImageNet	ViT-B	0.4862 \pm 0.0037	0.4561 \pm 0.0031	0.5365 \pm 0.0100	0.4886 \pm 0.0084
EndoFM	ViT-B	0.4523 \pm 0.0146	0.4323 \pm 0.0072	0.5409 \pm 0.0061	0.4984 \pm 0.0054
GSViT	EfficientViT	0.3513 \pm 0.0258	0.3436 \pm 0.0268	0.3938 \pm 0.0234	0.3778 \pm 0.0197
EndoViT	ViT-B	0.5120 \pm 0.0116	0.4663 \pm 0.0123	0.5723 \pm 0.0045	0.5192 \pm 0.0055
PeskaVLP	ResNet50	0.4857 \pm 0.0270	0.4731 \pm 0.0227	0.5789 \pm 0.0058	0.5241 \pm 0.0034
SurgeNet	CAFormer18	0.5400 \pm 0.0101	0.5301 \pm 0.0068	0.5998 \pm 0.0092	0.5596 \pm 0.0111
ZEN	ViT-B	0.5841 \pm 0.0071	0.5317 \pm 0.0037	0.6250 \pm 0.0054	0.5597 \pm 0.0074

Table 35 Depth estimation performance on the SCARED dataset using fine-tuned backbones.

Performance is evaluated using Abs Rel, Sq Rel, RMSE, RMSE log (lower is better), and δ (higher is better). The upper block reports results for self-supervised learning pretrained models, and the lower block reports results for existing pretrained models. Best-performing models for each metric are highlighted in bold. Values are reported as mean \pm standard deviation over five independent runs.

Method	Backbone	Abs Rel \downarrow	Sq Rel \downarrow	RMSE \downarrow	RMSE log \downarrow	$\delta \uparrow$
MIS-MAE	ViT-B	0.1416 \pm 0.0117	1.9033 \pm 0.3600	8.8798 \pm 0.7592	0.1544 \pm 0.0125	0.8163 \pm 0.0370
MIS-MoCoV3	ViT-B	0.1326 \pm 0.0120	1.6049 \pm 0.2371	8.2549 \pm 0.4240	0.1440 \pm 0.0078	0.8325 \pm 0.0162
MIS-MSN	ViT-B	0.1333 \pm 0.0088	1.6449 \pm 0.2098	8.3485 \pm 0.5328	0.1451 \pm 0.0095	0.8407 \pm 0.0231
MIS-DINO	ViT-B	0.1361 \pm 0.0071	1.6881 \pm 0.1999	8.5661 \pm 0.2402	0.1492 \pm 0.0039	0.8271 \pm 0.0095
MIS-DINOv2	ViT-B	0.1385 \pm 0.0046	1.7175 \pm 0.0622	8.4867 \pm 0.3943	0.1491 \pm 0.0073	0.8193 \pm 0.0123
MIS-DINOv2	ViT-L	0.1417 \pm 0.0040	1.7527 \pm 0.1226	8.7620 \pm 0.2505	0.1529 \pm 0.0040	0.8214 \pm 0.0143
ImageNet	ViT-B	0.1364 \pm 0.0155	1.7377 \pm 0.3488	8.5183 \pm 0.6496	0.1480 \pm 0.0122	0.8299 \pm 0.0317
EndoFM	ViT-B	0.1365 \pm 0.0145	1.7387 \pm 0.3745	8.5228 \pm 0.5233	0.1491 \pm 0.0090	0.8278 \pm 0.0309
GSViT	EfficientViT	0.2246 \pm 0.0228	4.3211 \pm 0.7802	13.3113 \pm 0.8691	0.2337 \pm 0.0154	0.6281 \pm 0.0362
EndoViT	ViT-B	0.1477 \pm 0.0146	2.1513 \pm 0.5365	9.0645 \pm 0.6363	0.1574 \pm 0.0097	0.8142 \pm 0.0244
PeskaVLP	ResNet50	0.1545 \pm 0.0125	2.1260 \pm 0.3175	9.9993 \pm 0.7286	0.1748 \pm 0.0133	0.7835 \pm 0.0423
SurgeNet	CAFormer18	0.1329 \pm 0.0111	1.5100 \pm 0.2089	8.1794 \pm 0.3829	0.1438 \pm 0.0074	0.8473 \pm 0.0322
ZEN	ViT-B	0.1306 \pm 0.0128	1.5402 \pm 0.2908	7.9178 \pm 0.4724	0.1386 \pm 0.0097	0.8592 \pm 0.0232

Table 36 Depth estimation performance on the Hamlyn dataset using fine-tuned backbones.

Performance is evaluated using Abs Rel, Sq Rel, RMSE, RMSE log (lower is better), and δ (higher is better). The upper block reports results for self-supervised learning pretrained models, and the lower block reports results for existing pretrained models. Best-performing models for each metric are highlighted in bold. Values are reported as mean \pm standard deviation over five independent runs.

Method	Backbone	Abs Rel \downarrow	Sq Rel \downarrow	RMSE \downarrow	RMSE log \downarrow	$\delta \uparrow$
MIS-MAE	ViT-B	0.1908 \pm 0.0116	3.9669 \pm 0.3956	14.6177 \pm 1.1492	0.2206 \pm 0.0177	0.6661 \pm 0.0595
MIS-MoCoV3	ViT-B	0.1745 \pm 0.0048	3.4721 \pm 0.2579	14.1841 \pm 0.5051	0.2127 \pm 0.0074	0.6921 \pm 0.0141
MIS-MSN	ViT-B	0.1727 \pm 0.0070	3.6208 \pm 0.2635	14.4188 \pm 0.4736	0.2151 \pm 0.0079	0.6836 \pm 0.0193
MIS-DINO	ViT-B	0.1802 \pm 0.0090	3.8866 \pm 0.4094	14.9283 \pm 0.6281	0.2257 \pm 0.0111	0.6449 \pm 0.0366
MIS-DINOv2	ViT-B	0.1714 \pm 0.0133	3.5428 \pm 0.5843	14.2567 \pm 1.0107	0.2134 \pm 0.0172	0.6858 \pm 0.0423
MIS-DINOv2	ViT-L	0.1614 \pm 0.0073	3.1527 \pm 0.2854	13.1128 \pm 0.6479	0.1953 \pm 0.0103	0.7304 \pm 0.0264
ImageNet	ViT-B	0.1864 \pm 0.0036	4.1933 \pm 0.2394	15.0118 \pm 0.4344	0.2236 \pm 0.0065	0.6848 \pm 0.0099
EndoFM	ViT-B	0.1817 \pm 0.0041	4.0425 \pm 0.0905	14.8925 \pm 0.1973	0.2213 \pm 0.0031	0.6884 \pm 0.0113
GSViT	EfficientViT	0.2407 \pm 0.0287	6.0054 \pm 1.2287	17.0957 \pm 1.3735	0.2585 \pm 0.0192	0.5751 \pm 0.0378
EndoViT	ViT-B	0.1906 \pm 0.0031	4.2328 \pm 0.2870	15.4385 \pm 0.5967	0.2323 \pm 0.0100	0.6519 \pm 0.0306
PeskaVLP	ResNet50	0.1812 \pm 0.0069	3.9584 \pm 0.3029	14.8482 \pm 0.5933	0.2257 \pm 0.0098	0.6583 \pm 0.0345
SurgeNet	CAFormer18	0.1715 \pm 0.0067	3.6143 \pm 0.2836	14.1965 \pm 0.5329	0.2125 \pm 0.0087	0.6836 \pm 0.0374
ZEN	ViT-B	0.1554 \pm 0.0098	2.8806 \pm 0.3651	12.5496 \pm 0.7705	0.1870 \pm 0.0122	0.7351 \pm 0.0496

Table 37 Depth estimation performance on the SCARED dataset using frozen backbones.

Performance is evaluated using Abs Rel, Sq Rel, RMSE, RMSE log (lower is better), and δ (higher is better). The upper block reports results for self-supervised learning pretrained models, and the lower block reports results for existing pretrained models. Best-performing models for each metric are highlighted in bold. Values are reported as mean \pm standard deviation over five independent runs.

Method	Backbone	Abs Rel \downarrow	Sq Rel \downarrow	RMSE \downarrow	RMSE log \downarrow	$\delta \uparrow$
MIS-MAE	ViT-B	0.2117 ± 0.0201	3.9499 ± 0.5276	12.3165 ± 0.7439	0.2140 ± 0.0155	0.6661 ± 0.0354
MIS-MoCoV3	ViT-B	0.1504 ± 0.0117	2.0385 ± 0.2570	9.2167 ± 0.4940	0.1629 ± 0.0088	0.7803 ± 0.0234
MIS-MSN	ViT-B	0.1504 ± 0.0066	2.0154 ± 0.0918	9.4050 ± 0.2375	0.1675 ± 0.0067	0.7812 ± 0.0245
MIS-DINO	ViT-B	0.1557 ± 0.0068	2.2076 ± 0.2312	9.5348 ± 0.3725	0.1675 ± 0.0059	0.7798 ± 0.0178
MIS-DINOv2	ViT-B	0.1472 ± 0.0068	2.0371 ± 0.1705	8.7419 ± 0.4077	0.1567 ± 0.0073	0.7814 ± 0.0264
MIS-DINOv2	ViT-L	0.1340 ± 0.0081	1.6110 ± 0.2032	8.2607 ± 0.3470	0.1458 ± 0.0059	0.8091 ± 0.0165
ImageNet	ViT-B	0.1595 ± 0.0135	2.3831 ± 0.2941	9.8408 ± 0.6187	0.1712 ± 0.0107	0.7671 ± 0.0276
EndoFM	ViT-B	0.1541 ± 0.0134	2.1728 ± 0.2640	9.5215 ± 0.7185	0.1712 ± 0.0146	0.7631 ± 0.0479
GSViT	EfficientViT	0.2646 ± 0.0169	5.5267 ± 0.5563	15.3095 ± 0.7114	0.2674 ± 0.0118	0.5511 ± 0.0291
EndoViT	ViT-B	0.2034 ± 0.0111	3.6276 ± 0.2977	12.4025 ± 0.4216	0.2160 ± 0.0096	0.6468 ± 0.0300
PeskaVLP	ResNet50	0.1984 ± 0.0097	3.2513 ± 0.2617	12.4412 ± 0.3488	0.2188 ± 0.0061	0.6728 ± 0.0207
SurgeNet	CAFormer18	0.1701 ± 0.0084	2.4920 ± 0.2443	10.7763 ± 0.2705	0.1884 ± 0.0045	0.7268 ± 0.0138
ZEN	ViT-B	0.1309 ± 0.0069	1.6220 ± 0.2034	8.1781 ± 0.3220	0.1431 ± 0.0055	0.8242 ± 0.0096

Table 38 Depth estimation performance on the Hamlyn dataset using frozen backbones. Performance is evaluated using Abs Rel, Sq Rel, RMSE, RMSE log (lower is better), and δ (higher is better). The upper block reports results for self-supervised learning pretrained models, and the lower block reports results for existing pretrained models. Best-performing models for each metric are highlighted in bold. Values are reported as mean \pm standard deviation over five independent runs.

Method	Backbone	Abs Rel \downarrow	Sq Rel \downarrow	RMSE \downarrow	RMSE log \downarrow	$\delta \uparrow$
MIS-MAE	ViT-B	0.1897 ± 0.0133	4.2759 ± 0.6031	14.7664 ± 0.6432	0.2213 ± 0.0099	0.6902 ± 0.0208
MIS-MoCoV3	ViT-B	0.1753 ± 0.0073	3.4550 ± 0.2221	14.1648 ± 0.4104	0.2131 ± 0.0069	0.6884 ± 0.0285
MIS-MSN	ViT-B	0.1689 ± 0.0062	3.2287 ± 0.3055	13.7272 ± 0.6784	0.2060 ± 0.0093	0.7086 ± 0.0229
MIS-DINO	ViT-B	0.1691 ± 0.0087	3.2971 ± 0.4387	13.9077 ± 0.8205	0.2096 ± 0.0122	0.7003 ± 0.0248
MIS-DINOv2	ViT-B	0.1680 ± 0.0131	3.3986 ± 0.5651	13.8990 ± 1.2661	0.2075 ± 0.0200	0.7102 ± 0.0476
MIS-DINOv2	ViT-L	0.1579 ± 0.0128	3.0895 ± 0.4933	12.9146 ± 1.0656	0.1923 ± 0.0164	0.7373 ± 0.0327
ImageNet	ViT-B	0.1831 ± 0.0060	4.1421 ± 0.0952	14.9893 ± 0.2588	0.2243 ± 0.0065	0.6684 ± 0.0232
EndoFM	ViT-B	0.1830 ± 0.0023	3.9253 ± 0.0524	14.3977 ± 0.1409	0.2153 ± 0.0022	0.6968 ± 0.0120
GSViT	EfficientViT	0.2470 ± 0.0170	6.2404 ± 0.7032	17.8172 ± 0.7431	0.2670 ± 0.0091	0.5720 ± 0.0221
EndoViT	ViT-B	0.2177 ± 0.0070	5.2286 ± 0.2621	17.2679 ± 0.5594	0.2695 ± 0.0108	0.5444 ± 0.0263
PeskaVLP	ResNet50	0.1886 ± 0.0078	4.2342 ± 0.3281	14.9181 ± 0.5209	0.2221 ± 0.0076	0.6901 ± 0.0125
SurgeNet	CAFormer18	0.1929 ± 0.0055	4.1303 ± 0.2559	15.5793 ± 0.4399	0.2381 ± 0.0076	0.6144 ± 0.0164
ZEN	ViT-B	0.1621 ± 0.0100	3.2286 ± 0.3645	13.2018 ± 0.7469	0.1971 ± 0.0125	0.7273 ± 0.0345

Table 39 Closed-ended VQA performance on PitVQA. F-score, balanced accuracy, and recall are reported for frozen and fine-tuned backbones. The upper block shows self-supervised learning pretrained models and the lower block shows existing pretrained models. Best-performing models are highlighted in bold. Values are reported as mean \pm standard deviation over five independent runs.

Method	Backbone	Frozen backbone			Fine-tuning backbone		
		F1 score \uparrow	B. Accuracy \uparrow	Recall \uparrow	F1 score \uparrow	B. Accuracy \uparrow	Recall \uparrow
MIS-MAE	ViT-B	0.4291 \pm 0.0120	0.4619 \pm 0.0137	0.4852 \pm 0.0138	0.5465 \pm 0.0197	0.5549 \pm 0.0221	0.5684 \pm 0.0218
MIS-MoCoV3	ViT-B	0.4783 \pm 0.0237	0.4923 \pm 0.0042	0.5127 \pm 0.0052	0.5381 \pm 0.0121	0.5425 \pm 0.0192	0.5563 \pm 0.0227
MIS-MSN	ViT-B	0.2708 \pm 0.0190	0.2848 \pm 0.0194	0.2943 \pm 0.0273	0.4047 \pm 0.0175	0.4221 \pm 0.0041	0.4357 \pm 0.0130
MIS-DINO	ViT-B	0.5281 \pm 0.0094	0.5290 \pm 0.0158	0.5447 \pm 0.0196	0.5523 \pm 0.0055	0.5568 \pm 0.0184	0.5715 \pm 0.0230
MIS-DINOv2	ViT-B	0.5447 \pm 0.0118	0.5446 \pm 0.0085	0.5585 \pm 0.0103	0.5658 \pm 0.0128	0.5668 \pm 0.0107	0.5785 \pm 0.0129
MIS-DINOv2	ViT-L	0.5610 \pm 0.0174	0.5680 \pm 0.0240	0.5851 \pm 0.0257	0.5920 \pm 0.0126	0.5928 \pm 0.0127	0.6038 \pm 0.0133
ImageNet	ViT-B	0.4770 \pm 0.0220	0.4952 \pm 0.0081	0.5121 \pm 0.0111	0.5523 \pm 0.0138	0.5617 \pm 0.0117	0.5749 \pm 0.0158
EndoFM	ViT-B	0.4759 \pm 0.0162	0.4820 \pm 0.0178	0.4995 \pm 0.0163	0.5209 \pm 0.0221	0.5306 \pm 0.0083	0.5464 \pm 0.0088
GSViT	EfficientViT	0.2574 \pm 0.0338	0.2737 \pm 0.0273	0.2957 \pm 0.0284	0.2490 \pm 0.0112	0.2681 \pm 0.0094	0.2903 \pm 0.0138
EndoViT	ViT-B	0.4163 \pm 0.0212	0.4426 \pm 0.0099	0.4650 \pm 0.0097	0.5078 \pm 0.0187	0.5221 \pm 0.0228	0.5413 \pm 0.0204
PeskaVLP	ResNet50	0.4438 \pm 0.0182	0.4555 \pm 0.0078	0.4738 \pm 0.0100	0.5364 \pm 0.0127	0.5452 \pm 0.0180	0.5590 \pm 0.0191
SurgeNet	CAFormer18	0.4708 \pm 0.0161	0.4846 \pm 0.0178	0.5018 \pm 0.0200	0.5917 \pm 0.0235	0.5984 \pm 0.0175	0.6094 \pm 0.0126
ZEN	ViT-B	0.5510 \pm 0.0125	0.5537 \pm 0.0048	0.5673 \pm 0.0085	0.6043 \pm 0.0140	0.6071 \pm 0.0105	0.6190 \pm 0.0119

Table 40 Closed-ended VQA performance on LLS48-VQA. F-score, balanced accuracy, and recall are reported for frozen and fine-tuned backbones. The upper block shows self-supervised learning pretrained models and the lower block shows existing pretrained models. Best-performing models are highlighted in bold. Values are reported as mean \pm standard deviation over five independent runs.

Method	Backbone	Frozen backbone			Fine-tuning backbone		
		F1 score \uparrow	B. Accuracy \uparrow	Recall \uparrow	F1 score \uparrow	B. Accuracy \uparrow	Recall \uparrow
MIS-MAE	ViT-B	0.1457 \pm 0.0063	0.1742 \pm 0.0107	0.2957 \pm 0.0240	0.1934 \pm 0.0067	0.2286 \pm 0.0107	0.3447 \pm 0.0191
MIS-MoCoV3	ViT-B	0.1730 \pm 0.0165	0.1944 \pm 0.0228	0.2584 \pm 0.0424	0.1718 \pm 0.0140	0.1981 \pm 0.0226	0.2701 \pm 0.0353
MIS-MSN	ViT-B	0.0399 \pm 0.0037	0.0606 \pm 0.0047	0.0606 \pm 0.0047	0.1240 \pm 0.0108	0.1442 \pm 0.0129	0.1570 \pm 0.0198
MIS-DINO	ViT-B	0.1883 \pm 0.0182	0.2261 \pm 0.0236	0.3640 \pm 0.0349	0.1944 \pm 0.0171	0.2305 \pm 0.0205	0.3484 \pm 0.0252
MIS-DINOv2	ViT-B	0.1923 \pm 0.0096	0.2322 \pm 0.0165	0.3699 \pm 0.0308	0.2041 \pm 0.0127	0.2459 \pm 0.0201	0.3791 \pm 0.0245
MIS-DINOv2	ViT-L	0.2130 \pm 0.0138	0.2600 \pm 0.0232	0.4027 \pm 0.0280	0.2174 \pm 0.0063	0.2664 \pm 0.0161	0.4020 \pm 0.0285
ImageNet	ViT-B	0.1483 \pm 0.0107	0.1780 \pm 0.0199	0.3160 \pm 0.0407	0.1595 \pm 0.0124	0.1898 \pm 0.0172	0.3139 \pm 0.0299
EndoFM	ViT-B	0.1375 \pm 0.0100	0.1680 \pm 0.0146	0.3130 \pm 0.0246	0.1431 \pm 0.0123	0.1725 \pm 0.0182	0.3098 \pm 0.0316
GSViT	EfficientViT	0.0526 \pm 0.0064	0.0683 \pm 0.0060	0.0738 \pm 0.0076	0.0568 \pm 0.0072	0.0734 \pm 0.0080	0.0780 \pm 0.0082
EndoViT	ViT-B	0.1366 \pm 0.0114	0.1536 \pm 0.0121	0.2539 \pm 0.0167	0.1645 \pm 0.0104	0.1904 \pm 0.0176	0.2951 \pm 0.0322
PeskaVLP	ResNet50	0.1528 \pm 0.0133	0.1796 \pm 0.0172	0.3002 \pm 0.0335	0.1764 \pm 0.0138	0.2085 \pm 0.0148	0.3273 \pm 0.0244
SurgeNet	CAFormer18	0.1646 \pm 0.0171	0.2013 \pm 0.0130	0.3558 \pm 0.0247	0.2048 \pm 0.0199	0.2396 \pm 0.0225	0.3425 \pm 0.0225
ZEN	ViT-B	0.2076 \pm 0.0134	0.2532 \pm 0.0209	0.3950 \pm 0.0302	0.2335 \pm 0.0190	0.2806 \pm 0.0240	0.4006 \pm 0.0346

Table 41 Open-ended visual question answering sentence generation performance on the **LLS48-VQA** dataset with fine-tuned backbones. Performance is evaluated using BLEU-1 to BLEU-4, ROUGE-L, and METEOR (higher is better). The upper block reports results for self-supervised learning pretrained models, and the lower block reports results for existing pretrained models. Best-performing models for each metric are highlighted in bold. Values are reported as mean \pm standard deviation over five independent runs.

Method	Backbone	BLEU-1 \uparrow	BLEU-2 \uparrow	BLEU-3 \uparrow	BLEU-4 \uparrow	ROUGE-L \uparrow	METEOR \uparrow
MIS-MAE	ViT-B	0.5131 \pm 0.0108	0.4212 \pm 0.0119	0.3601 \pm 0.0122	0.3149 \pm 0.0121	0.4391 \pm 0.0123	0.2616 \pm 0.0054
MIS-MoCoV3	ViT-B	0.4980 \pm 0.0107	0.4060 \pm 0.0117	0.3455 \pm 0.0118	0.3010 \pm 0.0117	0.4268 \pm 0.0129	0.2558 \pm 0.0064
MIS-MSN	ViT-B	0.4926 \pm 0.0129	0.4019 \pm 0.0143	0.3423 \pm 0.0158	0.2983 \pm 0.0167	0.4197 \pm 0.0124	0.2515 \pm 0.0057
MIS-DINO	ViT-B	0.5116 \pm 0.0080	0.4197 \pm 0.0083	0.3582 \pm 0.0082	0.3126 \pm 0.0080	0.4384 \pm 0.0099	0.2614 \pm 0.0049
MIS-DINOv2	ViT-B	0.5173 \pm 0.0116	0.4250 \pm 0.0123	0.3629 \pm 0.0126	0.3167 \pm 0.0127	0.4432 \pm 0.0093	0.2657 \pm 0.0038
MIS-DINOv2	ViT-L	0.5245 \pm 0.0082	0.4336 \pm 0.0094	0.3725 \pm 0.0094	0.3270 \pm 0.0091	0.4529 \pm 0.0104	0.2727 \pm 0.0047
ImageNet	ViT-B	0.5006 \pm 0.0037	0.4066 \pm 0.0050	0.3443 \pm 0.0052	0.2985 \pm 0.0053	0.4237 \pm 0.0088	0.2505 \pm 0.0052
EndoFM	ViT-B	0.4917 \pm 0.0115	0.3958 \pm 0.0119	0.3328 \pm 0.0122	0.2869 \pm 0.0122	0.4152 \pm 0.0091	0.2448 \pm 0.0041
GSViT	EfficientViT	0.4167 \pm 0.0118	0.3102 \pm 0.0148	0.2468 \pm 0.0156	0.2022 \pm 0.0155	0.3363 \pm 0.0170	0.1926 \pm 0.0092
EndoViT	ViT-B	0.5009 \pm 0.0133	0.4086 \pm 0.0136	0.3476 \pm 0.0141	0.3028 \pm 0.0144	0.4275 \pm 0.0109	0.2537 \pm 0.0053
PeskaVLP	ResNet50	0.5000 \pm 0.0094	0.4085 \pm 0.0108	0.3479 \pm 0.0113	0.3034 \pm 0.0115	0.4300 \pm 0.0133	0.2558 \pm 0.0066
SurgeNet	CAFormer18	0.5186 \pm 0.0085	0.4284 \pm 0.0089	0.3678 \pm 0.0087	0.3228 \pm 0.0083	0.4445 \pm 0.0081	0.2672 \pm 0.0034
ZEN	ViT-B	0.5244 \pm 0.0126	0.4340 \pm 0.0131	0.3734 \pm 0.0129	0.3282 \pm 0.0122	0.4519 \pm 0.0119	0.2726 \pm 0.0054

Table 42 Open-ended visual question answering sentence generation performance on the **LLS48-VQA** dataset with **frozen backbones**. Performance is evaluated using BLEU-1 to BLEU-4, ROUGE-L, and METEOR (higher is better). The upper block reports results for self-supervised learning pretrained models, and the lower block reports results for existing pretrained models. Best-performing models for each metric are highlighted in bold. Values are reported as mean \pm standard deviation over five independent runs.

Method	Backbone	BLEU-1 \uparrow	BLEU-2 \uparrow	BLEU-3 \uparrow	BLEU-4 \uparrow	ROUGE-L \uparrow	METEOR \uparrow
MIS-MAE	ViT-B	0.4873 \pm 0.0053	0.3937 \pm 0.0062	0.3323 \pm 0.0068	0.2873 \pm 0.0072	0.4125 \pm 0.0073	0.2443 \pm 0.0040
MIS-MoCoV3	ViT-B	0.5002 \pm 0.0155	0.4079 \pm 0.0163	0.3473 \pm 0.0167	0.3027 \pm 0.0167	0.4244 \pm 0.0137	0.2527 \pm 0.0063
MIS-MSN	ViT-B	0.3992 \pm 0.0233	0.2924 \pm 0.0230	0.2288 \pm 0.0236	0.1842 \pm 0.0234	0.3272 \pm 0.0143	0.1933 \pm 0.0114
MIS-DINO	ViT-B	0.5062 \pm 0.0080	0.4138 \pm 0.0080	0.3524 \pm 0.0080	0.3071 \pm 0.0080	0.4345 \pm 0.0075	0.2594 \pm 0.0041
MIS-DINOv2	ViT-B	0.5110 \pm 0.0103	0.4167 \pm 0.0105	0.3542 \pm 0.0103	0.3081 \pm 0.0102	0.4347 \pm 0.0099	0.2596 \pm 0.0041
MIS-DINOv2	ViT-L	0.5175 \pm 0.0100	0.4238 \pm 0.0112	0.3618 \pm 0.0114	0.3159 \pm 0.0112	0.4419 \pm 0.0127	0.2639 \pm 0.0055
ImageNet	ViT-B	0.4846 \pm 0.0074	0.3882 \pm 0.0077	0.3248 \pm 0.0083	0.2787 \pm 0.0088	0.4066 \pm 0.0076	0.2401 \pm 0.0041
EndoFM	ViT-B	0.4820 \pm 0.0055	0.3883 \pm 0.0078	0.3267 \pm 0.0086	0.2819 \pm 0.0090	0.4079 \pm 0.0095	0.2389 \pm 0.0086
GSViT	EfficientViT	0.3838 \pm 0.0382	0.2862 \pm 0.0313	0.2261 \pm 0.0269	0.1843 \pm 0.0238	0.3292 \pm 0.0135	0.1861 \pm 0.0172
EndoViT	ViT-B	0.4824 \pm 0.0103	0.3857 \pm 0.0114	0.3226 \pm 0.0121	0.2770 \pm 0.0123	0.4077 \pm 0.0092	0.2403 \pm 0.0041
PeskaVLP	ResNet50	0.4817 \pm 0.0142	0.3869 \pm 0.0154	0.3256 \pm 0.0160	0.2808 \pm 0.0160	0.4068 \pm 0.0130	0.2417 \pm 0.0070
SurgeNet	CAFormer18	0.5030 \pm 0.0129	0.4097 \pm 0.0140	0.3479 \pm 0.0144	0.3023 \pm 0.0144	0.4285 \pm 0.0111	0.2550 \pm 0.0048
ZEN	ViT-B	0.5148 \pm 0.0057	0.4227 \pm 0.0062	0.3615 \pm 0.0061	0.3162 \pm 0.0058	0.4402 \pm 0.0094	0.2648 \pm 0.0062

Table 43 Cross-modal retrieval performance on the LLS48-VQA dataset. Image-to-text and text-to-image retrieval performance is reported using Recall@1, Recall@5, Recall@10, and mean recall. Values indicate mean \pm standard deviation computed across videos.

Method	Recall@1	Recall@5	Recall@10	Mean Recall
Image-to-Text				
PeskaVLP	0.0814 \pm 0.0666	0.3116 \pm 0.1666	0.5176 \pm 0.1928	0.3035 \pm 0.1328
ZEN	0.0770 \pm 0.0638	0.3053 \pm 0.1676	0.5169 \pm 0.1962	0.2997 \pm 0.1323
Text-to-Image				
PeskaVLP	0.0675 \pm 0.0559	0.2760 \pm 0.1498	0.4577 \pm 0.1700	0.2671 \pm 0.1165
ZEN	0.0703 \pm 0.0560	0.2793 \pm 0.1521	0.4723 \pm 0.1774	0.2740 \pm 0.1193

Table 44 Zero-shot surgical phase recognition performance. Models are evaluated without task-specific training on Cholec80, MultiBypass140, and AutoLaparo datasets. Performance is reported in terms of video-level F1 score and accuracy. Values indicate mean \pm standard deviation across test videos in each dataset.

Method	Cholec80		MultiBypass140		AutoLaparo	
	F1 score	Accuracy	F1 score	Accuracy	F1 score	Accuracy
PeskaVLP	0.3056 \pm 0.0567	0.4272 \pm 0.0938	0.1748 \pm 0.0490	0.2963 \pm 0.0868	0.2433 \pm 0.0608	0.3310 \pm 0.0873
ZEN	0.3135 \pm 0.0546	0.4427 \pm 0.0908	0.1822 \pm 0.0517	0.3099 \pm 0.0907	0.2445 \pm 0.0628	0.3299 \pm 0.0911

Table 45 Summary of upstream datasets used for pretraining. Overview of surgical videos and frames across different anatomical regions and procedures.

Dataset	Anatomical region	Surgical procedure	Videos	Frames
Upstream datasets				
SMC	Hepatobiliary	Hepatectomy	100	507,568
hSBD-instrument		Cholecystectomy	24	18,064
HeiChole		Cholecystectomy	30	54,199
Cholec80		Cholecystectomy	40	84,629
Endoscapes		Cholecystectomy	201	55,809
HeiCo	Colon & Rectum	Proctocolectomy	30	91,760
		Rectal resection		100,995
		Sigmoidectomy		71,457
ART-Net	Pelvis	Hysterectomy	29	1,538
LapGyn4		Gynecologic procedure	500	30,682
SurgicalAction160		Gynecologic procedure	59	759
GLENDAA		Gynecologic procedure	400	25,682
ESAD		Prostatectomy	4	51,552
MultiByPass140	Stomach	Gastric bypass	80	417,518
Sisvse		Gastrectomy	30	4,510
SurgToolLoc2022	Others	Porcine procedure	N/A	745,196
Surgical YouTube	Hepatobiliary	Cholecystectomy	3,253	315,666
		Hepatectomy		16,467
		Splenectomy		20,865
	Abdominal wall	Hernia repair		133,360
	Esophageal	Heller myotomy		81,226
		Esophagectomy		48,641
	Appendix	Appendectomy		54,403
	Stomach	Gastrectomy		856
		Gastrojejunostomy		10,077
		Fundoplication		11,358
	Colon	Colectomy		290,423
		Hemicolecotomy		8,466
		Sigmoidectomy		11,741
	Rectum	Rectopexy		15,092
	Colon & Rectum	Colorectal and rectal cancer surgery		131,127
	Small bowel	Ladd's procedure		7,058
	Others	Unsorted procedures		897,666
			Total	4,780+
				4,316,410

Table 46 Summary of baseline models.

Model	Backbone	Pretraining data	Training strategy
ViT	ViT-B	ImageNet	Supervised
GSViT	EfficientViT	70M frames	Next frame prediction
EndoFM	ViT-B	5M frames	Teacher–student spatiotemporal matching
EndoViT	ViT-B	700k+ frames	MAE
PeskaVLP	ResNet50	26k clip–narration pairs	Video–text contrastive learning
SurgeNet	CAFormer18	4.7M+ frames	DINO

Table 47 Summary of downstream datasets and tasks. Internal and external datasets used for evaluating surgical understanding across multiple tasks.

Dataset	Surgical procedure	Task
Internal datasets		
Cholec80	Cholecystectomy	Surgical phase recognition
		Zero-shot phase recognition
CholecT50	Cholecystectomy	Surgical action triplet recognition
CholecSeg8k	Cholecystectomy	Semantic segmentation
MultiByPass140	Gastric bypass surgery	Surgical phase recognition
		Zero-shot phase recognition
LLS48	Hepatectomy	Surgical action triplet recognition
LLS48-VQA	Hepatectomy	VQA (Closed- and open-ended)
		Cross-modal retrieval
External datasets		
AutoLaparo	Hysterectomy	Surgical phase recognition
		Zero-shot phase recognition
DSAD	Rectal surgery	Semantic segmentation
GraSP	Radical prostatectomy	Semantic segmentation
		Instance segmentation
PitVQA	Pituitary surgery	VQA (Closed-ended)
SCARED	Porcine procedure	Depth estimation
Hamlyn	In vivo endoscopic video	Depth estimation

Table 48 Public surgical datasets used in this study.

Dataset	Link
Cholec80	https://camma.unistra.fr/datasets/
CholecT50	https://github.com/CAMMA-public/cholect50
CholecSeg8k	https://www.kaggle.com/datasets/newslab/cholecseg8k
Cholec80-CVS	https://github.com/ManuelRios18/CHOLEC80-CVS-PUBLIC
hSBD-instrument	https://hsdb-instrument.github.io/
Sisvse	https://sisvse.github.io/
HeiChole	https://www.synapse.org/Synapse:syn18824884/wiki/591922
Endoscapes	https://github.com/CAMMA-public/Endoscapes
ART-Net	https://github.com/kamruleee51/ART-Net
ESAD	https://saras-esad.grand-challenge.org/
AutoLaparo	https://autolaparo.github.io/
MultiByPass140	https://github.com/CAMMA-public/MultiBypass140
LapGyn4	https://ftp.itec.aau.at/datasets/LapGyn4
SurgicalAction160	https://ftp.itec.aau.at/datasets/SurgicalActions160
GLENDAA	https://ftp.itec.aau.at/datasets/glendaa
HeiCo	https://www.synapse.org/Synapse:syn21903917/wiki/601992
SurgToolLoc2022	https://surgtoolloc23.grand-challenge.org/surgtoolloc-2022-resources/
DSAD	https://www.kaggle.com/datasets/anindyamajumder/the-dresden-surgical-anatomy-dataset
GraSP	https://github.com/BCV-Uniandes/GraSP
SCARED	https://endovissub2019-scared.grand-challenge.org/
Hamlyn	https://hamlyn.doc.ic.ac.uk/vision/
PitVQA	https://github.com/mobarakol/PitVQA
Surgical Youtube	https://github.com/TimJaspers0801/SurgeNet